Development of an integrated reservoir-hydropower-hydrologic model in tropical climate basins and its application to reservoir operation assessment under climate change and real-time optimization

Thatkiat Meema

2021

Development of an integrated reservoir-hydropower-hydrologic model in tropical climate basins and its application to reservoir operation assessment under climate change and real-time optimization

by

Thatkiat Meema

A dissertation

submitted in partial fulfillment of the requirement

for the degree of Doctor of Philosophy

Dept. of Civil and Earth Resources Engineering

Kyoto University, Japan

2021

Declaration of authorship

I declare that this thesis titled “Development of an integrated reservoir-hydropower-hydrologic model in tropical climate basins and its application to reservoir operation assessment under climate change and real-time optimization” and the work presented in its entirely are my investigation, except where specifically indicated in the text. I confirm that this research was done wholly at Kyoto University. Any part of this dissertation has not been submitted for a degree or any other qualification at any other University or institution.

Thatkiat Meema

Acknowledgements

The author would like to express the deepest gratitude to his advisor, Prof. Yasuto Tachikawa for his valuable guidance and suggestion–not only academic aspect but other aspects also–during the whole research period under a full-time PhD. program in the Laboratory of Hydrology and Water Resources Research, Department of Civil and Earth Resources Engineering, Graduate School of Engineering, Kyoto University.

I would also like to acknowledge with much appreciation other professors of Hydrology and Water Resources Research Laboratory–Assoc. Prof. Yutaka Ichikawa, Assoc. Prof. Sunmin Kim, Junior Assoc. Prof. Kazuaki Yorozu and Asst. Prof. Tomohiro Tanaka–who provided me valuable suggestions and discussions for conducting this research.

My special thanks to the Electricity Generating Authority of Thailand (EGAT), Royal Irrigation Department of Thailand (RID), Thai Meteorological Department (TMD), TEAM Consulting Engineering and Management PCL. (TEAM GROUP) and Mr. Bounhome Kimmany (Faculty of Water Resources, National University of Laos) for their kind cooperation and support of relevant data and other information for this thesis.

The acknowledgments are also made to all faculties, staff especially Ms. Iwasa and all laboratory members, who have given all their support. Furthermore, I would like to acknowledge my laboratory seniors Dr. Supattana Wichakul, Dr. Donprapob Manee, Dr. Patinya Hanittinan and Dr. Theerawat Ram-Indra for the spontaneous help and support to the author in any other way during the study.

The author also thankfully acknowledges the Japanese Government (Monbukagakusho: MEXT) association with Human Security Engineering (HSE) program for granting the scholarship during studying in Japan, providing me an opportunity to study at Kyoto University.

I greatly thank all staff at Mekong River Commission (MRC), especially Dr. Janjira Chuthong for their cooperation and support during the internship period.

The author is sincere thanks to family who always support and encourage me.

The author would like to thanks all other individuals who did not mention above, the author would appreciate their kind support.

Abstract

Regarding the rapid regional growth of Southeast Asia, water resources have become a highly essential resource for their economy and society. As a dam reservoir is an effective tool in water management, several dams have been developed in various stages ranged from operated to planned in this region. However, the operation of a dam becomes challenging due to the high uncertainty of hydrologic conditions in the tropical climate basin with distinct wet and dry seasons providing a primary effect on reservoir operation increased the risk of water disasters such as flood and drought. This challenge becomes increasingly driven by climate change which increases in extreme events.

To investigate the effect of climate change on reservoir operation is an important and interesting finding for effective management of reservoirs to cope with future hydrologic conditions. The main goal of this thesis is to develop the approaches to assess the impact of climate change on reservoir operations and introduce the strategies to manage the reservoir coping with the uncertainty of water resources in the tropical climate basin.

Chapter 2 proposes the structural improvement of a distributed hydrological model for better results on long-term river discharge prediction in a tropical climate basin, by incorporating bedrock aquifers as part of the slope flow component of the original model structure. Using an application of this improved model, the simulated long-term river discharge results in better performance compared to the original model structure.

Chapter 3 proposes the development of an integrated model that combined reservoir-hydropower model and a distributed hydrological model to evaluate the effect of dam operation on river discharge and power generation. The model performed well which the results agree with the actual operation record. The coupling model is applied to assess the impact of hydropower development in a tropical climate basin such as the Nam Ngum Basin in Lao PDR in various stages of dam development. The results showed the primary change in river flow regulated by the upstream cascade dams.

Chapter 4 proposes the sensitivity assessment of the Nam Ngum 1 reservoir in Laos PDR to the uncertainty of water resources driven by a combination of climate change and upstream cascade dam development using a large ensemble of future climate projections.

The integrated model (Chapter 3) was applied with the projected climate to project future river flow and hydropower production. Even though the results showed a wide range of changes, the future inflow and generated energy tend to decrease when the projected temperature increase. The strategies to cope with the effect of climate change on hydropower generation are discussed.

Chapter 5 proposes the approaches for introducing ensemble weather forecast to real-time reservoir optimization for hydropower and irrigation benefit in Thailand. The medium-range ensemble precipitation forecasts are employed with the hydrologic model in adaptive mode to predict real-time reservoir inflow. Real-time optimization for determining one-week advance water release strategy is conducted with different scenarios using dynamic programming considering inflow predictions. The real-time reservoir inflow prediction performed well compared to the observation. The result of reservoir implementation presented that considering ensemble forecasts in real-time reservoir optimization provided more efficient operating decisions than employing historical data.

Table of contents

List of figures

List of tables

Chapter 1 Introduction

1.1 Background

Southeast Asia is one of the fastest-growing regions in the world in terms of both economy and population, with urbanization expected to continue at a high pace in the coming years (Vinayak *et al*., 2014). As human populations and economies grow, water resources become very important for maintaining an adequate food supply and a productive environment for all living organisms (Kılıç, 2020). Although water is considered a renewable resource because it depends on rainfall, its availability is finite in terms of the amount available per unit of time in any one region (Paz *et al*., 2000).

According to the regional growth of Southeast Asian Countries, water resource is a highly essential resource for the region where agriculture and hydropower are the one of main income of their economy. Although water is required to serve the region's growth, water disasters such as floods and drought are prevalent in this region which is naturally disaster-prone (ESCAP-UNISDR, 2012). Moreover, increasing water consumption due to population and economic growth is the most crucial feature and will continue at an accelerating rate so long as current attitudes and patterns of water utilization remain unchanged (Abu-Zeid and Shiklomanov, 2004). Therefore, the efficient management of water resources becomes an important role for the region.

A dam reservoir, which controls rivers for both water use and flood control, can play a significant role in effectively managing water resources (Nohara *et al*., 2016). It is an effective tool to store water when a severe flood occurs for mitigation of the huge loss, damage of lives and economics (Manee, 2016). According to rapid regional growth and energy demands in Southeast Asia, several dams in main rivers have been developed in various stages ranged from operated to planned especially in the Lower Mekong Basin, numerous dams along the mainstream and tributaries are planned to build (Kummu and Varis, 2007).

Even though building dams can boost their economies, dam operation is challenging due to the uncertainty (unpredictable) on hydrologic conditions in the tropical climate basin with a large difference between wet and dry seasons providing the primary effect on reservoir operation increased the risk of water disasters (Tingsanchali and Boonyasirikul, 2006) such as flood and drought.

Several studies (Bates *et al*., 2008; Milly *et al*., 2005; Palmer *et al*., 2008) indicated that climate change will affect the supply and demand for water resources resulting in an impact on freshwater ecosystems and ecosystem services worldwide. An increase in extreme events such as floods and drought has been predicted (Bates *et al*., 2008). However, current water management may not adequately cope with the impacts of climate change on the reliability of water supply, flood risk, health, agriculture, energy generation and aquatic ecosystems (Palmer *et al*., 2008).

Also, many studies indicate the impact of climate change on water resources in Southeast Asian Basins such as the Chao Phraya Basin (Hunukumbura and Tachikawa, 2012; Wichakul *et al*., 2015), Mekong Basin (Lauri *et al*., 2012; Perera *et al*., 2017) and Irrawaddy (Sirisena et al., 2020). Previous studies have also indicated the combined effects of climate change and existing (or planned) reservoirs on the river flow of Mekong's tributaries (Ngo *et al*., 2018; Piman *et al*., 2015). In addition, (MRC, 2018) reported a significant decrease in hydropower production in Southeast Asia Countries such as Thailand, Laos, Vietnam and Cambodia by 2060 during the GISS scenario. Therefore, predictions of climate change effect cloud increase the awareness of decision-makers to adopt policies and management procedures for rivers and infrastructure (Pahl-Wostl, 2007).

Several studies indicated the advantages of considering forecast information to improve reservoir operation efficiency (Alemu *et al*., 2011; Faber and Stedinger, 2001; Kim *et al*., 2007; Nohara *et al*., 2016; Nohara and Hori, 2018). Another approach that may improve the efficiency of decision-making on reservoir operation is to consider forecast information.

To assess the effect of climate change on water resources, a hydrological model is widely used. The distributed hydrologic model based on a kinematic wave approximation

with surface and subsurface flow components (DHM-KWSS) is a well-known model and applicable to basins with climatic conditions similar to those of such Japanese basins (Kim *et al*., 2011; Sayama *et al*., 2006; Takasao and Shiiba, 1988). However, describing hydrological behavior under different conditions is difficult (Hunukumbura *et al*., 2012). Therefore, improving the DHM-KWSS structure for estimating long-term river discharge in a tropical climate basin is an initial requirement for assessing the change of hydrologic conditions due to climate change. Furthermore, to assess the effect of reservoir operation on river flow and hydropower production under various climate scenarios, the integrated model that combines a distributed hydrologic model and reservoir-hydropower plant model is required to develop.

Assessment of the effect of climate uncertainty on reservoir operations and its introduction on the approaches to operate the large-scale reservoir in a tropical climate basin such as in the Southeast Asian region to cope with the effect is a key and interest for water management effectively in hydropower production and irrigation purpose as well. Furthermore, introducing forecast information to the real-time decision-making for increasing the effectiveness of reservoir operation should be examined. This information will be helpful for stakeholders to propose the strategies of water resources management.

1.2 Objective

The main goal of this thesis is to assess the impact of climate change on reservoir operations and examine the approaches to operate the large-scale reservoir in a tropical climate basin on the uncertainty of hydrologic conditions driven by the future climate conditions. The specific objectives of each interest are as follows.

- To improve the structure of a distributed hydrological model to predict the long-term river flow that is an initial requirement for reservoir operation study in a tropical climate basin where there is a primary difference in hydrologic condition between wet and dry seasons.
- To couple the hydrologic model with the reservoir-hydropower plant process for assessing the impact of reservoir operation on river flow and energy production.

- To predict future river flow and energy production in various climate change scenarios using a large ensemble climate model.
- To introduce the strategies on reservoir operation for hydropower generation to cope with the effect of climate change.
- To examine the approaches for introducing the real-time ensemble weather forecast to reservoir operation for hydropower and irrigation benefit.

1.3 Outline of thesis

This thesis mainly focuses on the effect of future climate on a large-scale reservoir operation and introduces the approach to cope with the uncertainty on the hydrologic condition. For this purpose, the integrated model that combines hydrologic and reservoir-hydropower plant models have been developed to access the impact on water resources and to examine the operation of the reservoir.

Therefore, all contents in a total of six (6) chapters are related to the step-by-step developments of an integrated model, projection of future river flow and hydropower production, and the introduction of the real-time forecast for optimization of reservoir operation.

Chapter 2 illustrates the structural improvement of a distributed hydrological model for better results on long-term river discharge prediction in the Nam Ngum River, the main tributary of the Mekong River, by incorporating bedrock aquifers as part of the slope flow component of the original model structure. To find the suitable model structure, three types of bedrock groundwater structures are configured to incorporate with the original model structure. The parameter set is optimized based on the available physical data for each structure type. Using an application of this improved model, the simulated long-term river discharge results in better performance compared to the original model structure.

Chapter 3 illustrates the development of a reservoir-hydropower plant model and incorporates it into a distributed hydrological model (Chapter 2) to evaluate the effect of dam operation on river discharge and power generation. The model composes of reservoir power generation and hydrological processes with a concept of a kinematic wave-based

assumption. The coupling model is applied to assess the impact of hydropower development in the Nam Ngum Basin in Lao PDR in various stages of dam development.

Chapter 4 assesses the sensitivity of the Nam Ngum 1 reservoir in Laos PDR to the uncertainty of water resources driven by a combination of climate change and upstream cascade dam development using a large ensemble of future climate projections. The future climate variables are projected based on the delta method in various scenarios. The climate variables such as precipitation, actual evapotranspiration and reservoir evaporation are input into the coupling model (Chapter 3) as forcing data to project future river flow and hydropower production. The strategies to cope with the effect of climate change on hydropower generation is discussed.

Chapter 5 examines the approaches for introducing ensemble weather forecast to reservoir operation for hydropower and irrigation benefit in Thailand. The medium-range ensemble precipitation forecasts are employed with the hydrologic model to predict real-time reservoir inflow. Data assimilation is applied to determine the initial condition of the model before performing the inflow forecasts. Moreover, the effect of the initial conditions on inflow forecast has been assessed based on differences in data assimilation procedures. Real-time optimization of the one-week advance water release strategy for hydropower generation and irrigation is conducted with different scenarios using dynamic programming considering inflow predictions.

Finally, the chapter 6 presents concluding remark of the thesis.

Chapter 2 Structural improvement of a kinematic wave-based distributed hydrologic model to estimate long-term river discharge in a tropical climate basin

A distributed hydrologic model based on a kinematic wave approximation with surface and subsurface flow components is applicable to basins that have temperate climatic conditions similar to basins in Japan. However, it is difficult to present long-term river discharge using the existing model structure in basins with different climatic conditions. This study aims to improve the model structure for better results of estimates of long-term discharge in the Nam Ngum River, the main tributary of the Mekong River, by incorporating bedrock aquifers as part of the slope flow component of the original model structure. Three bedrock groundwater structures are configured to incorporate with the original model structure. The results show that a combination of the original model component and one unconfined aquifer structure are the best representations of the river flow regime from the original model structure, in which the rate of infiltration from the layer into the bedrock aquifer was calculated using vertical hydraulic conductivity. The Nash–Sutcliffe efficiency coefficient of the original and improved models increased from 0.8 to 0.86 during the calibration period and from 0.56 to 0.62 during the validation period. The results of this study show that the improved model structure is applicable for long-term hydrologic predictions in Southeast Asian catchments with distinct dry and rainy seasons (Meema and Tachikawa, 2020).

2.1 Introduction

Rapid regional growth and energy demands from neighboring countries have prompted plans to build numerous dams along the mainstream and tributaries of the Mekong River (Kummu and Varis, 2007). A dam reservoir, which controls rivers for both water use and flood control, can play a significant role in effectively managing water resources (Nohara *et al*., 2016). Thus, the efficient operation of large-scale water infrastructure such as dam

reservoirs requires a good estimation of long-term river discharge for reservoir operation plans, water resource management, and flood control.

The distributed hydrologic model based on a kinematic wave approximation with surface and subsurface flow components (DHM-KWSS) is a well-known model used to describe rainfall-runoff processes for many river basins in Japan where most of the basins have steep slopes (Kim *et al*., 2011; Sayama *et al*., 2006; Takasao and Shiiba, 1988). The DHM-KWSS is applicable to basins with climatic conditions similar to those of such Japanese basins. However, describing hydrological behavior under different conditions, such as arid basins, is difficult (Hunukumbura *et al*., 2012). Tanaka and Tachikawa (2015) applied 1K-DHM with a DHM-KWSS structure to two river basins in Europe and Australia that have different climatic conditions than those in Japan for a long-term river flow simulation. The results of this study showed that the model structure of the DHMs-KWSS is applicable to river basins in temperate climatic conditions but has difficulty describing rainfall-runoff processes in semi-arid basins. Tanaka (2016) has suggested that to improve the long-term river flow estimation, especially in the dry season, future studies should incorporate a groundwater component into the model structure.

Katsura *et al*. (2008) found that the infiltration of water from soil into the weathered bedrock was the dominant factor and that the underlying bedrock makes important contributions to water flow. Several previous studies adopted a reservoir or multi-reservoir with linear, non-linear, or combined relationships to generate baseflow in hydrologic models (Ferket *et al*., 2010; Luo *et al*., 2012; Samuel *et al*., 2012).

In this study, the 1K-DHM was applied to estimate long-term river discharge in a tropical climate basin—the Ngum River basin in Lao People's Democratic Republic. The results show that explaining the hydrological behavior of a tropical climate basin using the original 1K-DHM model structure that includes only surface conditions (i.e. topography and land cover) and surface soil layer properties is difficult. Therefore, the main objective of this paper is to improve the DHM-KWSS structure for estimating long-term river discharge in a tropical climate basin by incorporating three bedrock groundwater structures, including unconfined and confined aquifers into the 1K-DHM. The parameter values for each model structure are identified using the SCE-UA algorithm,

and the performance of models with three aquifer structures was evaluated for five years, not including identification periods.

2.2 Applying 1K-DHM to the Nam Ngum River Basin

2.2.1 General description of 1K-DHM

The 1K-DHM is a distributed hydrological model based on a kinematic wave flow approximation that considers surface-subsurface flow. The elevation and flow direction are determined using topographical data provided by HydroSHEDS (Lehner *et al*., 2006) with digital elevation models (DEMs) at 30 second (approximately 1 km) resolution.

Each cell of 1K-DHM consists of river and slope flow components (Tanaka and Tachikawa, 2015). The schematic drawing of 1K-DHM is shown in **Fig. 2.1**. Discharge from the slope flow components on both sides of the river-channel component is estimated using rainfall input to the cell with the following discharge-storage relationship in **Eq. 2.1** that considers surface-subsurface flow components (Tachikawa *et al*., 2004). An influence of the catchment land cover in 1K-DHM is explained by considering the Manning's roughness coefficient of the surface flow condition on the soil surface component (n_s) as expressed in the equation below.

$$q_s(h_s) = \begin{cases} d_m k_m \left(\dfrac{h_s}{d_m}\right)^{\beta} i & (0 \le h_s \le d_m) \\ d_m k_m i + (h_s - d_m) k_a i & (d_m \le h_s \le d_a) \\ d_m k_m i + (h_s - d_m) k_a i + \dfrac{\sqrt{i}}{n_s} & (h_s - d_a)^m (d_a \le h_s) \end{cases} \quad (2.1)$$

where q_s is runoff per unit slope width, h_s is water depth, d_m is the maximum water content in the capillary pore, k_m is hydraulic conductivity when the capillary pore is saturated, β is an exponent parameter that describes the relationship between hydraulic conductivity and water content, d_a is the maximum water content in the effective porosity, k_a is saturated hydraulic conductivity, n_s is the Manning's roughness coefficient for surface flow in the slope flow component, i is slope gradient, and m = 5/3.

Eq. 2.1 represents the $q_s - h_s$ relationship for the surface and subsurface soil layer which realizes three flow mechanisms including subsurface flow through capillary pore,

subsurface flow through non-capillary pore and surface flow on the soil layer as shown in the conceptual soil model in **Fig. 2.3**. At a slope segment, when the water depth is lower than the equivalent water depth for unsaturated flow (d_m), flow is simulated by Darcy′s law with an unsaturated hydraulic conductivity (k_m). If the water depth exceeds the equivalent depth for unsaturated flow, the saturated subsurface flow is simulated by Darcy′s law with saturated hydraulic conductivity (k_a). And when the water depth is greater than the effective soil layer ($d_a = \gamma D$ where γ is the soil porosity and D is the total soil depth), the water flows as surface flow which is calculated by Manning′s equation. The water depth (h_s) and discharge per unit slope (q_s) can be calculated by combining **Eq. 2.2** with the continuity equation showed below.

$$\frac{\partial h_s}{\partial t} + \frac{\partial q_s}{\partial x} = r - e \tag{2.2}$$

The discharge from the slope flow component on both sides of the river channel ($2q_s$) as shown in **Fig. 2.1** is distributed into the river-channel component as the lateral discharge per unit length. The discharge from upper cells is assigned as the boundary condition into the river-channel component of the cell. River flow of the river-channel component is simulated by the following 1-D kinematic wave equations

$$Q = \alpha A^m \tag{2.3}$$

$$\frac{\partial A}{\partial t} + \frac{\partial Q}{\partial x} = 2q_s \tag{2.4}$$

where Q is the river discharge, A is the cross-sectional area, $\alpha = \sqrt{i_o}/(nB^{m-1})$ (where n is the Manning′s roughness coefficient of the channel; i_o is the slope gradient of the channel and B is the channel width), $m = 5/3$ and q_s is the total runoff from the slope flow component of a unit cell.

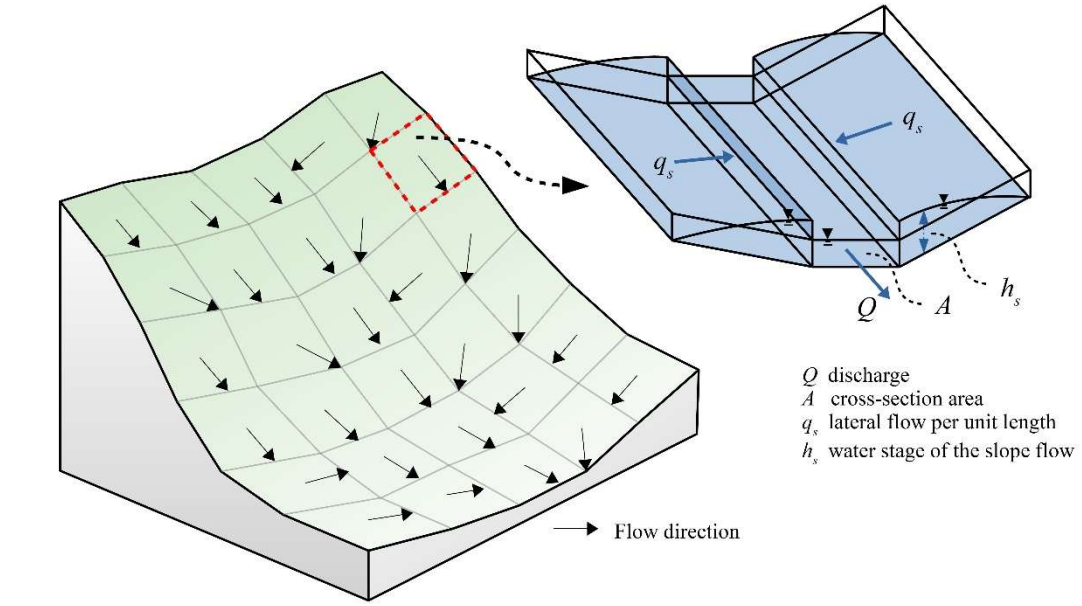

Fig. 2.1 Schematic of flow simulation in 1K-DHM.

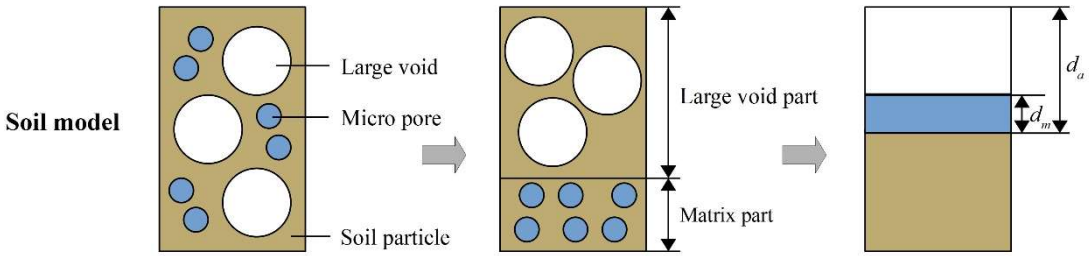

Fig. 2.2 Conceptual of soil surface model.

To calculate water depth (h_s) and discharge per unit slope (q_s), the combination of **Eq. 2.1 and Eq. 2.2** is derived as a nonlinear first-order partial differential equation which describes the change of q_s and h_s in time and space. This equation can be solved by using numerical methods. There are several methods such as the finite difference method, the finite element method, and the finite volume method. For 1K-DHM, the finite difference

method is used to solve the equation. There are two types of finite difference method which are explicit and implicit methods. Explicit methods evaluate all spatial derivatives in a partial differential equation at the time level where the solution is known. Implicit methods evaluate all spatial derivatives at the time level where the solution is unknown. Generally, implicit methods are more complex than explicit methods. However, the implicit method is better in numerical stability.

To apply the finite difference method for the numerical solution of the kinematic wave model, the propagation velocity (c) is introduced. Regarding to **Eq. 2.1**, the propagation velocity of the kinematic wave is determined as follows.

$$c = \frac{dq_s}{d\hbar_s} = f'\left(\hbar_s\right) = \begin{cases} \beta k_m \left(\frac{\hbar_s}{d_m}\right)^{\beta-1} i & \left(0 \le \hbar_s \le d_m\right) \\ k_a i & \left(d_m \le \hbar_s \le d_a\right) \\ m\frac{\sqrt{i}}{n_s}\left(\hbar_s - d_a\right)^{m-1} + k_a i & \left(d_a \le \hbar_s\right) \end{cases} \tag{2.5}$$

So, the continuity equation in the **Eq. 2.2** can be rewritten as.

$$\frac{\partial q_s}{\partial t} + c\left(\frac{\partial q_s}{\partial x} - (r-e)\right) = 0 \tag{2.6}$$

Following a finite difference solution (Beven, 1979), the **Eq. 2.6** can be rewritten by using the grid scheme as shown in **Fig. 2.3** that sets the values of ${q_s}_j^i$, ${q_s}_{j+1}^i$ and ${q_s}_j^{i+1}$ to determine the value of ${q_s}_{j+1}^{i+1}$ which can be written as

$$\boldsymbol{{q_s}_{j+1}^{i+1}} = \frac{\boldsymbol{{q_s}_{j+1}^{i} + \theta c_{j+1/2}^{i+1} \Delta t\left(\frac{{q_s}_j^{i+1}}{\Delta x} + \left(r^{i+1} - e^{i+1}\right)\right) - (1-\theta) c_{j+1/2}^{i} \Delta t\left(\frac{{q_s}_{j+1}^{i} - {q_s}_j^{i}}{\Delta x} - \left(r^{i} - e^{i}\right)\right)}}{\boldsymbol{1 + \theta c_{j+1/2}^{i+1} \frac{\Delta t}{\Delta x}}} \tag{2.7}$$

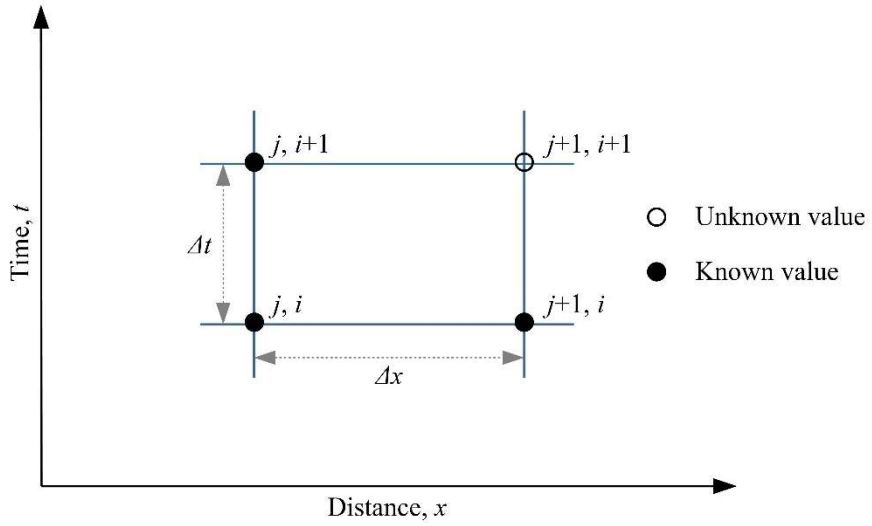

Fig. 2.3 Finite difference mesh used in kinematic model.

2.2.2 Nam Ngum River Basin and data input

The Nam Ngum River basin located in the central part of Lao People's Democratic Republic is one of the main tributaries of the Mekong River. The catchment area of the Nam Ngum River basin at the Naluang station is approximately 4852 km^2. The basin has a tropical climate condition where the whole area of the basin has distinct dry and rainy seasons. The mean annual precipitation in the basin is approximately 1765 mm, and high discharge always occurs in the wet season from May to October. Rainfall during this period accounts for 85% of the annual rainfall. During the dry season, there is less rainfall, however, the basin can maintain and contribute low flow to the river. According to a map of the depth to bedrock (DTB) (Shangguan *et al*., 2017) as shown in **Fig. 2.4**, the average DTB in the study basin is 3.1 m with a standard deviation of 2.55 m. Daily precipitation from 4 stations (Xiengkhuang, Kasy, Vangvieng and Naluang) and observed river discharge at the Naluang station were collected for use in this study.

For long-term river discharge simulation, actual evapotranspiration (AET) is required. Information on evapotranspiration is not available in the study area. Therefore, AET was estimated based on water balance calculated from observed annual river discharge at the

Naluang station and the annual amount of basin rainfall. The estimation of AET over the basin is shown in **Fig. 2.5**.

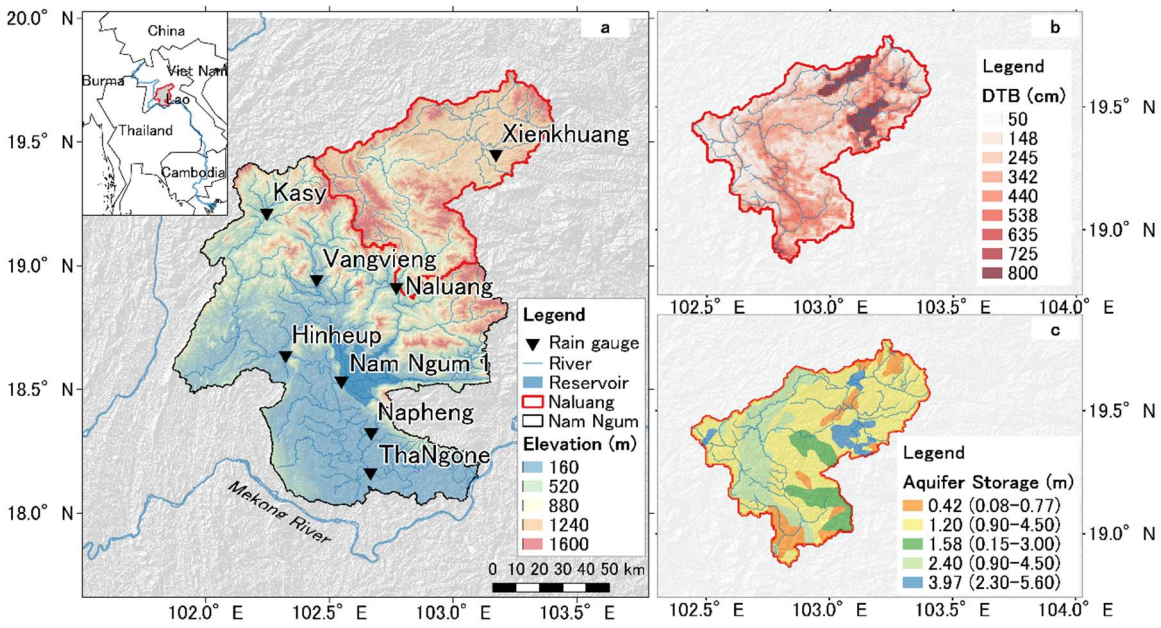

Fig. 2.4 General physical condition of Nam Ngum River Basin (a) watershed boundary with rain gauges location; (b) DTB map of Naluang catchment (Shangguan *et al*., 2017); (c) aquifer storage map of Naluang catchment (Viossanges *et al*., 2018).

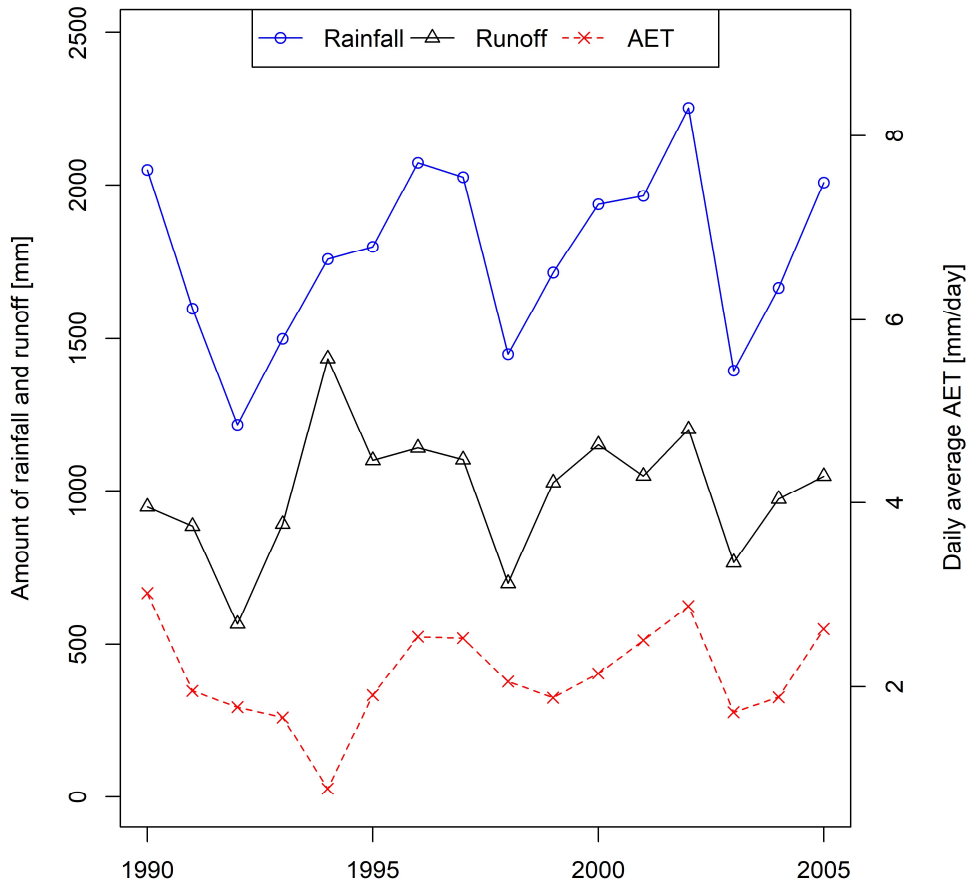

Fig. 2.5 Estimation of long-term actual evapotranspiration.

2.2.3 Result and discussion on applying 1K-DHM to the basin

The simulation optimized soil depth parameters – such as effective soil porosity depth (d_a) – to be much larger than the average DTB of the basin as shown in **Fig. 2.4b** so as to maintain river discharge in the dry season. The range of porosity for an unconsolidated deposit is approximately 0.25–0.7 (Freeze and Cherry, 1979); thus, the range of d_a should be from 0.8–2.2 m. However, the calibrated soil depth of the original 1K-DHM structure is much larger (the value is shown in a later section). The thick soil layer also resulted in an underestimation of the river discharge during the transition from the dry to the wet season. Thus, the existing model structure that considers only surface conditions (i.e. topography and land cover) and the properties of the soil surface layer does not explain

the hydrological behavior of a tropical climate basin that has distinct dry and rainy seasons. Therefore, this study aims to improve the model structure of the 1K-DHM for a better estimation of long-term river discharge in the basin.

2.3 Improvement of the model structure

Shallow and deep bedrock aquifers are analyzed in this study based on the literature on conceptual aquifer models described in the introduction section. Three aquifer structures are configured to incorporate the 1K-DHM by adding a single or multi aquifer of bedrock into the surface-subsurface component (soil surface) of the original model structure. The schematic of each slope flow model and discharge-storage relationship for each component are summarized in **Fig. 2.6**, and the description of each structure is provided below.

2.3.1 Model structure 1 (M1)

M1 consists of the surface-subsurface flow, shallow aquifer, and deep aquifer components on the slope unit.

2.3.1.1 Surface-subsurface flow component

The surface-subsurface flow component has the same structure as the original 1K-DHM (M0) (explained in Section 2.2.1). Thus, the discharge-storage relationship applies the same formula as M0, as expressed in **Eq. 2.1**. To consider the vertical infiltration from the surface-subsurface flow component into the shallow aquifer bedrock, the continuity equation of the soil surface layer is modified as follows:

$$\frac{\partial h_s}{\partial t} + \frac{\partial q_s}{\partial x} = r - e - p_u \tag{2.8}$$

where t is time, x is the space coordinate, r is rainfall intensity, e is actual evapotranspiration (AET), h_s is the water depth in the soil surface component, q_s is the discharge per unit width of the soil surface component, and p_u is the vertical infiltration rate from the surface soil layer into the shallow aquifer.

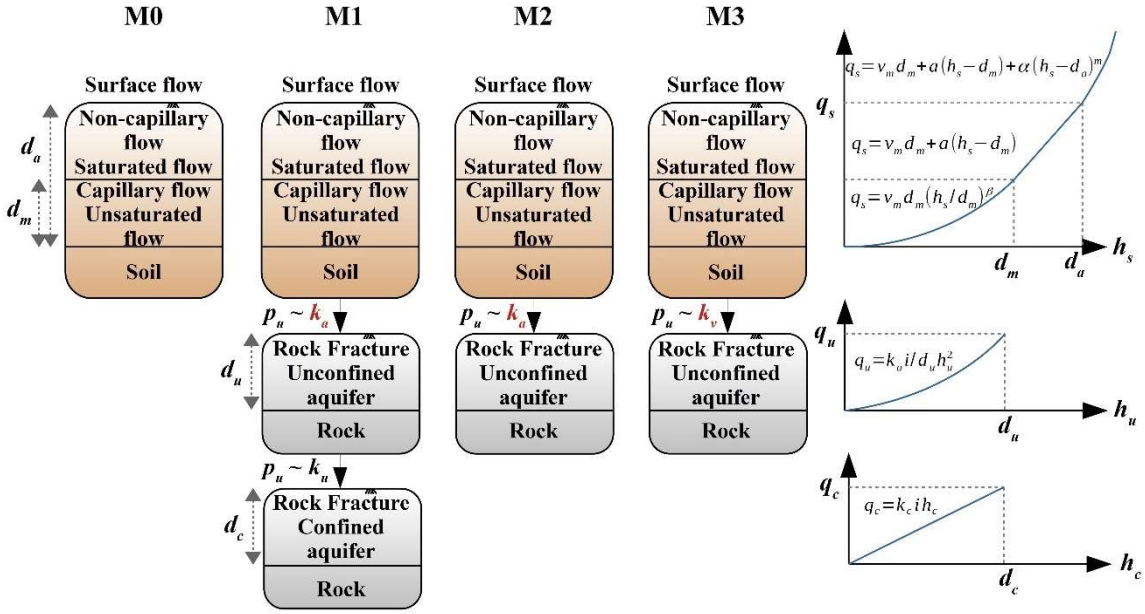

Fig. 2.6 Schematic conceptual of all model structures and their discharge-storage relationship.

2.3.1.2 Unconfined aquifer component

The shallow groundwater aquifers of river basins are predominantly unconfined, suggesting that the relationship between baseflow and storage is nonlinear (Wittenberg, 1999). Banks *et al*., (2009) described the flow through bedrock as being controlled by the fracture network and connectivity. This study assumed that some part of the groundwater flowed out from the soil layer boundary, infiltrated into the bedrock, flowed through the underlying bedrock and the connected rock fracture, and contributed to the river discharge. According to Darcy's law, the total discharge per unit width of the unconfined aquifer $q_u(h_u)$ is expressed as:

$$q_u(h_u) = k_u(h_u) i h_u = k_u \left(\frac{h_u}{d_u}\right) i h_u = \alpha_u {h_u}^2 \tag{2.9}$$

where d_u is the total effective depth of rock fracture in the unconfined bedrock aquifer as shown in **Fig. 2.7**; h_u is the total water depth in the fracture of the aquifer; k_u is the

hydraulic conductivity that corresponds to the actual cross-sectional area of flow in the rock fracture. In the unconfined aquifer, the hydraulic conductivity is assumed to decrease when h_u decreases; therefore, the hydraulic conductivity is assumed to be $k_u(h_u) = k_u(h_u/d_u)^{\beta_u}$, where β_u is a parameter that corresponds to the reduction of hydraulic conductivity in the unconfined aquifer (in this study , β_u is assumed to be 1), i is the gradient of the hillslope, and $\alpha_u = k_u i/d_u$.

The unconfined aquifer in a slope unit is calculated by the following continuity equation:

$$\frac{\partial h_u}{\partial t} + \frac{\partial q_u}{\partial x} = p_u - p_c \tag{2.10}$$

where p_c is the vertical infiltration from the unconfined aquifer to the confined aquifer.

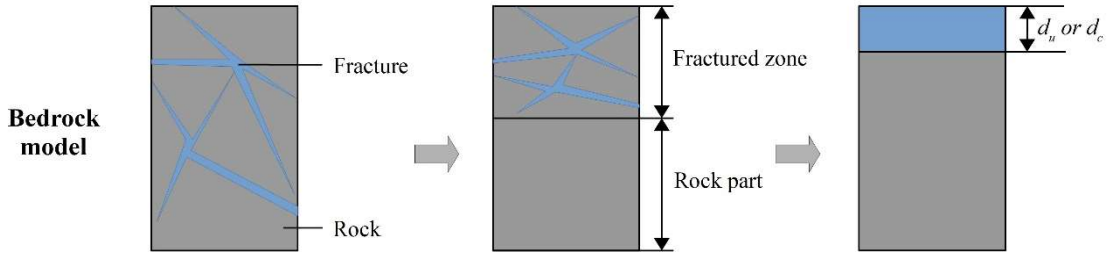

Fig. 2.7 Conceptual of bedrock aquifer model.

2.3.1.3 Confined aquifer component

A deep aquifer can be defined as a confined aquifer with a linear discharge-storage relationship. For the confined aquifer, d_c is the total effective depth of the rock fracture in the confined bedrock aquifer, and h_c is the total water depth in the rock fracture of the aquifer. k_c is the hydraulic conductivity that corresponds to the actual cross-sectional area of the flow in the rock fracture. Thus, the total discharge per unit width $q_c(h_c)$ can be calculated by:

$$q_c(h_c) = k_c i h_c = \alpha_c h_c \tag{2.11}$$

where $\alpha_c = k_c i$.

The confined aquifer in a slope unit is calculated by the following continuity equation:

$$\frac{\partial h_c}{\partial t} + \frac{\partial q_c}{\partial x} = p_c \tag{2.12}$$

The total discharge from all slope flow components on both sides of the river channel ($2q_s$, $2q_u$, and $2q_c$) contributes to the river channel component as the lateral discharge per unit length. Consequently, the continuity equation of a river channel flow model was modified as follows:

$$\frac{\partial A}{\partial t} + \frac{\partial Q}{\partial x} = 2(q_s + q_u + q_c) \tag{2.13}$$

where A is the river cross-section area, Q is the river discharge, and the relation $Q = \alpha A^m$ ($\alpha = \sqrt{i_o}/(nB^{m-1})$ where n is the Manning's roughness coefficient of the channel; i_o is the slope gradient of the channel and B is the channel width, m = 5/3) is assumed based on the kinematic wave flow assumption.

2.3.2 Model structure 2 (M2)

The structure of M2 is similar to that of M1 but consists of only an unconfined aquifer. Thus, M2 consists of two main components on the slope unit – the surface-subsurface flow and the unconfined aquifer components.

The surface-subsurface flow component is calculated with the same discharge-storage relationship as M1 with the continuity equation in **Eq. 2.8**. For the unconfined aquifer component, the discharge per unit width (q_u) is calculated using **Eq. 2.9** and the continuity equation in **Eq. 2.10**, where the vertical infiltration from the unconfined aquifer to the confined aquifer (p_c) is set to 0. For a river channel flow model, the total lateral discharge from the confined aquifer component (q_c) in **Eq. 2.13** is set to 0.

2.3.3 Model structure 3 (M3)

The structure of M3 is similar to that of M2 and consists of two main components on the slope unit: the surface-subsurface flow and the unconfined aquifer components. The difference between M3 and M2 is the estimation of the vertical infiltration from the soil surface layer to the unconfined aquifer (p_u), in which M3 is introduced as the vertical hydraulic conductivity (k_v) to calculate the infiltration rate.

2.3.4 Estimation of vertical infiltration

To estimate the amount of vertical infiltration into the bedrock, the storage routing technique (Arnold *et al*., 1998) was adopted. The storage routing technique is based on the equation

$$\frac{dS}{dt} = -p \tag{2.14}$$

where p is infiltration rate and S is the water content in the layer which can be expressed with following storage function:

$$S_{(t)} = k \cdot exp\left(-\frac{t}{T}\right) \tag{2.15}$$

where k is the constant value, t is the current time and T is the infiltration time of water from the upper layer.

The estimation of the vertical infiltration rate from the soil layer to the unconfined aquifer (p_u) in this model follows the assumption that the infiltration process occurs when the water content in the soil layer exceeds the unsaturated flow condition ($h_s > d_m$). Thus, by adopting the storage routing technique, p_u can be calculated using the numerical solution as follows:

$$p_u = \begin{cases} 0 & (0 \le h_s \le d_m) \\ (h_s - d_m)\left[1 - exp\left(\frac{-\Delta t}{T}\right)\right]/\Delta t & (d_m < h_s) \end{cases} \tag{2.16}$$

where d_m is the capillary depth, Δt is the time step and T is calculated by $T = (h_s - d_m)/k$. For M1 and M2, the saturated hydraulic conductivity in the soil layer (k_a) is used for k; the vertical hydraulic conductivity (k_v) is used for M3.

Only the M1 structure considers the confined aquifer, and the vertical infiltration from the unconfined aquifer to the confined aquifer (p_c) is calculated using the numerical solution as follows:

$$p_c = h_u\left[1 - exp\left(\frac{-\Delta t}{T}\right)\right]/\Delta t \tag{2.17}$$

where $T = h_u/k_u$.

The infiltration from the upper component does not occur when the storage in the aquifer component is filled full of water.

2.4 Numerical solution for the improved models

2.4.1 Surface-subsurface flow component

The numerical solution for the surface-subsurface flow component is similar to the original model. By adding the vertical infiltration (p_u) from the surface-subsurface flow component into the shallow aquifer bedrock into the continuity equation of the soil surface layer as expressed in **Eq. 2.1**, **Eq. 2.6** and **Eq. 2.7** can be rewritten as follows:

$$\frac{\partial q_s}{\partial t} + c\left(\frac{\partial q_s}{\partial x} - (r - e - p_u)\right) = 0 \tag{2.18}$$

$$q_{s}{}_{j+1}^{i+1} = \frac{q_{s}{}_{j+1}^{i} + \theta c_{j+1/2}^{i+1}\Delta t\left(\frac{q_{s}{}_{j}^{i+1}}{\Delta x} + (r^{i+1} - e^{i+1} - p_u{}^{i+1})\right) - (1-\theta)c_{j+1/2}^{i}\Delta t\left(\frac{q_{s}{}_{j+1}^{i} - q_{s}{}_{j}^{i}}{\Delta x} - (r^{i} - e^{i} - p_u{}^{i})\right)}{1 + \theta c_{j+1/2}^{i+1}\frac{\Delta t}{\Delta x}} \tag{2.19}$$

2.4.2 Unconfined aquifer component

For the numerical solution of the bedrock aquifer, a similar concept of kinematic wave assumption with the surface-subsurface layer is applied. Regarding to **Eq. 2.9**, the propagation velocity of the kinematic wave in the unconfined aquifer (c_u) is determined as follows.

$$c_u = \frac{dq_u}{dh_u} = f'(h_u) = \alpha_u h_u \tag{2.20}$$

And the continuity equation of the unconfined aquifer in the **Eq. 2.10** can be rewritten as.

$$\frac{\partial q_u}{\partial t} + c_u\left(\frac{\partial q_u}{\partial x} - (p_u - p_c)\right) = 0 \tag{2.21}$$

Following a finite difference solution (Beven, 1979), the **Eq. 2.21** can be rewritten by using the grid scheme as shown in **Fig. 2.3** that sets the values of $q_{u}{}_{j}^{i}$, $q_{u}{}_{j+1}^{i}$ and $q_{u}{}_{j}^{i+1}$ to determine the value of $q_{u}{}_{j+1}^{i+1}$ which can be written as follow;

$$q_{u_{j+1}}^{i+1} = \frac{q_{u_{j+1}}^{i} + \theta c_{u_{j+1/2}}^{i+1} \Delta t \left(\frac{q_{u_j}^{i+1}}{\Delta x} + \left({p_u}^{i+1} - {p_c}^{i+1} \right) \right) - (1-\theta) c_{u_{j+1/2}}^{i} \Delta t \left(\frac{q_{u_{j+1}}^{i} - q_{u_j}^{i}}{\Delta x} - \left({p_u}^{i} - {p_c}^{i} \right) \right)}{1 + \theta c_{u_{j+1/2}}^{i+1} \frac{\Delta t}{\Delta x}} \quad (2.22)$$

For M2 and M3, p_c is set to 0.

2.4.3 Confined aquifer component

Regarding to **Eq. 2.11** and **Eq. 2.12**, the propagation velocity of the kinematic wave (c_c) and the continuity equation in the confined aquifer layer can be expressed as follows.

$$c_c = \frac{dq_c}{dh_c} = f'(h_c) = \alpha_c \quad (2.23)$$

$$\frac{\partial q_c}{\partial t} + c_c \left(\frac{\partial q_c}{\partial x} - p_c \right) = 0 \quad (2.24)$$

To determine $q_{c_{j+1}}^{i+1}$, the values of $q_{c_j}^{i}$, $q_{c_{j+1}}^{i}$ and $q_{c_j}^{i+1}$ are set as known value in a finite difference equation as expressed below.

$$q_{c_{j+1}}^{i+1} = \frac{q_{c_{j+1}}^{i} + \theta c_{c_{j+1/2}}^{i+1} \Delta t \left(\frac{q_{c_j}^{i+1}}{\Delta x} + {p_c}^{i+1} \right) - (1-\theta) c_{c_{j+1/2}}^{i} \Delta t \left(\frac{q_{c_{j+1}}^{i} - q_{c_j}^{i}}{\Delta x} - {p_c}^{i} \right)}{1 + \theta c_{c_{j+1/2}}^{i+1} \frac{\Delta t}{\Delta x}} \quad (2.25)$$

2.5 Calibration and validation process of the improved model

The simulation is divided into the calibration and validation stages. Due to data availability and the condition of the basin (without upstream dam reservoirs), 1990 was selected as the calibration period, and 1991–1995 was selected as the validation period. For each model, the SCE-UA algorithm (Duan *et al.*, 1994) was applied to optimize the model parameters by searching for the parameter with the highest Nash–Sutcliffe efficiency coefficient (NSE). The important preparation to identify the parameter set is to design the range of the parameters.

As the optimization process using SCE-UA requires the range of each parameter, important preparation to identify the parameter set is needed to design the range value of

the additional parameters of the aquifer component in the improved models. According to the map of shallow groundwater storage in **Fig. 2.4c**, the average shallow groundwater storage (unconfined aquifer storage) in the basin is approximately 1.53 m (30 m of total depth of bedrock is considered) which can be ranged from 0.8–4.0 m. For the deep storage (confined aquifer storage), we assume that there is less of an influence on the river discharge than the shallow aquifer; thus, 15 m of the total depth of bedrock is considered. Therefore, the range of d_c can be 0.4–2.0 m (assuming that the bedrock is quite homogeneous and the porosity is similar to the shallow aquifer). To find k_u and k_c that represents the average hydraulic conductivity in the bedrock aquifers of the basin (k_c is set smaller than k_u based on the assumption that the deeper aquifer has slower hydraulic conductivity), the recession part (December, 1990– March, 1991) was manually simulated to match the recession hydrograph with the observation discharge in which the simulation is based on the assumption that river flow was contributed from the bedrock aquifer during that period. An initial condition was assigned to the model at the beginning of the simulation equivalent to the observed river flow at that moment.

We found that the parameters obtained from the recession part simulation should not directly be used when processing the optimization of parameters throughout the year simulation. This is because it is sometimes difficult to simulate the previous part to meet the flow condition at the beginning of the recession period. Therefore, the parameters were assigned as the range that is used to the SCE-UA algorithm. The k_v was introduced to control the amount of infiltration into the aquifer, thus the value of k_v should be in the range of input rainfall intensity. Due to the lack of hourly observed data in the study area, the input rainfall intensity was adopted by dividing the daily amount of rainfall into hourly rainfall intensity.

Finally, to optimize the parameters of M1-M3 with 5 more additional parameters, the range of d_u was designed as 0.8 – 4.0 m; the range of k_u was designed as 0.0001–0.001 m/s; the range of d_c was designed as 0.4 – 2.0 m; the range of k_c was designed as 0.00001–0.0001 m/s and the range of k_v was designed as 1.0×10^{-7} – 5.0×10^{-7}m/s. The results of optimized model parameters for each model compared with parameter sets obtained from river basins in Japan were presented in **Table 2.1**.

Table 2.1 Comparison of optimized model parameters.

Parameter (Units)	Nam Ngum				Kurokawa[1]	Katsura[1]
	M0	M1	M2	M3	M0	
Soil surface						
n_s ($m^{-1/3}/s$)	0.284	0.664	0.094	0.038	0.146	0.400
k_a (m/s)	0.0012	0.0085	0.0075	0.0038	0.0017	0.0005
d_a (m)	7.420	2.241	2.173	2.139	1.314	0.380
d_m (m)	7.381	2.071	2.069	1.951	0.987	0.160
θ (-)	24.93	28.68	25.29	27.30	7.87	6.00
Unconfined aquifer						
k_u (m/s)	-	0.00029	0.00032	0.00023	-	-
d_u (m)	-	2.417	2.486	1.570	-	-
k_v (m/s)	-	-	-	1.16×10^{-7}	-	-
Confined aquifer						
k_c (m/s)	-	7.83×10^{-7}	-	-	-	-
d_c (m)	-	0.572	-	-	-	-

* [1]Tanaka (2016)

2.6 Result and discussion

According to the optimized parameter sets for the Nam Ngum basin in **Table 2.1**, the effective soil depth parameters such as d_a and d_m are the primary difference between M0 and M1−M3. M0 attempted to simulate the base flow in the dry season by reflecting a soil depth value much larger than that of M1−M3. The comparison of optimized parameters between M1−M3 simulated in the Nam Ngum Basin and M0 simulated in Japanese basins shows no large difference in the effective soil depth parameters. Nevertheless, M0 for Japanese basins was simulated based on large flood events. Therefore, for the long-term simulation of M1−M3 in the Nam Ngum Basin, θ is set much higher to maintain the base flow during the dry season.

The observed and simulated discharge hydrographs during the calibration and validation stages obtained from each model structure at the Naluang station are compared in **Fig. 2.8**. **Fig. 2.9** shows the model performance indices, such as the NSE, Root mean

square error (RMSE), and Percent bias (PBIAS), of each model during the calibration and validation stages.

All the models presented the characteristics of long-term river discharge in the basin with distinct dry and rainy seasons. However, M0 attempts to maintain the base flow during the dry season by placing an emphasis on both soil and bedrock groundwater processes in only the soil layer component. This resulted in the overly thick d_a value shown in **Table 2.1**.

2.6.1 Improvement by M1 and M2

According to the simulation results, the M1 and M2 hydrograph and performance indexes showed similar tendencies. The combination of discharge generated by the confined and unconfined aquifers in M1 is similar to the discharge generated by the unconfined aquifer in M2. Moreover, the hydrologic processes in the soil layer component of the model structure are the same. On the one hand, the result of the river flow hydrograph at the basin outlet in M1 is very similar to that of M2. On the other hand, the incorporation of the bedrock aquifer into the 1K-DHM structure in M1 and M2 yielded better model performance indices than M0 for NSE and RMSE for all periods (annual, wet, and dry seasons) during the calibration stage. NSE and RMSE also showed a better performance in M1 and M2 than in M0 during the validation stage.

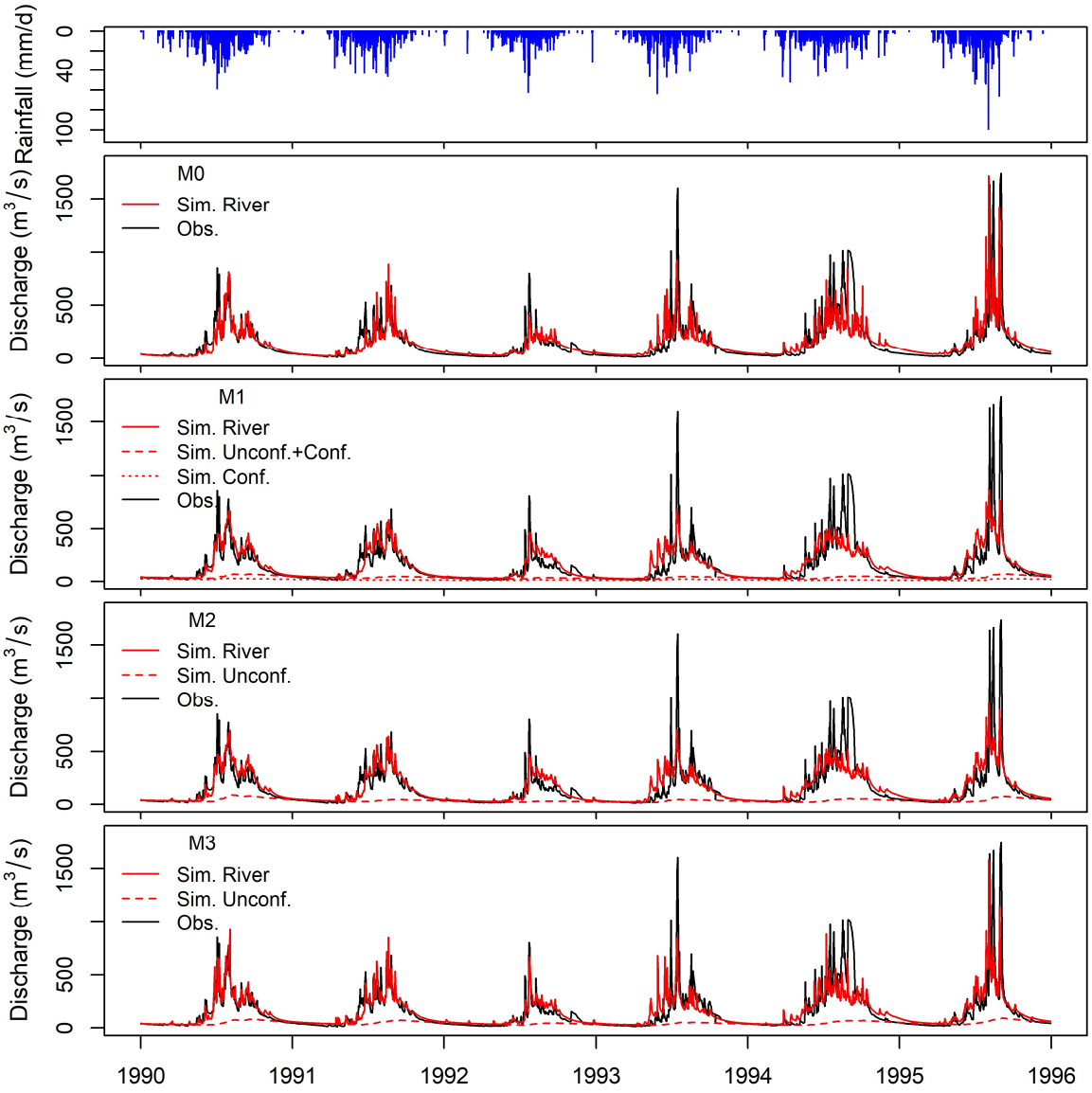

Fig. 2.8 Hydrograph of observed (black line) and simulated discharge (red line) at Naluang station including discharge generated by unconfined aquifer (dash red line; in M1 means combination of unconfined and confined aquifers) and confined aquifer (dot red line).

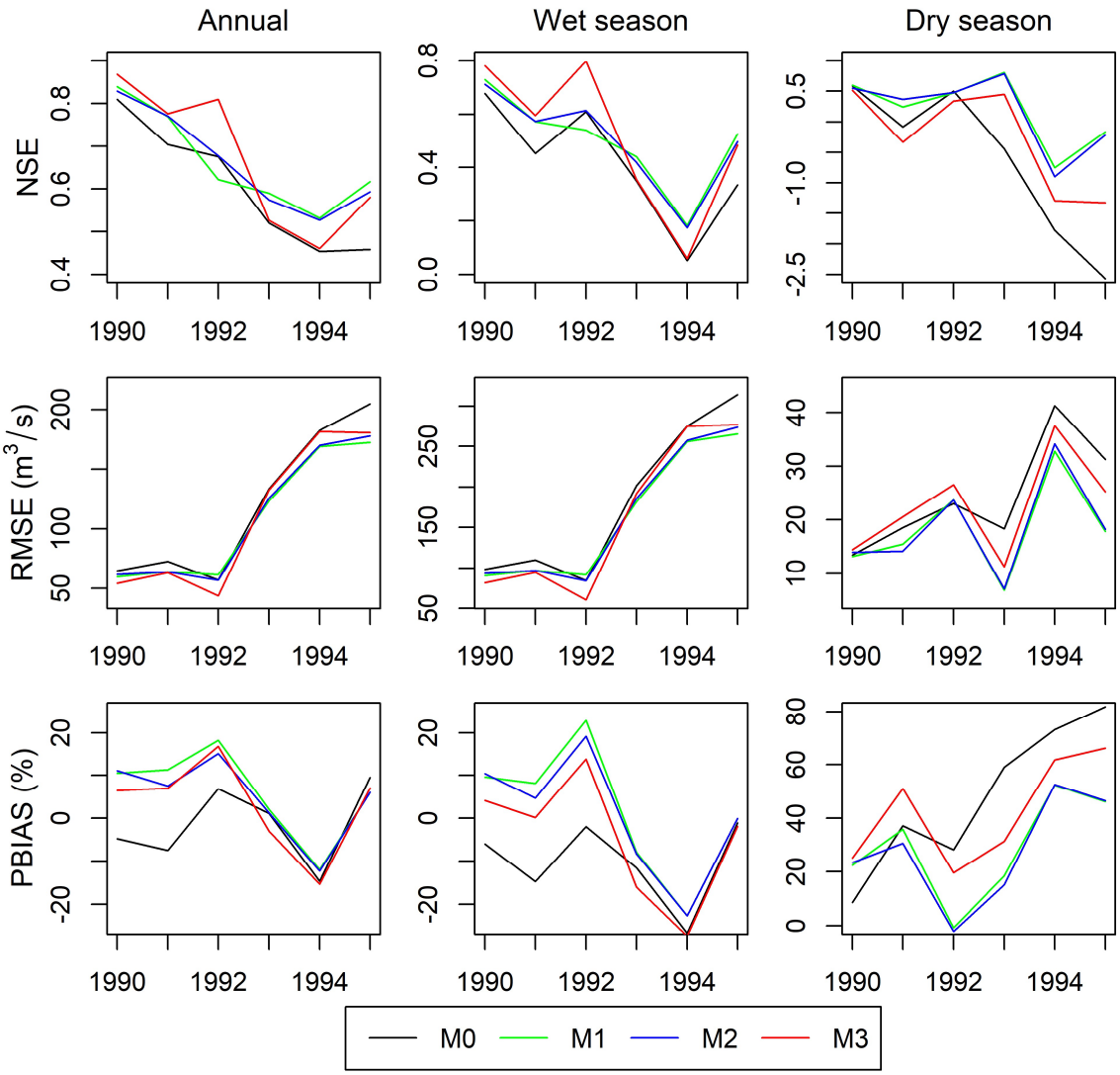

Fig. 2.9 Evaluation of model performances (Annual means throughout the year, wet season means May – October and dry season means January – April and November-December).

2.6.2 Disadvantages of M1 and M2

For M1 and M2, the optimized processes control the amount of infiltration by reflecting a high value of k_a to maintain unsaturated flow conditions in the soil layer. When high rainfall intensity causes the water stage in the soil layer (h_s) to exceed d_m, saturated flow conditions occur, and the vertical infiltration process begins. Most rainwater was

infiltrated into the bedrock aquifer because of high rates of k_a that caused the simulated river discharge at the beginning of the rainy season to be underestimated during the calibration stage (**Fig. 2.8**). Additionally, the recession part of simulated hydrograph during the calibration period was higher than the observed hydrograph because of a slow discharge rate in the aquifer and the time required to release the infiltrated water that is stored in the aquifer components. Therefore, the calculation of the vertical infiltration component is required to improve the simulation.

2.6.3 Improvement by M3

As mentioned above, the contribution of the confined aquifer in M1 is substituted by that of the unconfined aquifer in M2 for this study area. This suggests that developing M3 based on the M2 structure has more advantages than M1 because, to consider the confined aquifer in the model as M1, extra parameters are required which least to a more complicated calibration process.

To appropriately estimate the amount of infiltration, k_v was introduced into M3. The reduction in the amount of infiltration not only improved the simulation of base flow during the recession period, but also captured the peak flow at the beginning of the rainy season during the calibration stage (**Fig. 2.8**). Therefore, M3 provided the best performance for all indices such as NSE, RMSE, and PBIAS for all periods (annual, wet, and dry seasons) among the modified models during the calibration period. For the validation periods, the average annual NSE and RMSE in M3 are quite similar to those in M1 and M2; however, PBIAS is smaller, indicating that M3 improved the simulation of river discharge obtained in M1 and M2.

2.6.4 Prediction uncertainties due to limited data accuracy

Accurate data is necessary to evaluate the performance of the model. One of the reasons for the universally poor performance of the models in 1994 may be the uncertainty in the observed data. From Aug 29–Sep 15, the amount of rainfall in the basin was 69 mm; however, the amount of runoff in the basin reached 290 mm (more than 4 times the rainfall amount) (**Fig. 2.8**). These questionable results suggested underestimation of river discharge and explained the poor performance of the model.

Moreover, the lack of rainfall stations in the study basin may directly affect the performance of the model. By using the nearest neighbor method to distribute the amount of rainfall from 4 stations over the Naluang catchment, we found that only 3 main stations contributed rainfall values over the catchment as input for the model. This may lead to uncertainty in the amount and spatial distribution of rainfall estimation—one of the most important factors in the distributed hydrologic model.

The overestimation in the dry season by all the models may be caused by the AET estimation. In this study, AET was roughly estimated by adopting the difference between annual rainfall and discharge in the basin and using the average of this amount as daily AET input into the model. Consequently, AET might be underestimated during the dry season, which, in turn, may have resulted in overestimation of low flow during the dry season.

2.7 Conclusions

The model that combined the soil layer and the unconfined aquifer component with the estimation of the vertical infiltration based on k_v (M3) best reproduced the river in this study. The NSE values for M3 at the calibration and validation stages were 0.86 and 0.62, respectively, and notably improved the results of the original model (M0).

Therefore, by incorporating the bedrock aquifer into the DHM-KWSS model structure, the estimation of long-term river discharge – especially low flow in the dry season – was explained and improved remarkably. The model improved river discharge estimation and produced a reasonable set of parameters that agreed with physical data sets such as DTB and groundwater storage in the study area. Furthermore, the result of k_v value seemed to be reasonable. Maréchal *et al*. (2004) determined that a horizontal-to-vertical anisotropy ratio for hydraulic conductivity close to 10 (k_h/k_v~10) in the fractured rock aquifer. In this study, k_u/k_v is approximately 70 (consider k_u through the total aquifer depth) which shows a large difference between k_u and k_v. This may be caused by the fact that k_v responded as the infiltration threshold related to the input rainfall intensity (if rainfall intensity is smaller than k_v, all of rain water is infiltrated). Due to data limitations, the input rainfall intensity is estimated by using 24-hour mean rainfall (in which k_v of 1.16×10^{-7} m/s is

approximately 12 mm/24 hours). On the other hand, assuming that the 12 mm of rainfall occurs in 4 hours (assume that this value is the infiltration threshold), the input rainfall intensity might increase 6 times; then k_v values could be increased and k_u/k_v potentially close to 10.

The estimation of rainfall-runoff in the hydrologic model is subject to uncertainties in the accuracy of the data, such as the discharge and rainfall amount measurements, and the number of rain gauge stations in the basin. Furthermore, a better estimation of AET is required to improve long-term river flow prediction in basins with distinct dry and wet conditions. Additionally, further study is required to test the application of the improved model in other basins that have similar or different climatic conditions.

Chapter 3 Integrated reservoir-hydropower-hydrologic model for water resources and energy assessment

This chapter aims to develop a reservoir-hydropower plant model and incorporate it into a distributed hydrological model to evaluate the effect of dam operation on river discharge and power generation. The model was composed of a reservoir power generation and hydrological processes with a concept of a kinematic wave-based assumption. By using the integrated model to assess the impact of hydropower development in the Nam Ngum Basin in Lao PDR, the results indicated that the change of river discharge at the downstream of Nam Ngum 1 reservoir is +218.8% during the dry season and –28.5% during the wet season in the full development scenario from the natural condition. There is no primary effect on the inflow of the Nam Ngum 1 dam by the operation of the under-construction dam. On the other hand, the annual energy product of the Nam Ngum 1 has a minor increase (Meema *et al*., 2020).

3.1 Introduction

The Mekong River Basin (MRB) spans six countries—China, Myanmar, Lao PDR, Thailand, Cambodia, and Vietnam—with approximately 795,000 km2 of the total basin area. The catchment area of MRB in Laos PDR is approximately 25% of the total basin and contributes 35% of the total flow into the river considered as the most contributed country in MRB. Several dams are proposed to develop in the MRB due to rapid regional growth and energy demands from neighboring countries. Asian Development Bank (ADB, 2019) reported that the country's exploitable hydro potential is estimated to be 23,000 MW, and 5,172 MW of hydropower capacity had been operated as of 2017. Hydropower makes a significant contribution to the overall economy of the country. Based on an analysis of projects to be completed by 2030, total hydropower build-out for both domestic and export use will total 16,500 MW or around 70% of estimated potential.

Several studies reported that the development of large-scale hydropower reservoirs, which controls rivers for water use in power generation, can make a significant effect on

water resources. For example, Piman *et al*. (2016) indicated that development of all proposed dams in the major tributaries of the Mekong—Sekong, Sesan and Srepok Rivers (3S)—will significantly change the seasonal flows. It reported that 88.1% increase in dry season flows and 24.7% decrease in wet season flows at the 3S outlet.

The main objective of this study is to develop a distributed hydrologic model combined with a reservoir-hydropower plant process to assess the effect of large-scale hydropower dam operation in various scenarios of dam development on water resources and energy production. The developed model is applied to the Nam Ngum River Basin (NNRB)—a major tributary of the Mekong River—located in Laos PDR, and the effect of dam development in terms of change in river flows regime and power generation in various scenarios are analyzed.

3.2 Description of study area

3.2.1 The Nam Ngum River Basin

The Nam Ngum River Basin (NNRB) is the main Mekong tributary located in the central part of Lao PDR. The basin is one of the most important in Lao PDR, in terms of size (approximately 16,800 km^2 and 7% of the country area). Annual flows contributing to the mainstream at the Mekong River is approximately 14%, which is approximately 40% of country's contribution to the Mekong River flow. The headwaters of the Nam Ngum river are at an elevation of 2,800 m in the northeast of the basin and heads southwards for 420 km to its outlet at the Mekong River. Along the downstream of the Nam Ngum 1 reservoir, the Nam Ngum river has a gentle slope as it meanders along its course. The Vientiane Plain extends from each bank, covering an area of about 2,000 km^2 at elevations of 160 m to 180 m. During the wet season, the plain is influenced by flooding on the floodplain.

The average annual discharge of the Nam Ngum river to the Mekong is approximately 21,000 million cubic meters (mcm). The flows are very seasonal with the low flow from March to April and high flow from August to September. The climate of the Nam Ngum Basin is largely tropical with a distinct wet season from June to October and a dry season for the rest of the year. The highest temperature is in March and April, where average

temperatures range from 30°C to 38°C depending on location and altitude. The lowest temperatures occur between November and February on average of 15°C at higher elevations—Xiengkhuang Plateau. The mean annual rainfall of the basin is approximately 2,000 mm which ranges from 1,450 mm to 3,500 mm across the basin. The highest amount of rainfall occurs nearby the Vangvieng area and gradually decreases northeastward to the Xiengkhuang vicinity.

3.2.2 Water resources development

There are currently six hydroelectricity related schemes located in the NNRB with total reservoir storage of approximately 15,200 mcm and a combined electricity generation capacity of 990 MW. The first hydropower station in the basin is the Nam Ngum 1 (NN1) reservoir developed in 1971 with an existing installed capacity of 155 MW. The Nam Ngum 1 scheme—the largest among the six hydropower schemes—has a storage capacity of 7,010 mcm. The Nam Song diversion project (NS_DV) operated in 1996, diverts approximately 3650 mcm/year of water from the Nam Song River into the Nam Ngum 1 reservoir. The other two hydropower stations—Nam Ngum 2 (NN2) and Nam Lik 1/2 reservoirs—started operation in 2011 with the installed capacity of 615 MW and 100 MW respectively. The Nam Ngum 2 is the major power station located upstream of the NN1 reservoir with the largest power capacity and the second largest in storage volume of 6270 mcm (among the dams in the basin). In 2012, the Nam Ngum 5 (NN5) hydropower station started operation with an installed capacity of 120 MW. The dam is located on the tributary of the Nam Ngum River—Nam Ting River. In addition, the Nam Leuk (NL) and the Nam Mang hydropower dams, located outside of the Nam Ngum Basin which started operating in 2000 and 2005 respectively, diverting water from the Nam Leuk and Nam Mang Basins into the NN1 reservoir and the Vientiane plain, respectively.

As the NNBR has a significant hydropower potential with high rainfalls and large differences in elevation. An additional four dams are at various stages of development ranging from planning to construction. In the case that all dams are constructed, bringing the total power generation capacity of 1,900 MW and the total storage volume of 17,200 mcm which is approximately 80% of the total annual river discharge of the Nam Ngum River. The location of hydropower stations is shown in **Fig. 3.1** and the list of hydropower stations in the basin is summarized in **Table 3.1**.

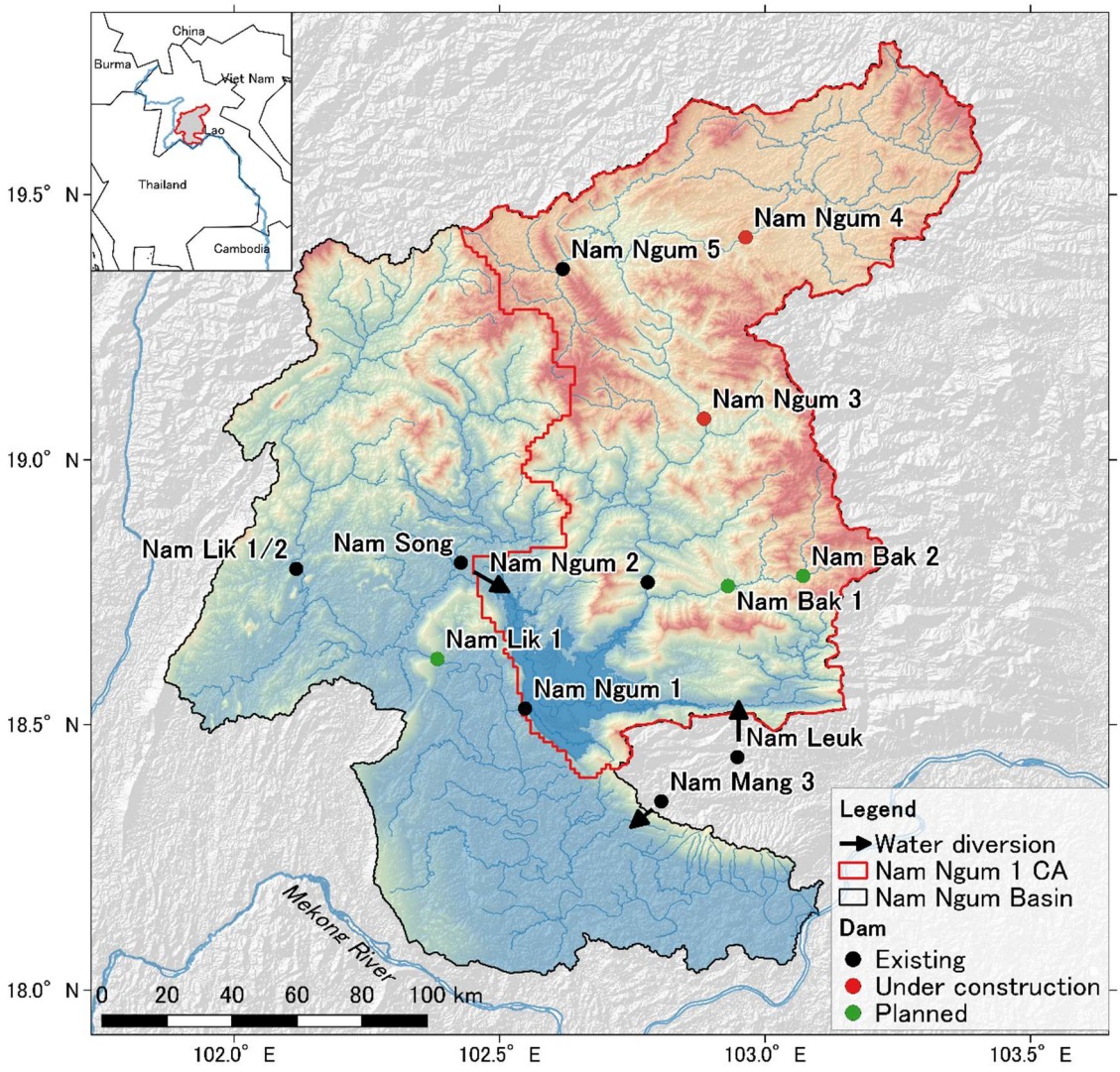

Fig. 3.1 Location of dams in the Nam Ngum River Basin.

Table 3.1 List of hydropower stations and other related water resources project in the basin.

Project	Status	Catchment area (km^2)	Annual inflow (mcm)	Storage at full supply (mcm)	Effective storage (mcm)	Installed capacity (MW)
Within the basin						
Nam Ngum 1	E	8460	12047	7010	4714	155
Nam Ngum 2	E	5640	6270	6774	2617	615
Nam Ngum 3	UC	3888	3090	1407	1070	440
Nam Ngum 4	UC	1748	1512	85.6	72.1	230
Nam Ngum 5	E	483	719	314	72.4	120
Nam Lik 1/2	E	1993	2690	1095	na	100
Nam Lik 1	P	5050	5786	61.3	na	61
Nam Bak 1	P	597	750	250	na	115
Nam Bak 2	P	320	400	190	na	68
Nam Song	E	1303	3072	14.2	na	-
Outside the basin						
Nam Mang 3	E	65	na	45	na	40
Nam Leuk	E	274	438	154	na	60

3.3 Modeling approach

The main model component can be divided into two parts—hydrologic process and reservoir-hydropower plant process—as shown in the schematic drawing of the integrated model in **Fig. 3.2**. The description of the model development is explained as follows.

3.3.1 Hydrologic process

The improved 1K-DHM that incorporates the bedrock aquifer into a slope component resulted better in long-term river discharge simulation is selected for the study. A model is explained by (Meema and Tachikawa, 2020).

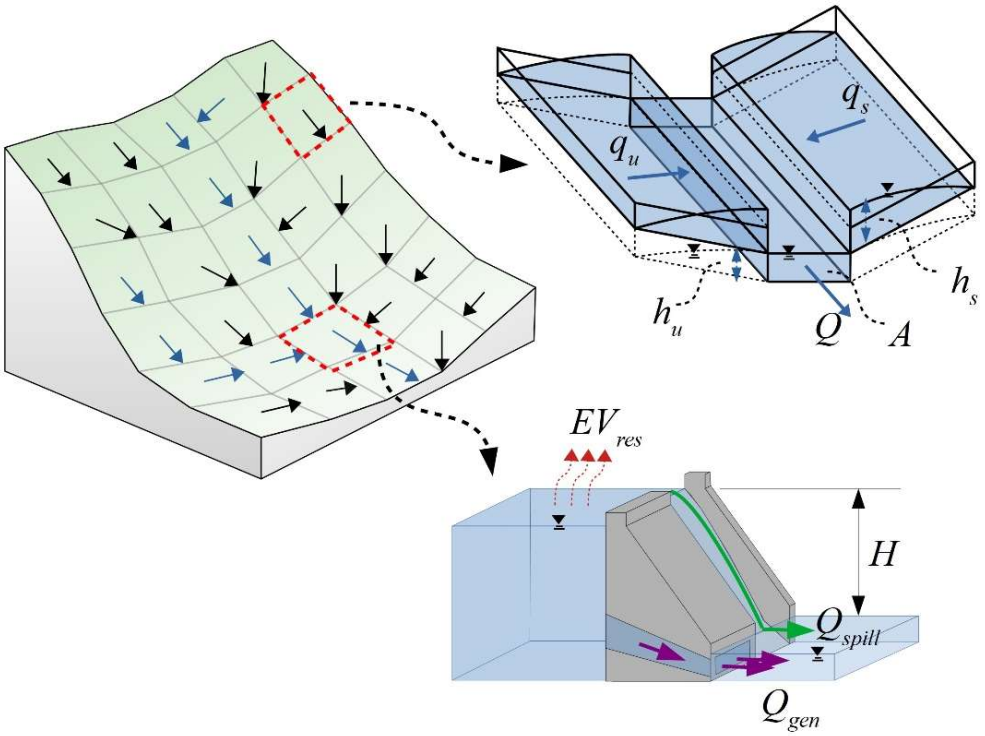

Fig. 3.2 Schematic drawing of the integrated model.

3.3.2 Reservoir-hydropower plant process

A reservoir-hydropower plant process is the process of reservoir routing that the release discharge to downstream grid is determined by using the reservoir guide curve method (see section 3.3.3). Release is specified for each time step, as well as reservoir level and spillage. The reservoir storage is simulated using the law of mass balance as below:

$$\frac{dS}{dt} = Q_{in} - (Q_{gen} + Q_{spill}) - S_{losses}/dt \tag{3.1}$$

where S is the reservoir storage; t is the time; S_{losses} is the reservoir storage losses; Q_{in} is reservoir inflow; Q_{gen} is the generated discharge through the turbine; and Q_{spill} is the spilled discharge expressed as below:

$$Q_{spill} = \begin{cases} 0, & S_{t+1} \leq S_{max} \\ S_{max} - S_{t+1}, & S_{t+1} > S_{max} \end{cases} \tag{3.2}$$

where S_{max} is the reservoir storage at the full supply level (*FSL*); S_{t+1} is the storage at the end of the time step; and Q_{gen} is estimated by using the release decision model based on the multiple zones of reservoir and their operating rules (see section 3.3.3). This process provides the target of energy generation (E) that evaluate the release to get the reservoir water level to the guide curve (rule curve) at the end of the time step as much possible based on the starting reservoir water level and current inflow (Q_{in}). Then, Q_{gen} is calculated as follow.

$$Q_{gen} = \frac{E}{\eta \cdot \rho \cdot g \cdot H} \tag{3.3}$$

where E is generated energy in the time step; η is turbine efficiency; ρ is water density; g is gravitational acceleration; and H is hydraulic head which can be calculated by

$$H = WL - TWL - H_{losses} \tag{3.4}$$

where WL is current reservoir water level obtained using the relationship between reservoir elevation−storage ($WL = f(S)$); TWL is downstream tailwater level; and H_{losses} is the hydraulic losses.

The reservoir storage losses (S_{losses}) due to reservoir surface evaporation can be expressed as;

$$S_{losses} = EV_{res} \cdot A_{res} \tag{3.5}$$

where EV_{res} is reservoir evaporation rate and A_{res} is the current reservoir surface area in which $A_{res} = f(WL)$.

3.3.3 Defining reservoir operation

The basic of reservoir operation can be described by a seasonal variation of target reservoir level which calls guide curve (rule curve). It is proposed as a guideline to determine the reservoir release with the basic objective of regulation that the release will increase when the reservoir level is above the guide curve and the release will decrease when the reservoir level is below the guide curve.

To simulate the reservoir operation using numerical modeling, determination of water release is required at each time step (see **Eq. 3.1**). For this purpose, the release decision scheme called “multiple zones of reservoir operation” is applied.

The multiple zones of reservoir operation consist of guide curves, zones and rules. "Zones" are operational subdivisions of the reservoir. Each zone is separated by a curve called zone separation curve (can have more than one curve for any reservoir). The full supply level (FSL) and minimum operation level (MOL) are considered as the zone separation also.

"Rule" is used to represent the target and constraints of release which are applied to each zone of the reservoir to define the release decision when the current reservoir level is within each zone.

The purpose of "guide curve" is to use to determine the release to get the target reservoir level at the end of the time step as much as possible based on the starting reservoir water level and current inflow of the time step. The guide curve can be used as the zone separation curve also.

3.4 Applying the integrated model to NNRB

3.4.1 Input precipitation

The daily observed data of rainfall from the stations over the NNRB were collected to create the gridded rainfall intensity using the nearest neighbor method. The summary of annual rainfall for each rain station is presented in **Table 3.2**. From 2006 to 2009, Vangvieng and Naluang are not available and Xaysomboun is incomplete in 2007.

Table 3.2 Summary of annual rainfall in study basin.

Station	Hinheup	Vangvieng	Kasy	Naluang	Xaysomboun	Xienkhuang
2002	1387.5	3974.5	1349.3	3357.3	2626.7	1862.3
2003	1278.6	3188.6	1085.5	2110.8	2694.3	1090.3
2004	2192.3	4104.9	1016.9	2480.1	2847.1	1371.9
2005	2603.9	4428.2	1140.0	2863.3	3337.7	1736.8
2006	1946.8		2210.9		2725.6	1364.3
2007	2528.9		2559.9			1001.5
2008	2155.6		3433.0		2946.6	1658.4
2009	2307.4		1983.8		2423.6	1317.9
2010		4213.8	2940.5		2588.0	1400.8
2011		4496.2	2844.0		3269.1	1581.7
2012		3412.5	2742.7		2393.9	1557.9
2013		4075.6	2549.3		3005.1	1614.8

3.4.2 Actual evapotranspiration

For long-term river flow simulations, actual evapotranspiration (AET) is required; however, however, it is the most difficult parameter to measure when calculating a site's water balance which is a function of precipitation, temperature, solar radiation, soil water storage, wind, canopy and understory interception, and growth rates (Kolka and Wolf, 1998). For this study, assuming that the error in the water balance calculated from AET is equal to zero, the annual AET (E_a) shown in **Fig. 3.3a** is estimated as follow;

$$E_a(i) = P(i) - Q(i) \tag{3.6}$$

where i is year; P is annual average basin rainfall; and Q is the annual river discharge (runoff depth) at the basin outlet.

To estimate monthly change of AET, the historical data set in a database for Policy Decision making for Future climate change (d4PDF) (Mizuta *et al*., 2017) was used. A d4PDF is a data set simulated from a global atmospheric model, which include the estimation of the total amount of water transferred from the surface into the atmosphere. The monthly average ($\bar{e}_m$) of a combination of water transpiration from soil (*TS*), evaporation on soil (*ES*) and evaporation on leaf (*EL*) from d4PDF data set with 60-year (1951−2010) data and 100 ensembles is used to estimate the seasonal variation of the

reference annual AET (E_a). The monthly AET (e_a) for each year shown in **Fig. 3.3b** can be calculated as follow.

$$e_a(i,j) = \alpha(i)\bar{e}_m(j) \tag{3.7}$$

where i is year; j is month and $\alpha(i) = E_a(i)/\bar{E}_m$ in which $\bar{E}_m = \sum_{j=1}^{12} \bar{e}_m(j)$.

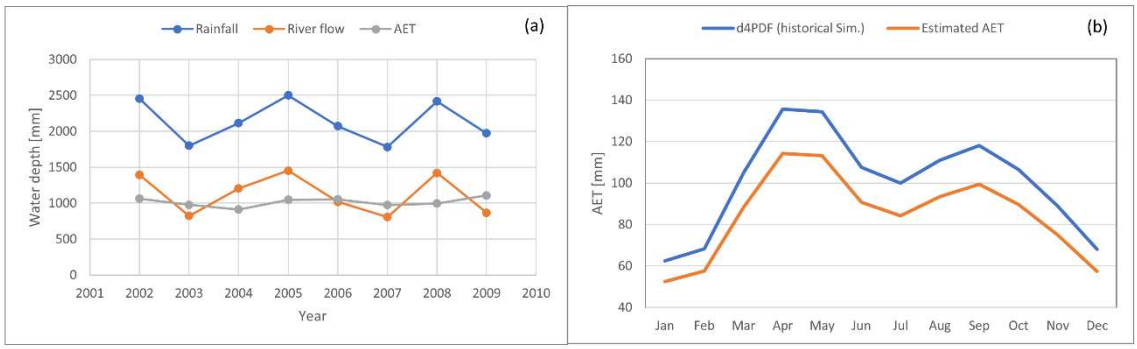

Fig. 3.3 (a) long-term estimated AET (b) comparison of mean monthly AET estimation

3.4.3 Selection of the large-scale dam and reservoir input data

In this study, we focused on the impact of large-scale hydropower reservoirs. Piman *et al*. (2016) defined the large-scale hydropower projects in tributaries of the Mekong with installed capacity above 300 MW and/or active storage over 1000 million cubic meters (mcm). Therefore, two existing dams—NN1 and NN2—and a proposed dam—Nam Ngum 3 (NN3)—met the criteria. The general reservoir data in **Table 3.1** is collected as the reservoir model input. The reservoir guide curve for NN1 is collected from JICA report (JICA, 2010). For NN2, this data is not available, so the reservoir guide curve is estimated based on the estimation of reservoir water level as shown in **Fig. 3.4**. The operation rule for each operation zone is estimated based on the operating historical record during the calibration period. For the future dam with no data record, the standard operation in this region is applied with the criterial that a reservoir tries to keep water in the wet season and releases in the dry season with 8-hour of minimum operation.

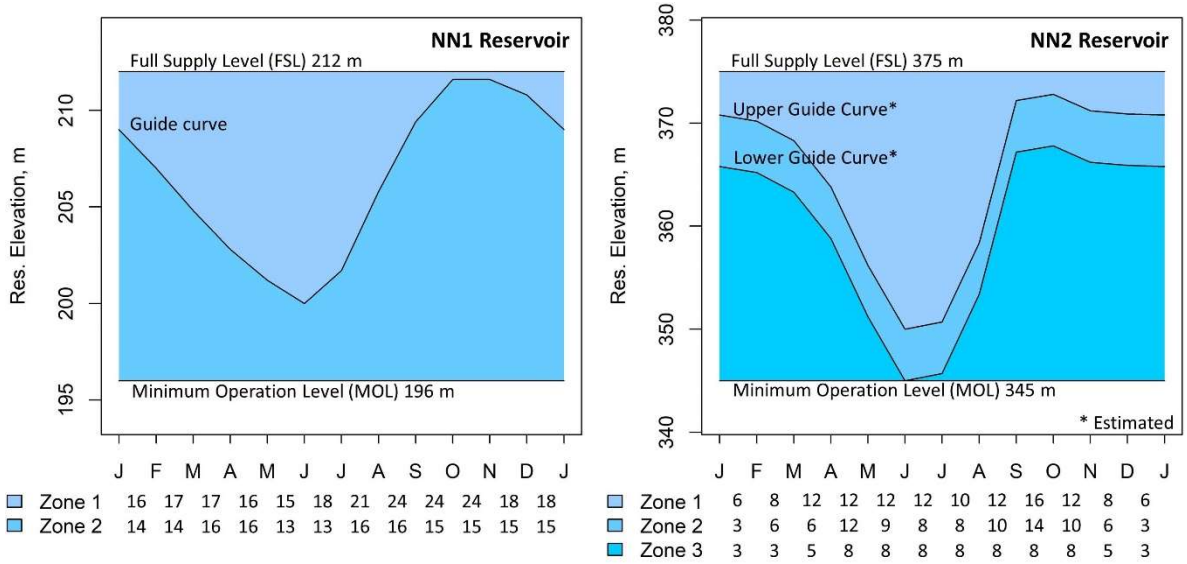

Fig. 3.4 Model input for multiple zones of reservoirs operation.

3.4.4 Reservoir evaporation losses

Winter (1981) suggests that one of the main approaches to estimate the evaporation of a water body is to use the pan coefficient. For this study, the evaporation from the reservoir (EV_{res}) can simply estimate by the following equation.

$$EV_{res} = k_p \cdot PEV \tag{3.8}$$

where k_p is pan coefficient (0.7), PEV is the potential evaporation.

Due to no pan measurement at the reservoirs, the potential evaporation of the basin (PEV_{basin}) is used in which estimated by adopting the mean monthly pan measurement at reference station (PEV_{ref}) with a monthly delta (Δ) of estimated potential evaporation (Thornthwaite, 1948) between using mean basin temperature ($\overline{PEV}^{TW}_{basin}$) and mean grid temperature ($\overline{PEV}^{TW}_{ref.grid}$) at the reference station extracted from the d4PDF historical data set (60-year ×100 ensembles). The mean monthly potential evaporation of the basin can be calculated as follow.

$$\overline{PEV}_{basin}(j) = \Delta(j) \cdot \overline{PEV}_{ref}(j) \tag{3.9}$$

where j is 1, 2, 3 …, 12 and

$$\Delta(j) = \overline{PEV}^{TW}_{basin}(j) / \overline{PEV}^{TW}_{ref.grid}(j) \quad (3.10)$$

For this study, the mean monthly pan measurement at Xiengkhuang station located in the upper part of the basin during 1989−1997 is used as reference data. **Fig 3.5b** presents the comparison of potential evaporation between the reference station (Xiengkhuang) and the estimation. The result showed that the estimation of basin averaged potential evaporation has a higher trend than the reference. This can describe using **Fig. 3.5a** that shows the mean temperature of the basin average higher than the reference. Furthermore, the estimation of reservoir evaporation quite agrees with the actual evaporation from the reservoirs in Thailand—considered as a similar climatic condition with the study area—in which the daily average range from 2.8 to 3.6 mm/day (Rittima *et al*., 2013). The estimated daily reservoir evaporation of 2.4 mm/day for NNRB shows a minor lower than the reservoirs in Thailand where the mean temperature is approximately 5−7 ˚C higher than the study area.

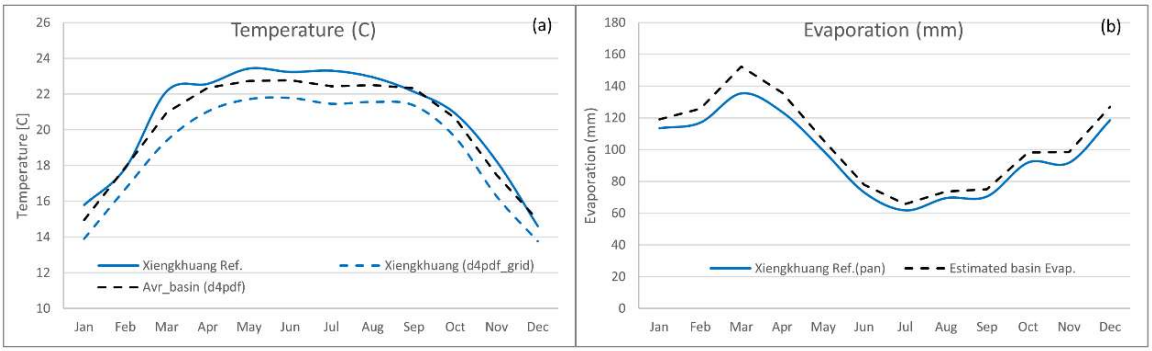

Fig. 3.5 (a) comparison of temperature (b) comparison of potential evaporation.

3.5 Model calibration and validation

The model setup with calibration and validation processes is required before applying the model to assess the impact of dam operation on water resources. The process can be divided into two parts as follow.

3.5.1 Hydrologic model part

To calibrate and validate the model for estimation of river discharge to the reservoir, the model is set as a natural condition (without dams and water diversion). The natural inflow estimated from the record of the NN1 (subtracted by diversion amount) is used to evaluate the result of the model. According to data availability, the period of 2002−2005 is selected to be a calibration period and 2006−2009 is selected to be a validation period. For the calibration process, the SCE-UA algorithm was applied to optimize the model parameters by searching for the parameters with the smallest root mean square error (RMSE). The design range of parameters in this study and the result of the optimized parameter set are shown in **Table 3.3**.

Table 3.3 The optimized hydrologic parameter set.

Parameter (Units)	Opt. parameter	Parameter range
n_s ($m^{-1/3}/s$)	0.173	0.05 − 0.5
k_a (m/s)	0.002	0.0005 − 0.005
d_a (m)	2.060	0.8 − 2.25
d_m (m)	1.831	
β (-)	27.03	9 − 30
k_u (m/s)	9.83E-05	5.0E-05 – 5.0E-04
d_u (m)	1.334	0.8 − 4.0
k_v (m/s)	1.79E-07	1.0E-07 − 5.0E-07

3.5.2 Integrated model part

The calibration period for reservoir operation of NN1 is 2002−2005. The operation record of this period is adopted to estimate the operation rule for each month in each zone of the reservoir; then, apply the same rules to validate the model. The multiple zones of the reservoirs and their operating rules (operation hour) are shown in **Fig. 3.4**. For the validation process, we divide the process into two stages due to the basin condition. The first validation period is 2006−2009 that refers to the stage of the basin before developing the NN2 reservoir. The second validation period is 2012−2013 that refers to the current stage of the basin. The description of simulation periods for calibration and validation of the integrated model are summarized in **Table 3.4**.

Table 3.4 Description of simulation periods for calibration and validation of the integrated model.

Period	Year	Dams	Remark
Calibration	2002 - 2005	NN1+NS_DV+NL	Before NN2 operation
Validation 1	2005 - 2009		
Validation 2	2012 - 2013	NN1+NS_DV+NL+NN2	Existing condition

3.6 Model performances results

3.6.1 Hydrologic model part

A comparison of river flow into the NN1 in **Fig. 3.6** indicated a good agreement between the simulation and the reference river discharge. The improved 1K-DHM performed well in a long-term river discharge simulation with the NSE and RMSE are 0.977 and 51.5 m^3/s respectively; and PBIAS is 2.4% for the calibration period. For the validation period, the NSE, RMSE, and PBIAS are 0.912, 81.2 m^3/s, and 5.2% respectively. The improved 1K-DHM is well reproducing a long-term river discharge simulation with a reasonable parameter set comparing with the available physical data in the basin.

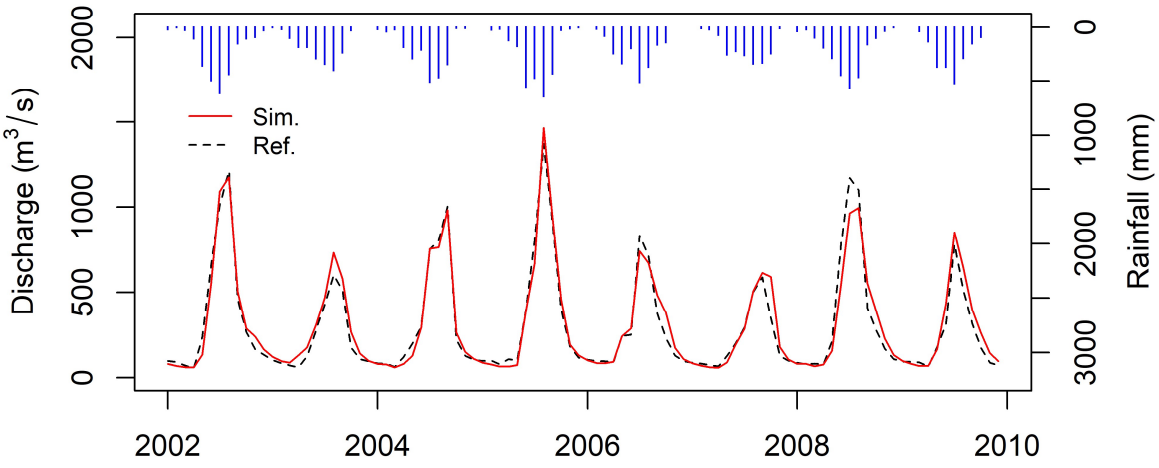

Fig. 3.6 Comparison of river discharge at the NN1 dam in natural condition between simulation and reference.

3.6.2 Integrated model part

A comparison of inflow to NN1, reservoir water level, generated energy and regulated flow between simulation and data record is shown in **Fig. 3.7** and the performances are summarized in **Table 3.5**. Even though the model results well in a simulation of reservoir inflow with PBIAS of 1.8% during the calibration period. However, an error in the volume of inflow affects other parameters. For example, in 2003, the overestimation of inflow results in an overestimation of water level in the reservoir because the reservoir requires larger storage to keep a larger amount of water. The higher level of reservoir results in an overestimation of released discharge for power generation leading to an overestimation of energy product as shown in **Fig. 3.7**. According to this reason, reducing an error of the hydrologic process can provide a better result of reservoir simulation.

The model results well in a simulation of the reservoir water level. For the NN1, the historical operation quite follows the reservoir guide curve; therefore, the simulation that tries to release discharge to keep the reservoir level at the guide curve target elevation as much possible at the end of time step provides a small RMSE of 1.0 m during a calibration period and lower than 1.4 m during validation periods It is very hard to capture the release

decision made by operators and current demands. On the other hand, the multiple zones model provided quite well result in a simulation of energy generation with the PBIAS of 3.5% during a calibration period and lower than 6.6% during validation periods. The model provided well performances with an agreement between the simulation result and the operation record. Thus, we consider that the model is applicable to simulate the reservoir operation and can be applied to access the impact of dam operation in various scenarios.

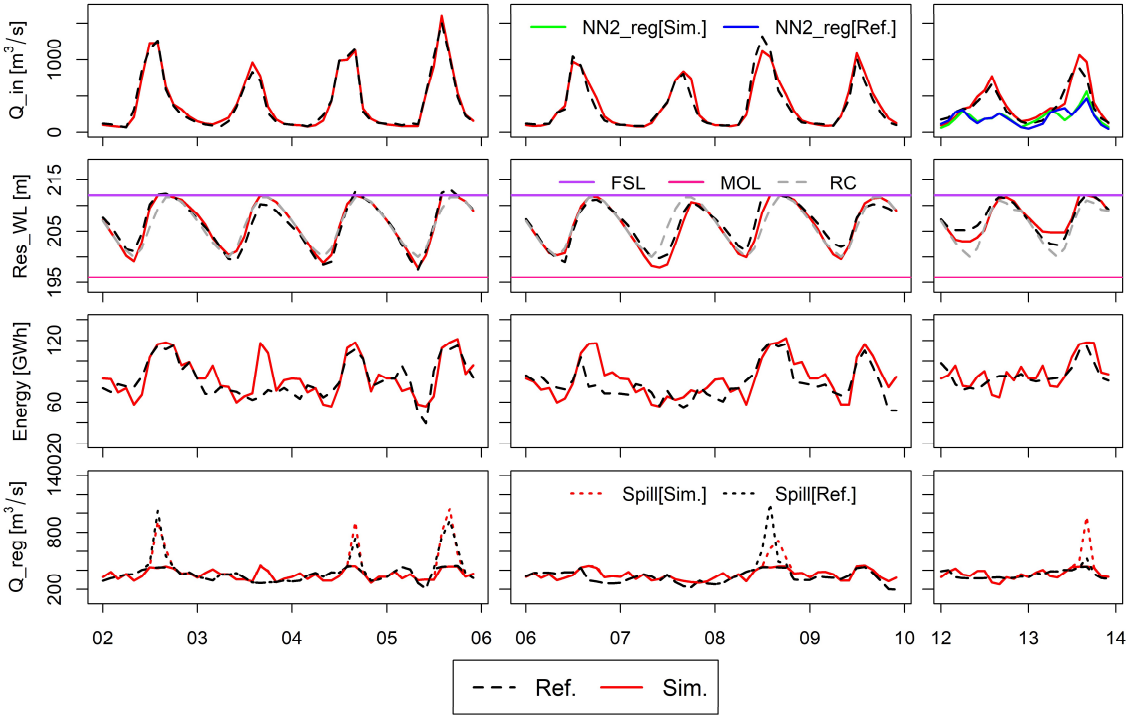

Fig. 3.7 Comparison of inflow (Q_in), reservoir water level (Res_WL), generated energy (Energy) and regulated flow (Q_reg) between simulation (Sim.) and reference data (Ref.) of the NN1 reservoir. For the horizontal axis, "02−06" is calibration period (2002−2005), "06−10" is validation period 1 (2006−2009), and "12−14" is validation period 2 (2012−2013). (RC: rule curve, FSL: full supply level, MOL: minimum operation level, NN2_reg: regulated discharge by NN2 and Spill: spill discharge through the NN1 spillway)

Table 3.5 Model performances of reservoir simulation for the NN1 power station (Q_in: reservoir inflow, Res_WL: reservoir water level, Energy: generated energy and Q_reg: regulated flow).

Variables	Calibration		Validation 1		Validation 2	
	RMSE	PBIAS	RMSE	PBIAS	RMSE	PBIAS
Q_in (m^3/s)	51.9	1.8	82.3	4.9	90.3	8.0
Res_WL (m)	1.0	0.1	1.2	-0.2	1.4	-0.1
Energy (GWh)	13.9	3.5	14.7	6.6	10.3	2.5
Q_reg (m^3/s)	69.2	1.7	99.3	4.3	100.4	8.1

3.7 Simulated scenarios

To access the effect of dam development in various stages in the study basin, the simulation scenarios can be defined as below. The summary of simulation scenarios is presented in the **Table 3.6** and the map showing dam location for each scenario is presented in **Fig. 3.8**.

3.7.1 Baseline scenario (BL)

The model is set to simulate the river flows in a natural condition (unregulated river flow) in which there are no dams and water diversion stations in the simulation.

3.7.2 Individual NN1 scenario (ID)

The simulation is considered only the NN1 reservoir. This scenario is referred to as the stage of the basin before developing the major water diversion into the NN1 reservoir.

3.7.3 NN1 and diversion scenario (DV)

The simulation is considered the NN1 reservoir including the water diversion from other river system (NL and NS_DV) into the NN1 reservoir. This scenario is referred to as the stage of the basin before developing the other major hydropower stations.

3.7.4 Existing dam scenario (ED)

This scenario is referred to as the current stage of the basin in which the simulation includes NN1 (with NL and NS_DV diversions) and NN2.

3.7.5 Future dam scenario (FD)

This scenario includes existing dams—NN1 (with NL and NS_DV diversions) and NN2—and a proposed large-scale dam (NN3).

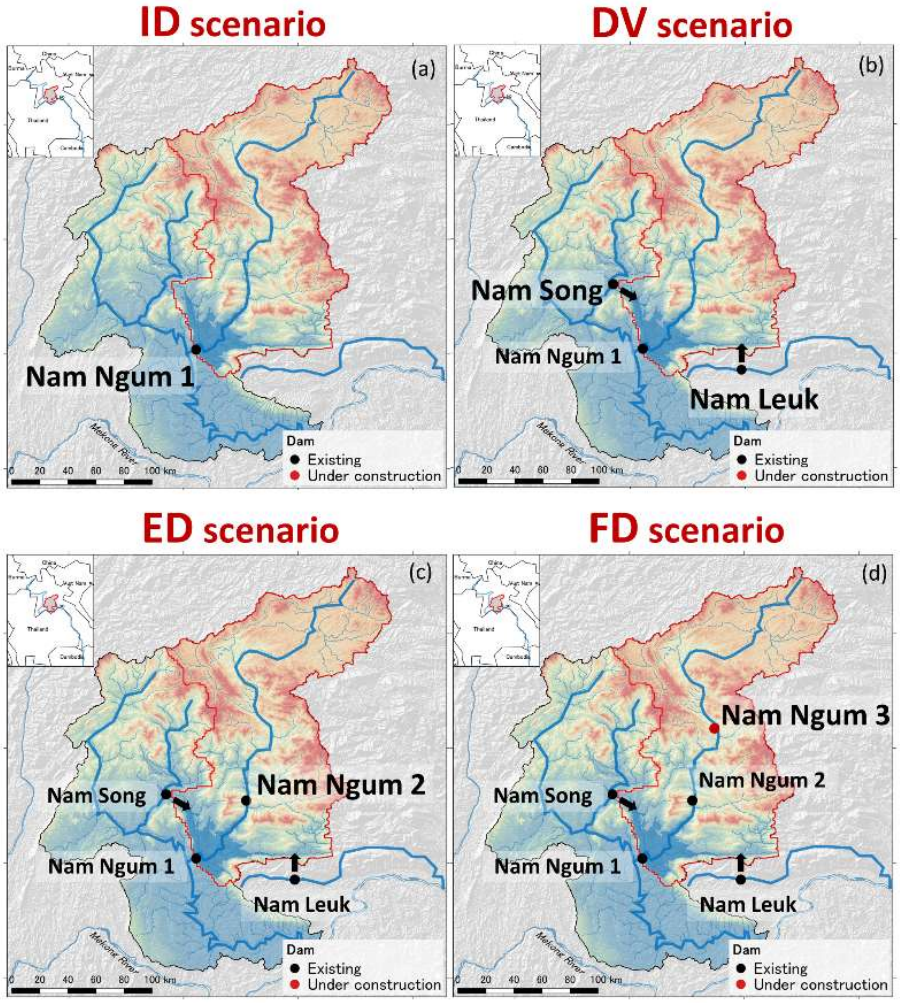

Fig. 3.8 Dam location for each scenario (a) for ID, (b) for DV, (c) for ED and (d) for FD.

Table 3.6 Summary of simulation scenarios.

Scenarios	Abbreviation	Dam	No. Dam	Purpose
Baseline	BL	-	0	Natural condition
NN1 individual	ID	NN1	1	Individual NN1
River diversion	DV	NN1+NS_DV+NL	3	Effect of diversion
Existing Dams	ED	NN1+NS_DV+NL and NN2	4	Effect of NN2
Future Dams	FD	All	5	Effect of proposed dam

3.8 Results and discussion on impact of hydropower development

Regarding to the simulation scenarios as shown in section 3.7, the results of simulation can be summarized in **Table 3.7**. The comparison of NN1 dam inflow (Q_in), Reservoir water level (Res_WL), generated energy (Energy) and regulated discharge (Q_reg) in different scenarios was shown in **Fig. 3.9**.

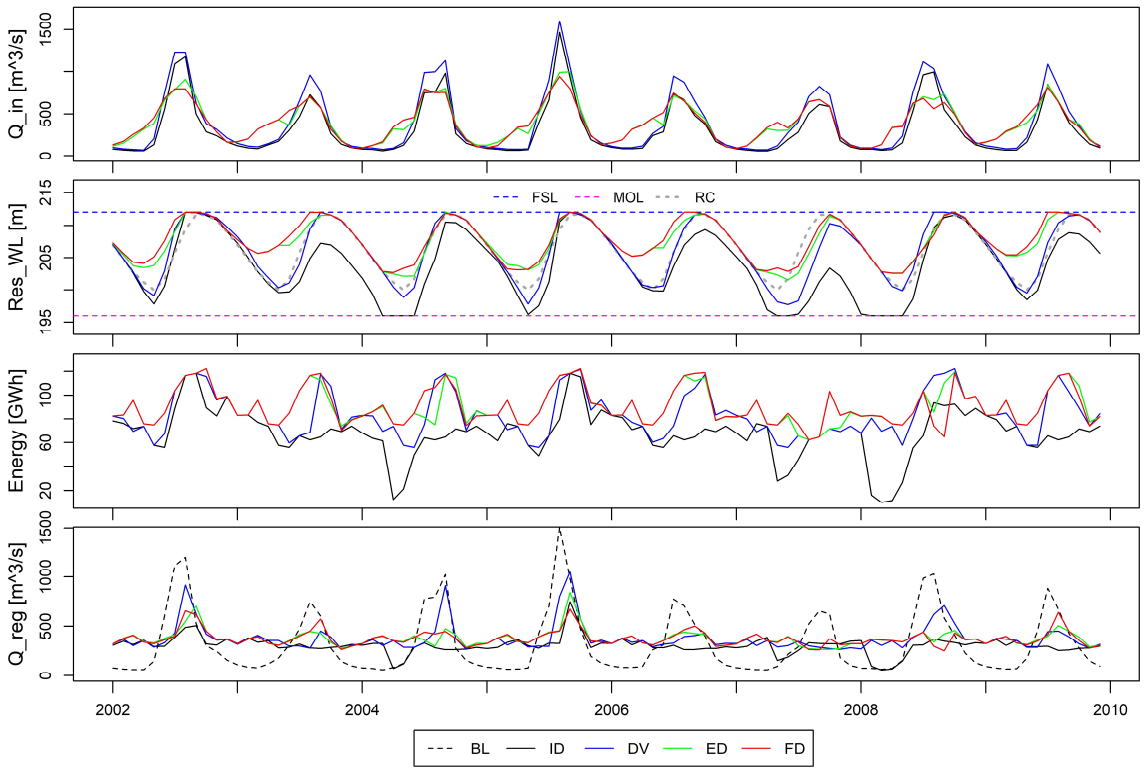

Fig. 3.9 Comparison of the NN1 reservoir simulation among the simulated scenarios.

Table 3.7 Summary of simulation results for various scenarios (wet season is June−October and dry season is November−May).

Scenarios	Q_in (m^3/s)			Energy (GWh)			Q_reg (m^3/s)			Spill (mcm)	Mean WL (m)
	Wet	Dry	Annual	Wet	Dry	Annual	Wet	Dry	Annual		
BL	592.7	108.9	310.5	-	-	-	592.7	108.9	310.5	-	-
ID	592.7	108.9	310.5	355.5	462.1	817.6	325.5	296.0	308.3	160.8	203.8
DV	740.4	134.4	386.9	459.0	542.8	1001.7	446.4	332.8	380.1	920.9	206.2
ED	614.2	224.5	386.9	498.7	582.0	1080.6	423.0	347.6	379.0	346.9	207.5
FD	603.7	233.6	387.8	503.9	581.8	1085.7	425.2	347.2	379.7	400.5	207.8

3.8.1 Effect of river diversion (DV)

The impact of river flow and energy of the NN1 due to river diversion is assessed by comparing the simulation results between DV and ID (only NN1). The diversion record in a period of 2002−2009 from the NS_DV and NL with the mean annual of water diversion of 3650 mcm and 350 mcm respectively is used in this simulation. The result of the simulation in **Table 3.7** presents that the amount of water diversion provides a primary increase in water budget for the NN1 reservoir (24.6% increase in the annual inflow) and provides a significant increase in the energy product (22.5% increase in the annual energy product). Diverted water also changes the seasonal river discharge of the Nam Ngum River. 12.4% increase during the dry season and 37.2% increase during the wet season in the downstream of the NN1 reservoir are found in this study.

3.8.2 Effect of the NN2 dam (ED) compared to DV

The NN2 dam has a large reservoir capacity with effective storage of 2,994 mcm, which can regulate 42% of the annual inflow. As shown in **Fig. 3.7**, the inflow to NN1 becomes much stable (seasonal variation is decreased) due to the regulating capability of the NN2. **Table 3.7** indicates that the mean inflow to the NN1 reservoir is increased by 67.1% during the dry season and decreased by 17.0% during the wet season. The annual energy product of the NN1 dam increases by 7.9% due to a high potential of power generation throughout the year.

The spilled water of NN1 decreases by 62.2% due to a decrease of inflow to the NN1 from the upstream during the wet season. The reduction of spilled water may conclude that the downstream flood risk is reduced also. Furthermore, the risk of water shortage is

reduced compared with the scenarios without NN2 especially in the drought year; for example, in 2007, as shown a comparison of the reservoir water stage for various scenarios in **Fig. 3.7**.

3.8.3 Effect of proposed dam (FD) compared to ED

The result of the simulation shows that there is no primary effect on the planed NN3 operation to the NN1 because its effective storage is small comparing to the total inflow of the NN1 reservoir (effective storage is 8.9% of NN1 total inflow). Furthermore, the major hydropower stations are already developed which regulate most of the river flows in the basin. On the other hand, the inflow to the NN1 reservoir has a minor increase in the dry season (4.0% increasing) and decreasing in the wet season (1.7% decreasing), the annual energy production has a minor increase (0.5% increase in the annual energy product) as shown in **Table 3.7**.

3.9 Conclusions

The integrated model has been developed to assess the effect of dam operation in the Nam Ngum River Basin, Laos PDR by combining the hydrologic and reservoir-hydropower processes. The integrated model performed well in calibration and validation processes that the result agrees with the actual operation record. By using the model to assess the impact of hydropower development in the NNRB, the results indicated a primary change in both annual and seasonal river discharge due to flow regulation by the cascade dams in full development (FD) compared to natural river flow condition (BL).

The regulated flow by the upstream cascade dams also results in the benefits in terms of energy production of the NN1 power station. Increasing river flow during the dry season has the benefits for the potential of water use for other purposes such as irrigation, domestic and industrial consumption with consideration to the effect of the change of water and sediment on the environment. The uncertainty of reservoir operation due to climate change in the NNRB will be implemented in further study.

Chapter 4 Uncertainty assessment of water resources and long-term hydropower generation using a large ensemble of future climate projections

This chapter aims to assess the sensitivity of the Nam Ngum 1 reservoir in Laos PDR to the uncertainty of water resources driven by a combination of climate change and upstream cascade dam development using a large ensemble of future climate projections. The results of study present that the precipitation projections of the basin under a 4 degree increase scenario vary in the range of −9.6% to +6.9% compared to the historical observed precipitation (present climate). The impacts of changing climate on hydropower resources were investigated. Based on a combined effect of climate change and upstream cascade dam development, the projected inflow of the Nam Ngum 1 reservoir at the full development stage will change from −16.0% to +6.5%, which resulted in a large range of annual energy production changes from −18.8% to +2.8% compared to the current condition (present climate and existing dam stage). Furthermore, water losses from the reservoir due to water discharge from spillway for extreme floods and evaporation are expected to increase when increasing temperature, which will lead to a loss in energy production. Our study indicated that the operation of hydropower should be adapted to the effect of climate change. This information will be used for stakeholders to propose the strategies of water resources management (Meema *et al*., 2021).

4.1 Introduction

The Mekong flows southward for approximately 4,800 km from its source (Tibetan Plateau) through China, Myanmar, Lao PDR, Thailand and Cambodia before entering the South China Sea via a complex delta system in Viet Nam with an approximately 795,000 km^2 of the total basin area. The Mekong ranks 10th amongst the world's great rivers based on mean annual flow (MRC, 2005). Rapid regional growth and energy demands from neighboring countries have prompted plans to build numerous dams along the mainstream and tributaries of the Mekong River (Kummu and Varis, 2007).

The catchment area of MRB in Laos PDR is approximately 25% of the total basin and contribute 35% of total flow into the river considered as the most contributed country in the Mekong River Basin (MRB) (MRC, 2005). The country has benefit in topography and water resources which provide a significant potential of hydropower development. ADB (2019) reported that the country's exploitable hydro potential is estimated to be 23,000 MW, and 5,172 MW of hydropower capacity had been operated as of 2017. Based on an analysis of projects to be completed by 2030, total hydropower build-out for both domestic and export use will total 16,500 MW or around 70% of estimated potential. However, the large variations of changes in hydropower generation across regions and even within regions due to the effect of climate change were reported (Hamududu and Killingtveit, 2012). The uncertainty of future hydropower generation is derived not only by the current river flow inter-annual variation but also the change in long-term river flow availability due to the effect of climate change (Blackshear *et al*., 2011).

Several of previous studies assessed the impacts of climate change on hydropower generation at a global scale (Hamududu and Killingtveit, 2012; van Vliet *et al*., 2016), continental-scale (IEA, 2020; Lehner *et al*., 2005), national scale (Fan *et al*., 2020; Grijsen and Patel, 2014) and basin-scale (Beyene *et al*., 2010; Kopytkovskiy *et al*., 2015; Mohor *et al*., 2015; Shrestha *et al*., 2016). Some studies have been conducted on the impact of climate change on hydropower generation related to the Mekong River Basin. Mekong River Commission (MRC, 2018) reported that the percentage change in the average energy production on hydropower in Laos PDR for the climate change scenarios during 2060 (RCP2.6−8.5) compared to the baseline ranges from +7.5% to −31.1%. Piman *et al*. (2015) reported that there a minor decrease in energy production of hydropower in the Mekong tributaries—Srepok, Sesan and Sekong (3S) basins—during the full development level driven by A2 and B2 emission scenarios (MPI_ECHAM4) compared to the baseline scenario.

However, the significant uncertainty in hydropower production assessment is associated with the variability of precipitation projections (Hamlet *et al*., 2010) resulted from the use of different general circulation models (GCMs). The model projections are affected by a range of uncertainties including emissions scenario uncertainty, internal variability of the climate system, and model response uncertainty (Hawkins and Sutton,

2009). The quantification of all aspects of model uncertainty requires multi-model ensembles, ideally as a complement to the exploration of single-model uncertainties through perturbed physics ensembles experiments (Tebaldi and Knutti, 2007). Several studies applied a large-ensemble to improve the uncertainties of future river discharge projections (Ayers *et al*., 2016; Mohammed et al., 2015; Thompson *et al*., 2017). Carvajal *et al*. (2017) use a large-ensemble (CMIP5) to assess the sensitivity and improve the reliability of hydropower generation to uncertain water resource availability driven by future climate change in Ecuador. A database for Policy Decision making for Future climate change (d4PDF) is a large GCM ensemble database with a high-resolution model that permits analysis of long-term trends and future changes in localized and severe events (Mizuta *et al*., 2017). A number of studies adopted the database to project the future hydroclimate e.g., precipitation (Endo *et al*., 2017; Hibino *et al*., 2018), extreme flood and river discharge (Hanittinan *et al*., 2020; Tanaka *et al*., 2020).

The information about the adaptability of hydropower generation to hydrologic changes and global warming effects in the region is scarce especially for the large-scale dam in the main tributaries of the Mekong. Thus, this study aims to assess a combined impacts of climate change and dam development in a tributary of the Mekong River in Laos PDR (Nam Ngum River) on hydropower generation using a large ensemble of climate projections. For this purpose, a physically-based distributed hydrologic model (Meema and Tachikawa, 2020) is adopted with the projected climate variables using the delta method for different climate scenarios obtained from a large GCM ensemble database, d4PDF. The mean of projected climate ensembles from each climate scenario was used to evaluate the change of water resources and power production with different dam development stages of the basin. Furthermore, the result of the study demonstrated that implementation strategies of an adaptive reservoir operation are needed to mitigate the impact of climate change.

4.2 Modeling approach

4.2.1 General description of the model application

In chapter 2, the 1K-DHM has been improved for long-term river flow simulation in a tropical climate basin and it was extended by incorporating the reservoir-hydropower plant process into the model for accessing the impact of hydropower development in the NNRB (as described in Chapter 3, (Meema *et al*., 2020)).

The coupled model (consist of hydrological and reservoir-hydropower plant processes) has been calibrated from 2002 to 2005 in which the hydrologic parameters and reservoir operation of the NN1 (operation rules) have been optimized to perform the simulation agree with the actual operation record. Two validation periods were proposed, validation period 1 (2006-2009) presents the condition without the NN2, and validation period 2 (2012-2013) presents the existing condition of the basin (including the NN2). The model resulted well with an agreement between simulation and reference data (inflows, regulated discharge, reservoir water level and energy production) of the NN1 power station during the calibration and validation processes (see **Fig. 3.7**).

Thus, to project the hydropower generation and dam regulation flow in various scenarios, the calibrated hydrologic parameters and reservoir operation (rule curve and operation rules as shown in **Fig. 3.4**) are collected to apply for this purpose.

4.2.2 Estimation of water diversion

As the basin has the structures that transfer water from other rivers into the Nan Ngum 1 Reservoir (NN1) as shown in **Fig. 3.1**. To calculate the amount of water diversion in this study, we assign the amount of water diversion as the boundary condition into the model. The diversion record in a period of 2002−2009 from the Nam Song Diversion Dam (NS_DV) and the Nam Leuk Dam (NL) is used as the diversion amount from the dams in the present climate scenario. To predict the amount of water diversion in different climate scenarios, we assume that the operation of the diversion dams is based on the amount of inflow.

Therefore, we adopted the monthly ratio between the simulated flow in the present climate condition and the discharge of the diversion record; then, we applied the ratio with the simulated river discharge for each climate scenario. The diverted water discharge

is limited to the maximum diversion capacity (200 m^3/s for NS_DV and 60 m^3/s for NL). The water diversion amount can be calculated as follow;

$$Q_{dv_{sim}}(i,j) = k(i,j) \cdot Q_{in_{sim}}(i,j) \quad (4.1)$$

where j is month, i is a year (2002, 2003, …, 2009), $Q_{in_{sim}}$is simulated inflow to the diversion dam, $Q_{dv_{sim}}$is simulated diversion discharge and k is diversion ratio in which can be calculated as follow;

$$k(i,j) = \frac{Q_{dv_{rec}}^{PS}(i,j)}{Q_{in_{sim}}^{PS}(i,j)} \quad (4.2)$$

where $Q_{dv_{rec}}^{PS}$ is record of mean monthly diversion discharge in the present condition and $Q_{in_{sim}}^{PS}$is simulation of mean monthly inflow in the present condition.

4.3 Future climate projection

4.3.1 Future climate projection data base (d4PDF)

A database for policy decision making for future climate change (d4PDF) contains the outputs from global warming simulations under the present, 4 degrees (+4K) and 2 degrees (+2K) temperature increase conditions using a 60-km atmospheric general circulation model (AGCM). The duration of each experiment is 60 years. Each set of experiments has 100 and 90 ensemble members for the historical and 4 degree increase experiments, in which the initial conditions and the lower boundary conditions are perturbed (Mizuta *et al*., 2017). The settings of the experiments are summarized in **Table 4.1**.

The historical climate is simulated with a 100-member ensemble. The observed monthly mean sea-surface temperature (SST), sea ice concentration (SIC) (Hirahara et al., 2014), and climatological monthly sea ice thickness (SIT) (Bourke and Garrett, 1987) are used as the lower boundary conditions of the AGCM.

For the +4K simulation, in which the global mean surface air temperature is 4 degrees warmer than in the pre-industrial era. The greenhouse gases (GHG) are set to the value in 2090 of the RCP8.5 scenario. The climatological SST warming patterns (ΔSSTs) from

six CMIP5 models−CCSM4 (CC), GFDL CM3 (GF), HadGEM2-AO (HA), MIROC5 (MI), MPI-ESM-MR (MP), and MRI-CGCM3 (MR)−are added to the observational SST after removing the long-term trend component. Each of the six ΔSSTs contains a 15-member ensemble, giving a total of 90 members.

For the +2K simulation, in which the global mean surface air temperature is 2 degrees warmer than in the pre-industrial era and the GHGs are set to the value in 2040 of the RCP8.5 scenario (Fujita *et al*., 2019). The same six CMIP5 models as in the +4K simulation were used as ΔSSTs of the AGCM. Each of the six ΔSSTs contains a 9-member ensemble, giving a total of 54 members.

Table 4.1 Simulation settings and description of the period, number of ensembles and future SST change obtained from CMIP5 model.

	Historical simulation	**+2K Future simulation**	**+4K Future simulation**	**CMIP5 model for obtaining ΔSST**	
Duration	60 (1951-2010)	60 (2031-2090)	60 (2051-2110)	**Model**	**Institution (Country)**
Members	100	9 (m101-m109)	15 (m101-m109)	CCSM4 (CC)	NCAR (United States)
(GCM)	(m001-m100)	× 6 SSTs	× 6 SSTs	GFDL CM3 (GF)	NOAA GFDL (United States)
				HadGEM2-AO (HA)	Met Office Hadley Center (United Kingdom)
				MIROC5 (MI)	AORI, NIES, JAMSTEC (Japan)
				MPI-ESM-MR (MP)	Max Planck Institute for Meteorology (Germany)
				MRI-CGCM3 (MR)	Meteorological Research Institute (Japan)
Greenhouse gases	Observed	Values at 2040 of RCP8.5	Values at 2090 of RCP8.5		

4.3.2 Climate projection scenarios using the delta method

One of the simplest ways to statistically downscale GCM projections is to use the delta or change factor method (Trzaska and Schnarr, 2014). The change factor (Δ) is the ratio between GCM simulations of future and current climate and is used as a multiplicative factor to obtain future regional conditions. This method assumes that GCMs more reliably

simulate relative change rather than absolute values (Hay *et al*., 2000). Thus, climate variables can be projected as follow,

$$V_F = \Delta(j) \cdot V_{PS} \tag{4.3}$$

where V_F is daily mean projected climate variable, V_{PS} is daily mean present climate variable (observed or references data) and $\Delta(j)$ is monthly change factor in which can be calculated as follow.

$$\Delta(j) = \frac{\bar{V}_F^{GCM}(j)}{\bar{V}_H^{GCM}(j)} \tag{4.4}$$

where j is month, $\bar{V}_H^{GCM}$ and $\bar{V}_F^{GCM}$ are mean monthly value of GCM variable for historical and future conditions respectively in which can be calculated as follow.

$$\bar{V}^{GCM}(j) = \frac{\sum_{n=1}^{N} \bar{V}_n^{GCM}(j)}{N} \tag{4.5}$$

where *N* is the number of the ensembles, *j* is month, n is the ensemble number (1, 2, 3, …, *N*) and $\bar{V}_n^{GCM}(j)$ is the mean monthly value of the GCM variable for the ensemble member *n* which is calculated as follows,

$$\bar{V}_n^{GCM}(j) = \frac{\sum_{i=1}^{60} V_{n,i}^{GCM}(j)}{60} \tag{4.6}$$

where *j* is month, *i* is a year number (1, 2, 3, …, 60) and $V_{n,i}^{GCM}(j)$ is the monthly value of the GCM variable for the n-th member.

4.3.2.1 Projection of precipitation

The observed daily rainfall from 2002 to 2009 over the basin is collected to represent the present climate condition. The future precipitation amount for different climate scenarios is projected using **Eq. 4.3**. To obtained the delta factor of precipitation for each month, monthly precipitation extracted from d4PDF is used as the j-th monthly value of the GCM climate variable ($V_{n,i}^{GCM}(j)$) for the i-th year in n-th member in **Eq. 4.6**. Then, the delta factor of precipitation for different climate scenarios can be obtained by following **Eq. 4.5** and **Eq. 4.4** respectively.

4.3.2.2 Projection of actual evapotranspiration

To simulate a long-term river flow, actual evapotranspiration (AET) is another necessary input parameter; however, it is the most difficult parameter to measure in the field of basin hydrology. Meema *et al*. (2020) estimated the AET for the NNRB with a daily average of 2.78 mm/day using the water balance method (the difference amount of water between annual precipitation and river discharge). For this study, we adopted this information as the AET of the present climate scenario.

To project future AET in different climate scenarios, **Eq. 4.3** is adopted. To calculate the delta factor for AET, a combination of the simulated amount of water transferred from the global surface into the atmosphere including the water transpiration from soil (TS), the evaporation on soil (ES) and the evaporation on the leaf (EL) in different climate scenarios obtained from d4PDF is used as the monthly value of the GCM climate variable in **Eq. 4.6**. Then, the delta factor of AET for different climate scenarios can be obtained by following **Eq. 4.5** and **Eq. 4.4** respectively.

4.3.2.3 Projection of reservoir evaporation

The estimated evaporation from a water body for NNBR with the mean daily value of 2.4 mm/day—estimated by Meema *et al*. (2020)—is adopted as the present reservoir evaporation loss.

For the future projection of reservoir evaporation loss due to the climate change (assume that the pan coefficient of 0.7 has no significant change in future condition), the delta factor of the basin potential evaporation between historical and future conditions is used to multiply with the present reservoir evaporation as similar to **Eq. 4.3**.

To calculate the delta factor of reservoir evaporation, the basin-average mean monthly temperature in different climate scenarios is extracted from d4PDF to estimate the potential evaporation of the basin using the Thornthwaite method (Thornthwaite, 1948) and use this as the monthly value of GCM variable in **Eq. 4.6**. Then, the delta factor can be calculated by following **Eq. 4.5** and **Eq. 4.4** respectively.

4.4 Simulation scenarios

The combination scenarios between upstream dam development and climate change are conducted to investigate the uncertainty on basin hydrology and dam operation. A list of simulated scenarios is shown in **Table 4.2**. The description of simulation scenarios is as follows.

4.4.1 Dam development scenarios

To assess the uncertainty due to dam development in the Nam Ngum River Basin as shown the dam location in **Fig. 3.1**, three stages of dam development—no dam (ND), existing dam (ED), and future dam (FD)—were conducted. In this study, we focused on the large-scale dam that has many effects on river flow due to its regulation. Based on the large-scale dam criteria in the Mekong tributaries (Piman *et al*., 2016), Nam Ngum 1 and Nam Ngum 2 met the criteria for the existing dam stage (ED) as shown in **Fig. 3.8c** , while Nam Ngum 3 (NN3) met the criteria for the future dam stage (FD) as shown in **Fig. 3.8d**.

4.4.2 Climate change scenarios

Fifteen scenarios of climate (1 for present, 7 for +2K, and 7 for +4K) were conducted to assess the uncertainty of different climate projections on precipitation and actual evapotranspiration. The present climate scenario (BL) is referred to the historical data—precipitation and actual evapotranspiration—in a period of 2002−2009. The +2K scenarios is referred to greenhouse gas levels at 2040 from the RCP8.5, six warming patterns (ΔSST)—+2K with CC pattern (2K_CC), +2K with GF pattern (2K_GF), +2K with HA pattern (2K_HA), +2k with MI pattern (2K_MI), +2K with MP pattern (2K_MP) and +2K with MR pattern (2K_MR)—and +2K with the mean value of warming patterns (2K_AVR) are carried out. The +4K scenarios is referred to greenhouse gas levels at 2090 from the RCP8.5, six warming patterns (ΔSST)—+4K with CC pattern (4K_CC), +4K with GF pattern (4K_GF), +4K with HA pattern (4K_HA), +4K with MI pattern (4K_MI), +4K with MP pattern (4K_MP) and +4K with MR pattern (4K_MR)— and +4K with the mean value of warming patterns (4K_AVR) are carried out.

Table 4.2 List of Simulation scenarios.

Climate scenario	ΔSST	Scenarios		
		Without dam (ND)	**Existing dams (ED)**	**Future dams (FD)**
Present	-	ND-PS	ED-PS	FD-PS
+2K Future	CC	ND-2K_CC	ED-2K_CC	FD-2K_CC
	GF	ND-2K_GF	ED-2K_GF	FD-2K_GF
	HA	ND-2K_HA	ED-2K_HA	FD-2K_HA
	MI	ND-2K_MI	ED-2K_MI	FD-2K_MI
	MP	ND-2K_MP	ED-2K_MP	FD-2K_MP
	MR	ND-2K_MR	ED-2K_MR	FD-2K_MR
	AVR	ND-2K_AVR	ED-2K_AVR	FD-2K_AVR
+4K Future	CC	ND-4K_CC	ED-4K_CC	FD-4K_CC
	GF	ND-4K_GF	ED-4K_GF	FD-4K_GF
	HA	ND-4K_HA	ED-4K_HA	FD-4K_HA
	MI	ND-4K_MI	ED-4K_MI	FD-4K_MI
	MP	ND-4K_MP	ED-4K_MP	FD-4K_MP
	MR	ND-4K_MR	ED-4K_MR	FD-4K_MR
	AVR	ND-4K_AVR	ED-4K_AVR	FD-4K_AVR

4.5 Results and discussion

4.5.1 Climate change projections

4.5.1.1 Precipitation

Fig. 4.1a shows the differences between reference data and 100-member ensemble d4PDF basin-averaged monthly precipitation estimates across the basin. The purpose is to demonstrate the performance of the GCM (d4PDF) compared to the observation. The analysis presented a difference in magnitude with the GCM (d4PDF) over-predicting precipitation during the dry season especially in March and April, under-prediction during the wet season in June and July. On the other hand, the climate model resulted well in capturing the seasonal variation with the observed data. This demonstrates that the historical experiment of GCM (d4PDF) shows an agreement in seasonal variation with the reference observed data and is appropriate to adopt to project the climate variables from the present climate in various scenarios using the delta change method to assess the uncertainty of climate projection for the NNRB.

Fig. 4.1b illustrates mean monthly basin precipitation trends of all climate scenarios in the 2 degree and 4 degree increase experiments from the GCM prediction. The monthly

delta changes factor obtained by analyzing the GCM data set for +2K scenarios is ranged from 0.73 to 1.36 and for +4K scenarios is ranged from 0.71 to 1.50. This shows that the range of change in precipitation is much larger when temperature increase. Although the range of the delta change in the dry season seems similar to the wet season (0.71−1.44 for the dry season and 0.73−1.50 for the wet season), a primary difference in prediction of precipitation magnitude occurs during the wet season, especially in July and August.

By using the delta factors obtained by analyzing the d4PDF data set with the observed precipitation (present climate), the precipitation projection in different climate scenarios is predicted as shown in **Fig. 4.1c**. Based on average daily accumulation for all climate scenarios, the climate projections describe a range of changes in mean annual precipitation (compared to historical observed data) from −5.5% to +4.9% for +2K scenarios and from −9.6% to +6.9% for +4K scenarios. Similar to the delta change factors, a significant change in amount of projected precipitation is in the wet season especially in July and August.

The average pattern of +2K climate scenario (2K_AVR) results in a slight increase (0.35% increase) in mean annual precipitation compared to the observation (present climate) and a slight reduction (0.64% reduction) has resulted for the average pattern of +4K climate scenario (4K_AVR).

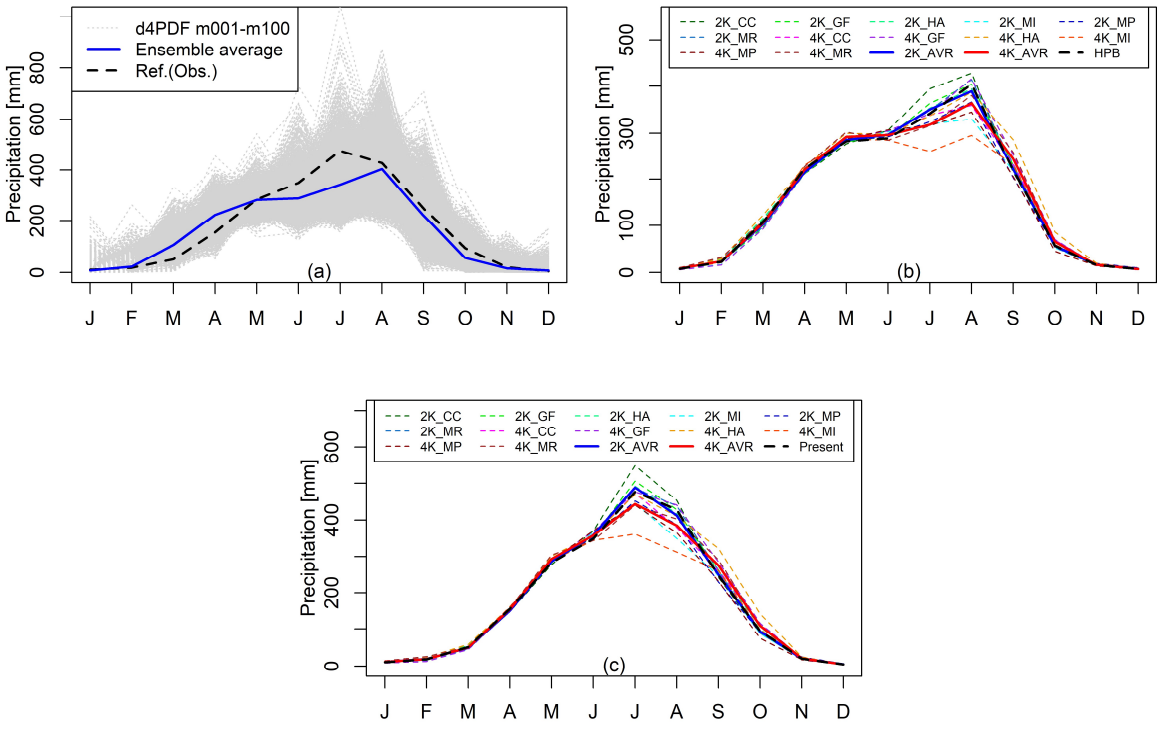

Fig. 4.1 (a) Comparison of reference data (Observation) and historical experiment of the 100-member ensemble d4PDF basin-averaged monthly precipitation, (b) comparison of basin-averaged monthly precipitation estimated by d4PDF in various climate scenarios in the 2 degree and 4 degree increase experiments and (c) comparison of projected basin-averaged monthly precipitation estimated by using delta change method in various climate scenarios. (HPB is historical data estimated by d4PDF and Present is present value collected from historical observed data).

4.5.1.2 Actual evapotranspiration projections

Fig. 4.2a shows the mean monthly AET in various climate scenarios obtained from the GCM (d4PDF) prediction. The estimated amount of water transfer to the atmosphere tends to increase when the temperature increase. The monthly delta changes factor obtained by analyzing the GCM data set for +2K scenarios is ranged from 0.91 to 1.10, for +4K scenarios is ranged from 0.91 to 1.15.

By using the delta factors obtained by analyzing the d4PDF data set (**Fig. 4.2a**) with the references AET, the AET projection in different climate scenarios is predicted as

shown in **Fig. 4.2b**. Under the climate projections, a range of increase in mean annual AET compared to the reference (present climate) is varied from +0.57% to +3.78% for +2K scenarios and from +4.50% to +7.94% for +4K scenarios. All climate scenarios show the highest amount of AET during April and May in which this period has a high temperature with a moderate precipitation amount. The average pattern of +2K climate scenario (2K_AVR) results in a 2.8 mm/day in the average daily value (0.57% increase from present climate) and a 2.95 mm/day (5.96% increase) has resulted for the average pattern of +4K climate scenario (4K_AVR).

According to the projected AET, it is distinct that increasing temperature results in an increase in the potential of water transferred to the atmosphere leading to fewer water resources availability in the basin.

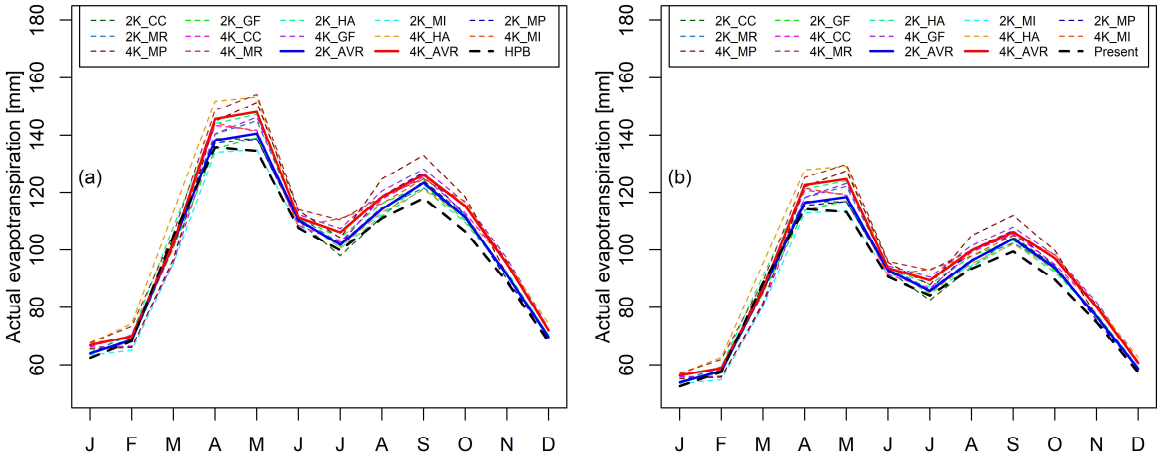

Fig. 4.2 (a) Comparison of basin-averaged monthly AET in various climate scenarios projected by d4PDF and (b) Comparison of projected basin-averaged monthly AET estimated by using delta change method in various climate scenarios. (HPB is historical data estimated by d4PDF and Present is present value estimated from historical data).

4.5.2 Climate change and hydropower development impact on river flow

Regarding the simulation scenarios described in section 4.4, **Table 4.3** presents the summary of simulation results on river flow (unregulated flow) at the NN1 dam site in

different climate scenarios with no dam condition.

Inflow and regulated flow (downstream river flow) of the NN1 reservoir were used to analyze the impact of climate change and hydropower development on annual and seasonal flow change. A comparison of annual and seasonal flow in different climate scenarios for existing (ED) and future dam (FD) conditions is summarized in **Table 4.4** and **Table 4.5**, respectively.

Table 4.3 Summary of simulation results on annual and seasonal flow at the Nam Ngum 1 damsite in different climate scenarios without dam condition (ND). "Change" is the percent of change from the ND-PS scenario.

	Wet season		Dry season		Annual	
Scenario	Flow (m^3/s)	change (%)	Flow (m^3/s)	change (%)	Flow (m^3/s)	change (%)
ND-PS	617.9	-	109.5	-	321.3	-
ND-2K_CC	643.5	4.1	109.3	-0.2	331.9	3.3
ND-2K_GF	604.5	-2.2	107.6	-1.7	314.6	-2.1
ND-2K_HA	606.3	-1.9	110.5	0.9	317.1	-1.3
ND-2K_MI	535.1	-13.4	100.0	-8.7	281.3	-12.5
ND-2K_MP	540.8	-12.5	103.2	-5.8	285.5	-11.1
ND-2K_MR	601.8	-2.6	107.5	-1.8	313.5	-2.5
ND-2K_AVR	588.3	-4.8	106.4	-2.8	307.2	-4.4
ND-2K_CC	570.2	-7.7	105.3	-3.9	299.0	-7.0
ND-2K_GF	613.7	-0.7	108.0	-1.3	318.7	-0.8
ND-2K_HA	633.8	2.6	117.3	7.1	332.5	3.5
ND-2K_MI	468.6	-24.2	96.6	-11.8	251.6	-21.7
ND-2K_MP	516.5	-16.4	95.7	-12.6	271.0	-15.7
ND-2K_MR	569.7	-7.8	107.3	-2.0	300.0	-6.6
ND-2K_AVR	561.2	-9.2	105.3	-3.9	295.2	-8.1

Table 4.4 Summary of simulation results on annual and seasonal inflow of the Nam Ngum 1 dam for Existing (ED) and Future Dam (FD) simulation scenarios. "Change" is the percent of change from the ND-PS scenario.

	Wet season		Dry season		Annual			Wet season		Dry season		Annual	
Scenario	Flow (m^3/s)	change (%)	Flow (m^3/s)	change (%)	Flow (m^3/s)	change (%)	Scenario	Flow (m^3/s)	change (%)	Flow (m^3/s)	change (%)	Flow (m^3/s)	change (%)
ED-PS	614.2	-0.6	224.5	105.1	386.9	20.4	FD-PS	603.7	-2.3	233.6	113.3	387.8	20.7
ED-2K_CC	668.5	8.2	224.7	105.2	409.6	27.5	FD-2K_CC	651.3	5.4	236.7	116.2	409.4	27.4
ED-2K_GF	625.8	1.3	223.2	103.8	390.9	21.7	FD-2K_GF	613.5	-0.7	232.9	112.7	391.5	21.8
ED-2K_HA	629.2	1.8	226.7	107.0	394.4	22.7	FD-2K_HA	618.5	0.1	235.2	114.8	394.9	22.9
ED-2K_MI	562.6	-9.0	206.4	88.5	354.8	10.4	FD-2K_MI	556.4	-10.0	214.0	95.4	356.7	11.0
ED-2K_MP	567.0	-8.2	210.9	92.6	359.2	11.8	FD-2K_MP	560.8	-9.2	218.1	99.2	360.9	12.3
ED-2K_MR	623.8	0.9	222.4	103.1	389.6	21.3	FD-2K_MR	610.7	-1.2	232.8	112.6	390.3	21.4
ED-2K_AVR	610.0	-1.3	220.7	101.5	382.9	19.2	FD-2K_AVR	598.0	-3.2	230.9	110.9	383.8	19.4
ED-4K_CC	592.7	-4.1	217.5	98.6	373.8	16.3	FD-4K_CC	583.2	-5.6	226.7	107.0	375.2	16.8
ED-4K_GF	635.3	2.8	224.5	105.0	395.6	23.1	FD-4K_GF	624.5	1.1	232.9	112.7	396.1	23.3
ED-4K_HA	655.6	6.1	237.9	117.3	412.0	28.2	FD-4K_HA	646.2	4.6	244.8	123.6	412.0	28.2
ED-4K_MI	506.9	-18.0	190.6	74.1	322.4	0.3	FD-4K_MI	505.9	-18.1	195.9	79.0	325.1	1.2
ED-4K_MP	545.5	-11.7	197.8	80.7	342.7	6.6	FD-4K_MP	543.6	-12.0	202.6	85.0	344.7	7.3
ED-4K_MR	591.5	-4.3	220.7	101.5	375.2	16.8	FD-4K_MR	582.6	-5.7	229.8	109.9	376.8	17.3
ED-4K_AVR	585.3	-5.3	216.3	97.5	370.1	15.2	FD-4K_AVR	576.6	-6.7	225.2	105.7	371.6	15.7

Table 4.5 Summary of simulation results on annual and seasonal flow at downstream of the Nam Ngum 1 dam (regulated flow) for Existing (ED) and Future Dam (FD) simulation scenarios. "Change" is the percent of change from the ND-PS scenario.

	Wet season		Dry season		Annual			Wet season		Dry season		Annual	
Scenario	Flow (m^3/s)	change (%)	Flow (m^3/s)	change (%)	Flow (m^3/s)	change (%)	Scenario	Flow (m^3/s)	change (%)	Flow (m^3/s)	change (%)	Flow (m^3/s)	change (%)
ED-PS	423.0	-31.5	347.6	217.5	379.0	17.9	FD-PS	425.2	-31.2	347.2	217.1	379.7	18.2
ED-2K_CC	473.6	-23.4	348.7	218.5	400.7	24.7	FD-2K_CC	474.1	-23.3	347.6	217.4	400.3	24.6
ED-2K_GF	429.1	-30.6	348.3	218.1	382.0	18.9	FD-2K_GF	431.5	-30.2	347.3	217.2	382.3	19.0
ED-2K_HA	436.6	-29.3	348.7	218.5	385.3	19.9	FD-2K_HA	439.0	-29.0	347.5	217.4	385.6	20.0
ED-2K_MI	354.8	-42.6	339.8	210.4	346.0	7.7	FD-2K_MI	366.0	-40.8	334.7	205.7	347.8	8.2
ED-2K_MP	362.6	-41.3	341.3	211.7	350.2	9.0	FD-2K_MP	372.4	-39.7	337.0	207.8	351.7	9.5
ED-2K_MR	426.2	-31.0	347.8	217.7	380.5	18.4	FD-2K_MR	428.2	-30.7	347.2	217.1	381.0	18.6
ED-2K_AVR	412.2	-33.3	346.5	216.5	373.9	16.3	FD-2K_AVR	414.7	-32.9	346.1	216.1	374.7	16.6
ED-4K_CC	388.1	-37.2	345.5	215.6	363.3	13.1	FD-4K_CC	393.1	-36.4	344.2	214.3	364.6	13.5
ED-4K_GF	434.9	-29.6	348.8	218.5	384.7	19.7	FD-4K_GF	438.1	-29.1	347.0	216.9	385.0	19.8
ED-4K_HA	471.6	-23.7	350.6	220.2	401.0	24.8	FD-4K_HA	475.0	-23.1	348.0	217.8	400.9	24.8
ED-4K_MI	313.1	-49.3	323.7	195.7	319.3	-0.6	FD-4K_MI	316.5	-48.8	324.1	196.0	320.9	-0.1
ED-4K_MP	338.9	-45.2	330.9	202.2	334.2	4.0	FD-4K_MP	344.5	-44.3	330.3	201.7	336.2	4.6
ED-4K_MR	389.9	-36.9	345.4	215.4	363.9	13.2	FD-4K_MR	394.7	-36.1	344.5	214.7	365.4	13.7
ED-4K_AVR	380.1	-38.5	344.1	214.2	359.1	11.8	FD-4K_AVR	384.5	-37.8	343.5	213.8	360.6	12.2

4.5.2.1 Climate change impact on natural condition flow

The simulation without dams is conducted to assess the impact of climate change on river flow without the impact of dam operation. **Fig. 4.3** shows a comparison of the average monthly flow in various climate scenarios. Comparison between different climate scenarios shows that the change of average annual flow compared to the present climate scenario (ND_PS) is ranged from −12.5% to +3.3% for +2K scenarios and from −21.7% to +3.5% for +4K scenarios with a significant difference in magnitude in the wet season—July, August, and September (similar to the projection of precipitation). The average of 2K (2K_AVR) and 4K (4K_AVR) climate scenarios show a reduction trend in the annual river flow with −4.4% and −8.1% respectively.

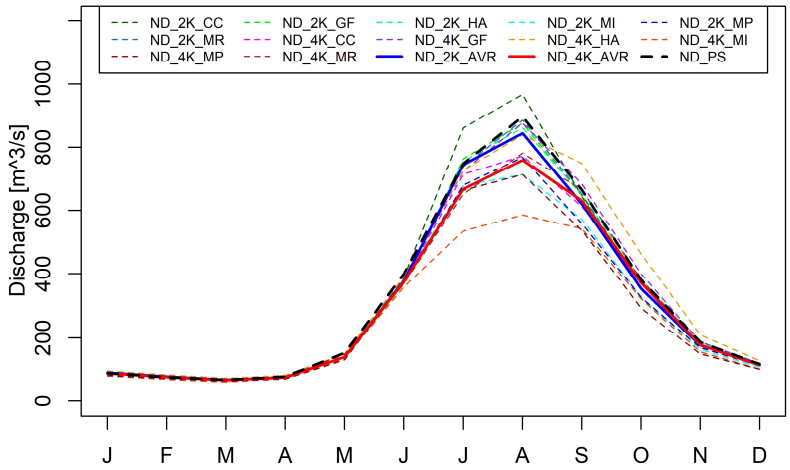

Fig. 4.3 Mean monthly projected river flow at the Nam Ngum 1 dam in different climate scenarios without dam (Unregulated flow).

4.5.2.2 Climate change impact on Nam Song water diversion

To predict the amount of water diversion in different climate scenarios, we adopted the ratio between the simulated flow in the present climate condition and the discharge of the diversion record; then, we applied the ratio with the simulated river discharge for each climate scenario. The diverted water discharge is limited to the maximum diversion capacity.

Fig. 4.4a presents a change of mean monthly water availability at the diversion headwork (Nam Song River) in different climate scenarios in which the mean annual flow is varied from −7.5% to + 6.3% for +2K scenarios and from −15.7% to + 8.1% for +4K scenarios compared with the present climate scenarios.

Fig. 4.4b presents a change of mean monthly water diversion from the Nam Song at diversion headwork to the NN1 reservoir in different climate scenarios, the mean annual diversion discharge is varied from −4.5% to +2.2% for +2K scenarios and from −9.6% to +6.1% for +4K scenarios compared with the present climate scenarios.

According to the result of simulations, climate change has less effect on the total amount of water diversion from the Nam Song River to the NN1 reservoir compared to the change of water availability at the diversion headwork (inflow of the Nam Song dam). For example, in the case of the 4K_MI climate scenario (the most reduction of river flow), a reduction of water transfer to the NN1 reservoir is only a 1.5% reduction from the NN1 reservoir total inflow compared to the present climate scenario with existing dam condition (ED_PS).

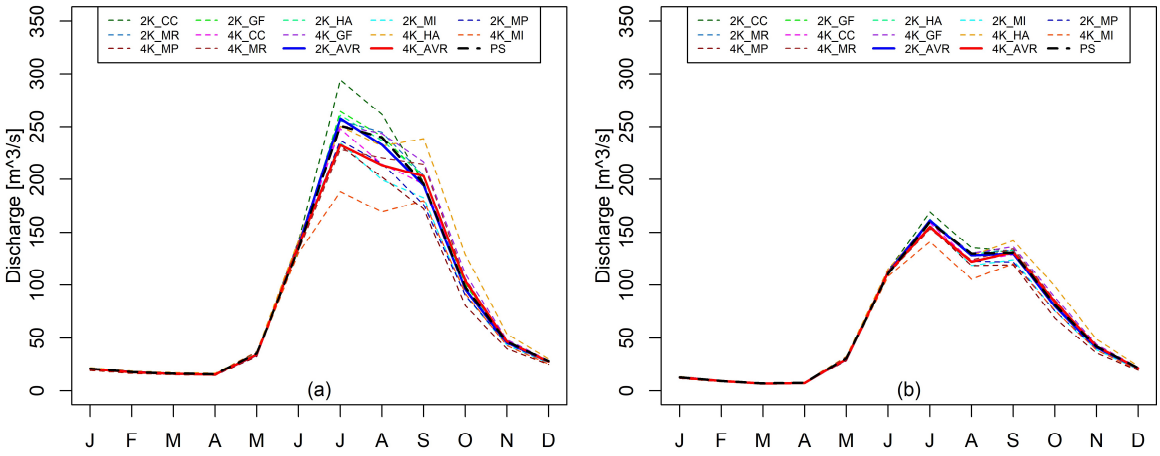

Fig. 4.4 Mean monthly projected flow at the Nam Song diversion dam in different climate scenarios (a) inflow of the Nam Song diversion dam and (b) diversion discharge to the Nam Ngum 1 reservoir.

4.5.2.3 Climate change impact on river flow with existing dam condition

Fig. 4.5a describes the impact of climate change on the inflow of the NN1 reservoir

with the existing dam condition. The change of the annual inflow is ranged from −8.3% to +5.9% for +2K scenarios and from −16.7% to +6.5% for +4K scenarios compared to the present climate scenario (ED_PS). To assess a combined effect of climate change and dam development, the degree of change in the river flow is compared with the natural flow condition (ND_PS), a range of change in the mean annual inflow from +0.3% to +28.2% was found. A significant change in seasonal flow (inflow of NN1) due to upstream dam development in different climate scenarios—compared with natural flow condition (ND_PS)—is varied from +74.1% to +117.3% in the dry season and −18% to +8.2% in the wet season. A significant alteration in the seasonal inflow of NN1 is mainly due to a regulation of the large storage dam such as NN2 with a 2617 mcm of the effective storage capacity.

Fig. 4.5b describes the impact of climate change on the regulated flow of the NN1 reservoir with the inflow from the existing upstream dam condition. The change of the annual regulated flow to downstream of the NN1 reservoir for different climate scenarios is ranged from −8.7% to +5.7% for +2K scenarios and from −15.8% to +5.8% for +4K scenarios compared to the present climate scenario (ED_PS).

The effect of the NN1 reservoir regulation with large effective storage of 4714 mcm is assessed by comparing the seasonal flow change between the predicted inflow (**Fig. 4.5a**) and regulated flow (**Fig. 4.5b**) for each climate condition. A simulation result shows a 49.0−22.9% reduction in the wet season and a 44.2−56.1% increase in the dry season.

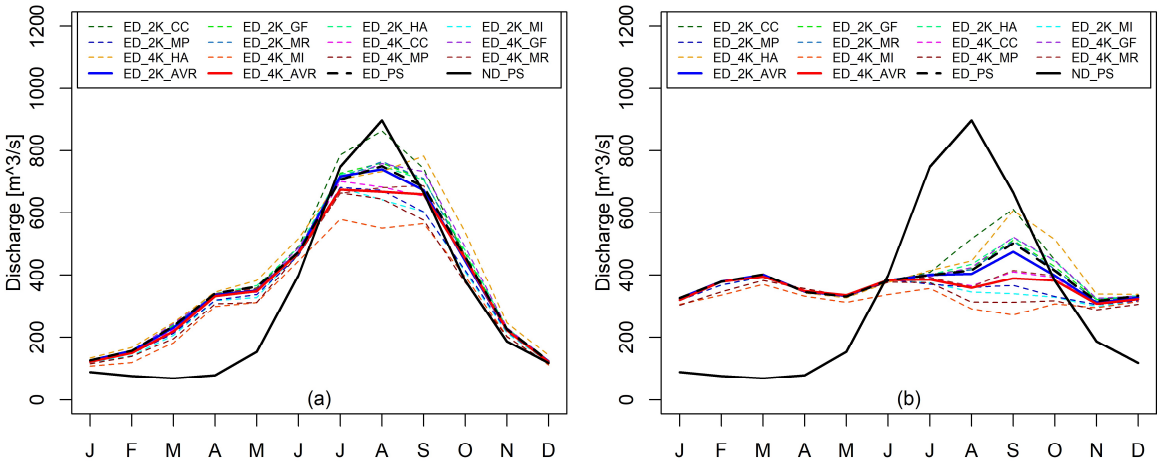

Fig. 4.5 Comparison of mean monthly river flow between base line (present climate without dam, ND_PS) and different climate scenarios with existing dam development stage (a) inflow of the Nam Ngum 1 reservoir and (b) regulated flow to downstream of the Nam Ngum reservoir.

4.5.2.4 Climate change impact on river flow with future dam condition

Fig. 4.6a shows the impact of climate change on the inflow of the NN1 reservoir with the regulated flow from the future upstream dam condition (NS_DV, NL, NN2, and NN3). The change of the annual inflow of the NN1 reservoir for different climate scenarios is ranged from −8.0% to +5.6% for +2K scenarios and from −16.2% to +6.3% for +4K scenarios compared with the present climate scenario (FD_PS). The inflow of the NN1 reservoir becomes more stable (slightly decrease in seasonal variation) due to an increase in regulated storage of the upstream dams. An additional power station—Nam Ngum 3 with effective storage of 1070 mcm—is taken into account in this simulation. To assess the impact of the NN3 regulation on the inflow of the NN1, the simulated inflow for future dam development condition (**Fig. 4.6a**) is compared with the existing dam condition (**Fig. 4.5a**) for each climate scenario. The results show that there is a slight reduction of 0.2−2.6% in the wet season inflow and a slight increase of 2.4−5.3% in the dry season inflow of the NN1 reservoir.

Fig. 4.6b shows the impact of climate change on the regulated flow of the NN1

reservoir to downstream with future dam conditions. The change of the annual river flow in downstream of the NN1 reservoir for different climate scenarios is ranged from −8.4% to +5.4% for +2K scenarios and from −15.5% to +5.6% for +4K scenarios compared with the present climate scenario (FD_PS). A primary change in seasonal river flow due to dam development in different climate scenarios—compared with natural flow condition (ND_PS) at the downstream of the NN1 reservoir—is varied from −48.8% to −23.1% in the wet season and +196.0% to +217.8% in the dry season.

To assess the impact of the NN3 operation on regulated flow of the NN1, the regulated flow with FD condition (as shown in **Fig. 4.6b**) is compared to the river flow with ED condition (as shown **Fig. 4.5b**) for each climate scenario, the result shows that there is no primary change in the regulated flow from the NN1 reservoir to the downstream because the regulated potential of the NN3 (effective storage of 1070 mcm) is approximately only 9.0% (range from 8.2% to 10.4%) of the mean predicted total inflow of the NN1 for different climate scenario with future dam condition. This agrees with Meema et al. (2020) that the major large-scale hydropower dams are already developed in which can regulate most of the river flows in the basin.

By comparing the individual effect between climate change and dam development with the natural flow condition (ND_PS), the changing climate has a primary effect in terms of the total amount of water availability (mean annual river flow) due to a combined effect of precipitation change and AET increasing. A significant effect occurs during the wet season due to a change in precipitation magnitude leading to a change in river flow. Only a slight change in seasonal flow driven by climate change was found in this study.

The dam development in the basin has a primary effect in terms of seasonal flow variation due to a regulation using its storage. Furthermore, not only a primary change in seasonal flow but dam development with a river diversion type from another catchment results in increasing of mean annual river flow also. The simulation result demonstrates that the large-scale dam reservoir—which can control a huge volume of water in the basin—has an important role in water resources management.

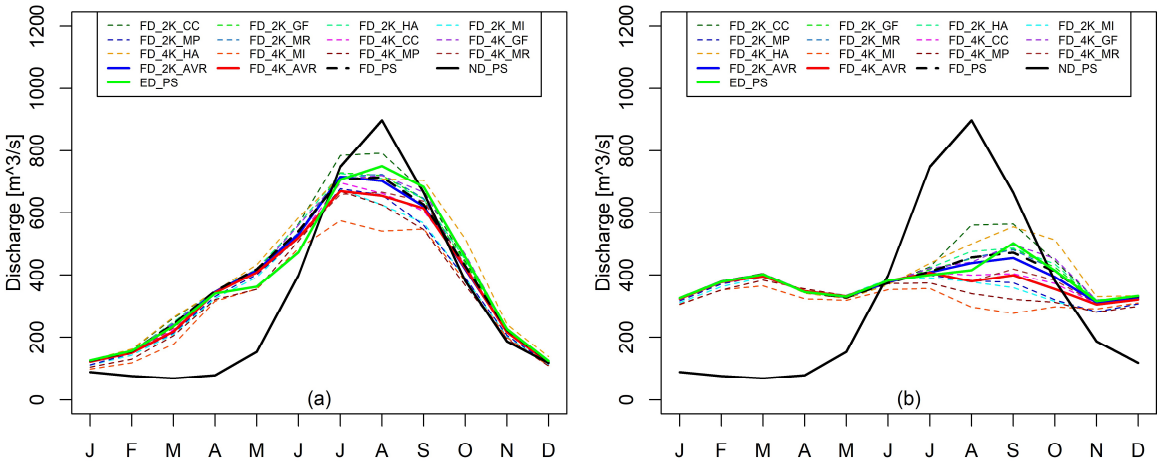

Fig. 4.6 Comparison of mean monthly river flow among present climate without dam (ND_PS), present climate with existing dam (ED_PS) and different climate scenarios with future dam development stage (a) inflow of the Nam Ngum 1 reservoir and (b) regulated flow to downstream of the Nam Ngum reservoir.

4.5.3 Linkage between projected precipitation, evaporation, inflow and regulated flow

The model has included the soil and bedrock aquifers that respond as natural storage of the basin. During the dry season, the amount of precipitation is lower than AET, river flow is mainly contributed by the basin storages. Although some effective rainfall happens (Precipitation > AET) during the beginning of the wet season (May and June), most rainwater is infiltrated into the aquifers. Therefore, the hydrograph of river flow (**Fig. 4.3**) shows a minor difference during these periods.

The highest amount of precipitation is in July and August, effective rainfall has much enough to become surface flow which the magnitude of river flow is depended on the amount of projected precipitation resulted in a primary difference in river flow hydrograph (as shown in **Fig. 4.3**).

In September and October, the storages are full filled from the previous months, most of the effective rainwater becomes surface runoff. A combination of groundwater and surface flow results in a higher significant difference in river flow compared to

precipitation.

The major difference in regulated flow among the scenarios is due to spillage water. In the study, we assume that the operation follows the present operation. So, during the dry season including the beginning of wet seasons such as June and July, the amount of reservoir inflow can be controlled by the reservoir storage (current storage; S_t <= maximum storage; S_{max}). So, the comparison of regulated flow for various scenarios is quite similar (as shown in **Fig. 4.5** and **Fig. 4.6**). During the mid to late wet seasons (August to October), much spill will happen ($S_t > S_{max}$) when river discharge has an increasing trend leading to the significant difference in regulated flow during this period (as shown in **Fig. 4.5** and **Fig. 4.6**).

Although a larger difference in precipitation was observed in July and August, the primary difference in regulated flow from the NN1 was found in August to October due to the storage capacity (regulated capacity) of the reservoirs. In this study, the hydrological residence time (HRT) of the NN1, NN2 and NN3 reservoirs for the present climate scenarios with future dam condition are 0.39, 0.46 and 0.41 year respectively (HRT [year] = effective storage capacity [MCM] / inflow [MCM/year]). On the other hand, when the HRT decreases, the regulated hydrograph will be closer to the inflow hydrograph.

4.5.4 Climate change impact on reservoir water level and water spill

Fig. 4.7a present a comparison of mean monthly water level of the NN1 reservoir in different climate scenarios with existing dam condition. A change of mean water level for different climate scenarios compared with present climate scenarios (ED_PS) is varied from −0.63 to + 0.12 m for +2K scenarios and from −2.86 to + 0.41 m for +4K scenarios. For the average climate scenarios such as 2K_AVR and 4K_AVR, the reduction in mean reservoir water level is 0.12 and 0.34 m respectively.

Fig 4.7b present a comparison of mean monthly water level of the NN1 reservoir in different climate scenarios with future dam condition. The tendency of the mean monthly reservoir water level is quite similar to the existing dam condition (**Fig. 4.7a**) but the trend is slightly increased. By using the same operation pattern, more stable inflow (increase in the dry season flow and decrease in the wet season) due to increasing the regulation capacity of the upstream dam results in a slightly higher water levels in the reservoir,

which a 0.18−0.36 m increase in mean reservoir water level compared with the existing dam condition for each climate scenario has resulted.

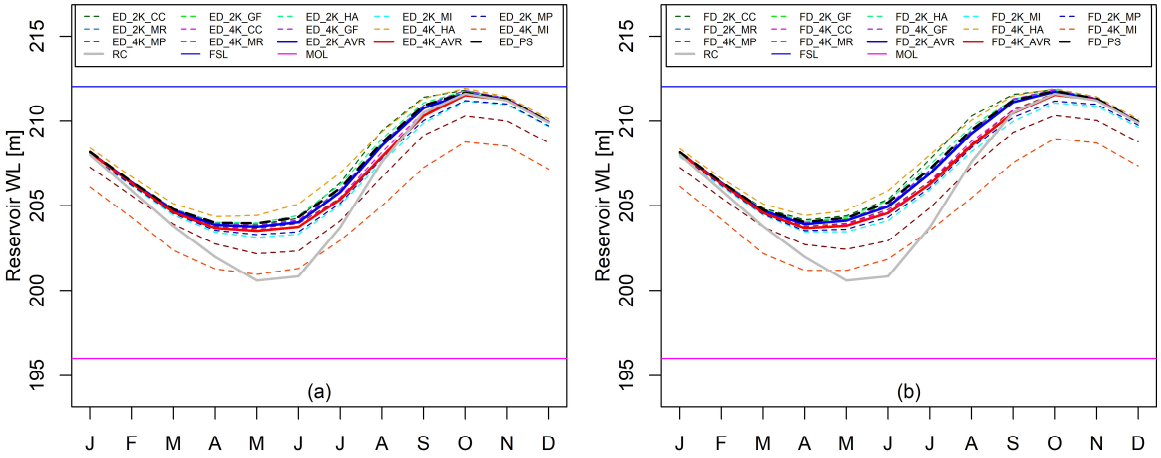

Fig. 4.7 (a) comparison of mean monthly reservoir water level for different climate scenarios with existing dam condition and (b) comparison of mean monthly reservoir water level between present climate scenario with existing dam (ED_PS) and different climate scenarios with future dam condition. (RC: rule curve, FSL: full supply level and MOL: minimum operation level).

Table 4.6 summaries the mean annual reservoir water and the total amount of water spill from the NN1 reservoir in different simulation scenarios. The mean annual amount of water spill for all simulation scenarios is ranged from 0 to 921.6 mcm. For each dam development condition, the mean annual water spill trends to increase when the mean reservoir water level increase.

To assess the effect of dam development on water spill from the NN1 reservoir, the amount of water spill for each climate scenario between existing dam (ED) and future dam (FD) conditions is compared. A comparison shows that even though all climate scenarios in FD result in an increase in mean water level compared with ED, some climate scenarios result in a reduction of a water spill. This demonstrated that the amount of water

spill is not only a function of water level but other factors also. For example, in the case 4K_MR, even though the mean water level in FD has a 0.2 m higher than ED, the water spill is reduced by 42.0%. Because most of the water level in FD is higher than ED during the period without spill (spill usual occurs in September and October) and the regulated flow from the upstream in FD condition is more appropriate for power generation; Thus, the most of amount of water is used to generate the power through the turbines leading to less water spill through the spillway.

The water level of the NN1 Reservoir seems to have less fluctuation when there are more reservoirs upstream due to its regulated flow that tends to increase the NN1 inflow in the dry season and decrease in the wet season.

Water spill is the amount of water released through the spillway without generating electricity when the current reservoir storage is exceeded the maximum storage. Thus, to use water effectively, the operation of the reservoir should be considered to avoid the amount of water spill.

Table 4.6 Summary of simulation result on the mean annual reservoir water and the total amount of water spill from the Nam Ngum 1 reservoir for different climate scenarios with the existing (ED) and future (FD) dam development conditions.

Existing dams (ED)	Water level (m)	Spill (mcm)	Future dams (FD)	Water level (m)	Spill (mcm)
ED-PS	207.5	348.1	FD-PS	207.8	399.4
ED-2K_CC	207.6	856.0	FD-2K_CC	208.0	911.6
ED-2K_GF	207.5	423.1	FD-2K_GF	207.8	458.7
ED-2K_HA	207.6	438.0	FD-2K_HA	207.9	541.5
ED-2K_MI	206.9	68.0	FD-2K_MI	207.1	85.2
ED-2K_MP	207.0	82.2	FD-2K_MP	207.2	84.7
ED-2K_MR	207.4	403.7	FD-2K_MR	207.8	414.2
ED-2K_AVR	207.4	310.8	FD-2K_AVR	207.7	308.9
ED-4K_CC	207.3	184.0	FD-4K_CC	207.5	146.0
ED-4K_GF	207.5	478.7	FD-4K_GF	207.8	538.9
ED-4K_HA	207.9	855.4	FD-4K_HA	208.2	921.6
ED-4K_MI	204.7	0.0	FD-4K_MI	204.9	0.0
ED-4K_MP	206.1	19.8	FD-4K_MP	206.3	59.1
ED-4K_MR	207.3	215.4	FD-4K_MR	207.5	124.9
ED-4K_AVR	207.2	151.9	FD-4K_AVR	207.4	104.2

4.5.5 Climate change impact on hydropower production

The hydrologic impact on hydropower production was analyzed considering an overall effect on climate change and upstream dam development. The simulation results of the mean annual energy production for the different simulation scenarios are provided in **Table 4.7**.

Fig. 4.8a presents a comparison of the mean monthly energy product of the NN1 power station in different climate scenarios with the existing dam development condition. Under projected climate scenarios, a difference in mean annual energy production compared to the present climate (ED_PS) is varied from –8.4% to +1.9% for +2K scenarios and from −19.5% to +2.8% for +4K scenarios. Its reduction in energy production due to a reduction in inflow to the reservoir and a decrease in reservoir water level (leading to generated hydraulic head reduction) results in less energy production.

Fig. 4.8b illustrates a comparison of the mean monthly energy product of the NN1 power station in different climate scenarios with the future dam development condition. A change in mean annual energy production from the present climate (FD_PS) for different projected climate scenarios is quite similar to a change in the existing dam development condition. To demonstrate the effect of upstream cascade dam development on energy production of the NN1 power station, the mean monthly energy between existing (**Fig. 4.8a**) and future (**Fig. 4.8b**) dam development conditions is compared for each climate scenario. Under the future dam development level, the annual energy production of the NN1 power station has a slight increase trend due to more upstream reservoirs in operation.

Construction of upstream cascade dams improves the stabilization between wet and dry season of inflow to the NN1 reservoir leading to improvement in reservoir water level results in an increase in the potential of power generation and an increase in total energy production. However, a general trend (2K_AVR and 4K_AVR) seems to indicate a reduction in the annual energy product when the projected temperature is increased.

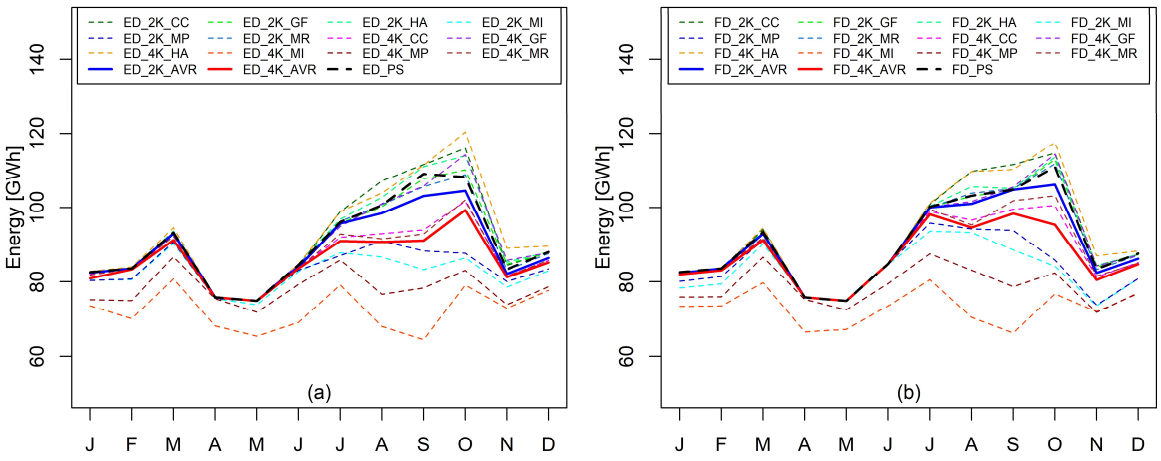

Fig. 4.8 (a) Comparison of energy production for NN1 power station with existing dam stage in different climate scenarios and (b) Comparison of energy production for NN1 power station with future dam stage in different climate scenarios.

Table 4.7 Summary of simulation result on the mean annual energy production of the Nam Ngum 1 power station for different climate scenarios with the existing (ED) and future (FD) dam development conditions. "Change" is the percent of change from the ED-PS scenario.

Scenario	Energy (GWh)	Change (%)	Scenario	Energy (GWh)	Change (%)
ED-PS	1080.6	-	FD-PS	1085.7	0.5
ED-2K_CC	1101.5	1.9	FD-2K_CC	1104.8	2.2
ED-2K_GF	1081.5	0.1	FD-2K_GF	1087.7	0.7
ED-2K_HA	1093.6	1.2	FD-2K_HA	1092.1	1.1
ED-2K_MI	989.8	-8.4	FD-2K_MI	998.1	-7.6
ED-2K_MP	1003.6	-7.1	FD-2K_MP	1013.4	-6.2
ED-2K_MR	1077.0	-0.3	FD-2K_MR	1086.6	0.6
ED-2K_AVR	1064.6	-1.5	FD-2K_AVR	1075.4	-0.5
ED-4K_CC	1040.9	-3.7	FD-4K_CC	1055.2	-2.3
ED-4K_GF	1084.9	0.4	FD-4K_GF	1087.9	0.7
ED-4K_HA	1110.8	2.8	FD-4K_HA	1110.5	2.8
ED-4K_MI	869.6	-19.5	FD-4K_MI	877.7	-18.8
ED-4K_MP	940.4	-13.0	FD-4K_MP	946.8	-12.4
ED-4K_MR	1039.5	-3.8	FD-4K_MR	1059.7	-1.9
ED-4K_AVR	1029.1	-4.8	FD-4K_AVR	1044.1	-3.4

4.5.6 Climate change impact on water loss from the reservoir

The mean monthly evaporation rate from the water body is placed at the reservoirs to account for the net amount of water loss due to evaporation from the water surface of the reservoirs. The difference in water loss from the NN1 reservoir for different simulation scenarios is summarized in **Table 4.8**.

Fig. 4.9a presents a comparison of the mean monthly amount of water loss from the NN1 reservoir in different climate scenarios with the existing dam development condition. The amount of water loss due to evaporation in different climate scenarios is varied from 9.2% to 13.4% for +2K scenarios and from 24.5% to 35.6% for +4K scenarios compared to the present climate with the existing dam development stage (ED_PS). Even though, evaporation loss rate in November and December has a significantly lower than in March and April (as shown in **Fig. 4.9c**), the net amount of water loss is quite similar (as shown in **Fig. 4.9a**). Because the operation pattern tries to maintain the water in the reservoir at a high level at the end of the rainy season and the beginning of the dry season leading to an increase in free water surface area in which results in a high amount of water loss.

Fig. 4.9b presents a comparison of the mean monthly amount of water loss from the NN1 reservoir in different climate scenarios with the future dam development condition. The tendency of water loss from the reservoir in different climate scenarios compared to the present climate (FD_PS) is quite similar tendency to the existing dam development condition. By comparing the result of simulation in different climate scenarios between the future dam condition (**Fig. 4.9b**) and the existing dam condition (**Fig. 4.9a**) to assess the impact of future dam development on the projected amount of water loss from the NN1 reservoir, there is a slight increase in actual water loss. As the water level increase (discussed in the previous section), there will be more reservoir water surface area in which results in an additional amount of water loss due to evaporation.

The amount of water loss from the reservoir in present (ED_PS) is approximately 2.4% of the total inflow of the NN1 reservoir. However, under the projected climate scenarios, the amount of water loss from the NN1 reservoir due to evaporation will be increased to be approximately 2.7% and 3.2% of the present mean annual inflow for 2K and 4K temperature increase scenarios respectively (2K_AVR and 4K_AVR). Assume that the

total amount of water loss due to evaporation can be used to utilize the hydropower, an approximately 3.6 and 9.4 GWh/year of additional energy production for the NN1 power station will be lost when the temperature increase 2K and 4K respectively (2K_AVR and 4K_AVR).

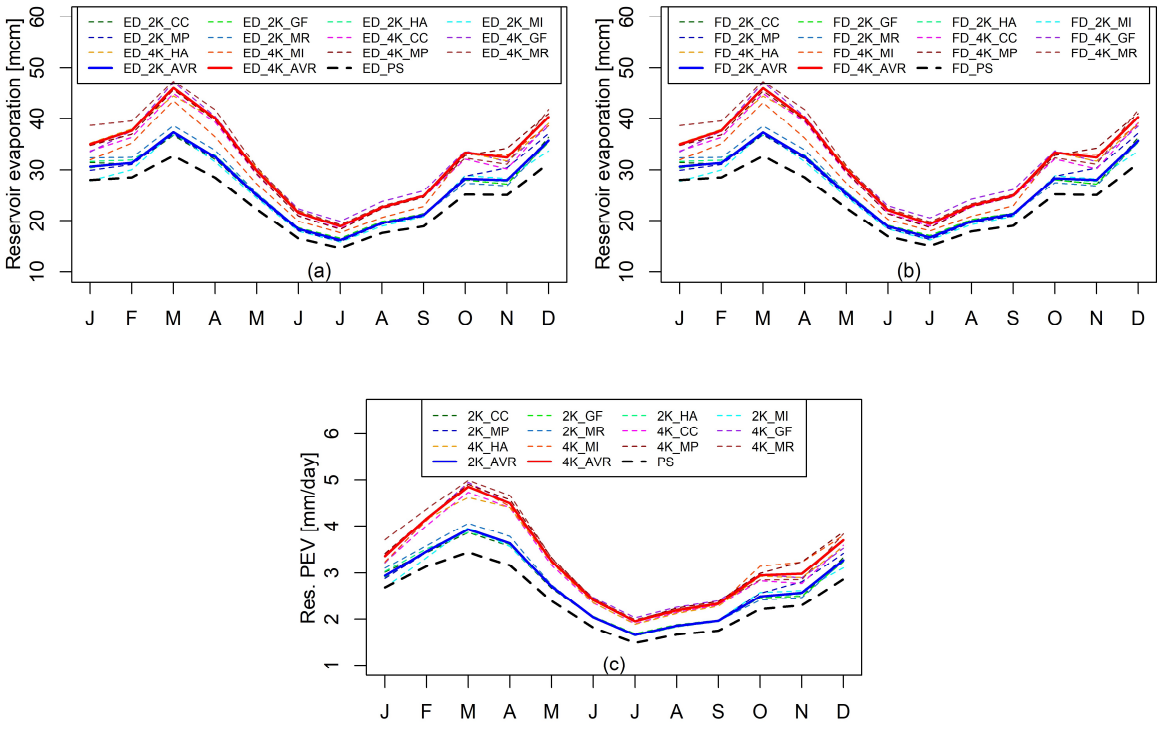

Fig. 4.9 (a) mean monthly net amount of water loss from the NN1 reservoir due to evaporation in different climate scenarios for existing dam development stage. (b) mean monthly net amount of water loss from the NN1 reservoir due to evaporation in different climate scenarios for future dam development stage. (c) mean monthly evaporation rate from water body in different climate scenarios.

Table 4.8 Summary of simulation result on the mean annual water loss due to evaporation from the Nam Ngum 1 reservoir for different climate scenarios with the existing (ED) and future (FD) dam development conditions. "Change" is the percent of change from the ED-PS scenario.

Existing dams (ED)	Loss (mcm)	Change (%)	Future dams (FD)	Loss (mcm)	Change (%)
ED-PS	289.2	-	FD-PS	290.8	0.5
ED-2K_CC	323.7	11.9	FD-2K_CC	326.0	12.7
ED-2K_GF	323.6	11.9	FD-2K_GF	325.5	12.6
ED-2K_HA	326.0	12.7	FD-2K_HA	327.7	13.3
ED-2K_MI	315.8	9.2	FD-2K_MI	316.9	9.6
ED-2K_MP	325.4	12.5	FD-2K_MP	326.8	13.0
ED-2K_MR	328.1	13.4	FD-2K_MR	330.1	14.1
ED-2K_AVR	324.3	12.1	FD-2K_AVR	326.1	12.7
ED-4K_CC	371.3	28.4	FD-4K_CC	373.1	29.0
ED-4K_GF	384.7	33.0	FD-4K_GF	386.9	33.8
ED-4K_HA	380.8	31.7	FD-4K_HA	382.4	32.2
ED-4K_MI	360.1	24.5	FD-4K_MI	361.2	24.9
ED-4K_MP	380.5	31.6	FD-4K_MP	381.9	32.0
ED-4K_MR	392.2	35.6	FD-4K_MR	394.0	36.2
ED-4K_AVR	382.7	32.3	FD-4K_AVR	384.3	32.9

4.5.7 Reservoir operation strategy to cope with climate change

As hydropower production strongly relate to inflow, the power generation for the NN1 power station could be varied significantly due to large variation in inflow projections. To mitigate the variability, implementing strategy such as changing the existing operation is necessary to address. **Fig. 4.10** shows the implementation of reservoir operation of the NN1 reservoir for the increasing trend of inflow (for example 4K_HA scenario). **Fig. 4.10a** shows the implementation by dropping the level of the NN1 rule curve to avoid a spill. By dropping the rule curve to a lower level, the results present that water spill is tended to decrease and energy production is tended to increase. Although dropping the level of rule curve over 2.5 m results in a higher reduction of the water spill, the head is reduced and result in less power output. The maximum increase in energy output has resulted when dropping the rule curve by 2.5 m with a 1.7% increase in energy production compared to the existing rule curve (dropping 0 m). **Fig. 4.10b** shows the implementation

by increasing installed power capacity. It is possible that in terms of the future inflow trend has increased, the stakeholders can consider installing more capacity to utilize additional water to get more power generation. The engineering design and construction processes are required. Furthermore, installing more power capacity, the implementation cost should be considered against the benefit of the increase in energy production. By increasing the capacity (with the existing rule curve), the results present that water spills are tended to decrease and energy production is tended to increase. Although the water spill is more decreased when increase capacity over 10%, it results in less energy output due to a large amount of water is discharged downstream which results in a reduction of water level in the reservoir (reduction head) leading to less power generation. The maximum increase in energy output has resulted when increasing the capacity by 10% with a 3.8% increase in energy production compared to the existing capacity.

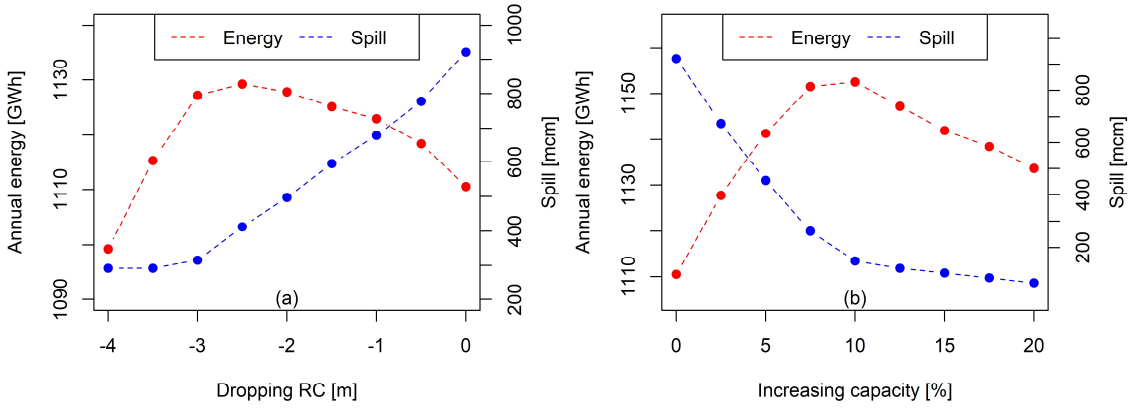

Fig. 4.10 (a) A relationship among dropping rule curve level, water spill and annual energy output of the NN 1 power station for FD_4K_HA. (b) A relationship among increasing installed capacity, water spill and annual energy output of the NN 1 power station for FD_4K_HA.

Fig. 4.11 shows the implementation of reservoir operation of the NN1 reservoir by changing the rule curve for the decreasing trend of inflow (for example FD_4K_MI scenario). **Fig. 4.11a** shows the shifting elevation of the NN1 rule curve at a different

level. **Fig. 4.11b** shows the implementation of the NN1 reservoir by shifting the rule curve to a higher level. By shifting the rule curve (as shown in **Fig. 4.11a**), a higher hydraulic head is provided due to higher reservoir water levels result in more energy production. As a result of the higher water level, the water spill is tended to increase. Although the water level in the reservoir is increased when shifting the rule curve with an average of shifting elevation higher than 2.5 m, the energy output is tended to decrease due to the higher water spill. The maximum increase in energy output has resulted when shifting the rule curve of the NN1 reservoir by 2.5 m on average with a 5.4% increase in energy production compared to the rule curve.

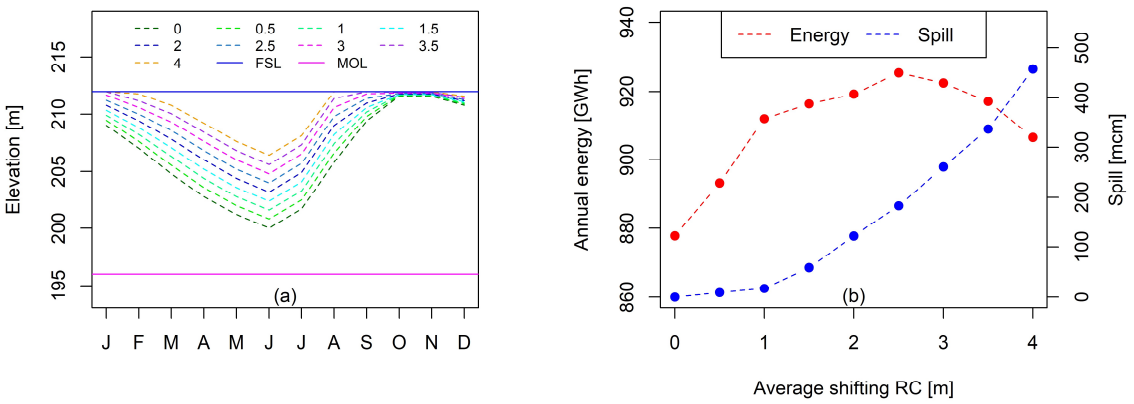

Fig. 4.11 (a) shifting elevation of the NN1 rule curve in different levels, the number shows the average shifting level of the rule curve from the existing in meter and (b) the relationship among annual energy, water spill and the shifting rule curve.

4.6 Conclusions

A change of long-term river flow projection covers a wide range dominated mainly by the difference in precipitation projections. The mean climate projection of +2K and +4K scenarios (2K_AVR and 4K_AVR) show a slight decrease in mean annual river flow. Even though the climate change dominates a primary effect on river flow in total annual amount, the impact on seasonal flow change is quite low compared to the effect of dam development. The effect of dam development shows a significant reduction in seasonal

flow variation at the downstream of the NN1 reservoir (regulated flow) in all climate scenarios compared to the natural flow condition (ND). At the full dam development stage (FD), all climate scenarios show a distinct trend of change in seasonal flow compared to the existing dam stage (ED) that there is a slight increase in the dry season and a slight decrease in the wet season due to an additional regulated storage of the under-construction dam (NN3).

Estimation of energy production of the NN1 power station under climate projections shows a large variation in mean annual energy output due to an uncertainty of river flow projections in different climate scenarios. At the full dam development stage (FD), the annual energy production has a slight increasing trend compared to the existing dam development stage (ED) due to the regulated flow from more storage of the upstream cascade dam.

As an increase in temperature projections, the NNBR seems to face a decrease trend in future precipitation. A combination of precipitation reduction and high temperature resulted in a reduction trend of river flow and hydropower production. Without any implementation, the existing operation will lead to loss in annual energy production. Thus, adaptive implementations are necessary to mitigate the impact of climate change on the long-term hydropower generation. Rule curve—a long-term hydropower operation is based—needs to be effectively managed to optimize hydropower production while other related purposes such as downstream flood risk, water demand deficit, ecosystems and social vulnerability are minimized.

Based on our approach for this study, there are some limitations. Firstly, by using delta method to project the climate variables, a lack of change in the variability and spatial patterns of climate. To access the spatial distribution and the variability of the projected climate, GCM downscale including bias correction process might be required.

Secondly, this study assumed that the hydrologic variables that have an influent in river flow projection (including basin land cover) are not change. For further study, land use change and upstream water use (irrigation or other purposes) might be taken into account.

As the operation of a large-scale dam with a large storage capacity can play a primary role in water resources management of the river basin. In order to improve the efficiency of reservoir operation, consideration of forecast information might be taken into account. However, the hydrological forecast contain a large uncertainty and it is difficult to

perfectly predict future conditions. Nohara *et al*. (2016) applied the ensemble prediction technique to support preliminary operation of the reservoir. The information including the possible conditions and the uncertainty of prediction can be important for more effective decision strategy for the reservoir real-time operation.

Chapter 5 Real-time optimization of a large-scale reservoir operation using adaptive river flow prediction

This chapter examines the application of ensemble weather forecasting for reservoir operations which provide hydropower and irrigation facilities in Thailand. Medium-range ensemble precipitation forecasts were employed using a hydrological model to predict the real-time reservoir inflow. The effects of initial conditions on the model inflow prediction were examined using different methods. Real-time optimization of the water release strategy, determined a week in advance, for hydropower generation and irrigation was conducted with different scenarios using dynamic programming considering inflow predictions. The medium-range ensemble precipitation forecast conducted by the European Centre for Medium Range Weather Forecasts was used to quantify precipitation for the study basin. The ensemble precipitation forecast with the hydrological model was employed for inflow prediction of the study basin (which was located in a tropical climate with a distinct wet and dry season). The initial conditions of the hydrological model influenced the real-time inflow forecast. To determine the initial conditions of the model, the empirical data assimilation considering a drainage area factor was utilized, and observed precipitation data were used as model input forcing data during the warmup period. This method improved the reservoir inflow prediction and reduced the computational cost. Real-time reservoir optimization using dynamic programming with considering ensemble forecasts provided more efficient operating decisions than employing historical data. This is despite the difficulties encountered while operating a reservoir in a tropical region with significant uncertainty regarding hydrological conditions. The resulting information will be useful for water resource management, which may be adapted to other basins in the study region.

5.1 Introduction

The Sirikit Dam is one of the two large reservoirs in the Chao Phraya River Basin (CPRB). The river basin is the largest (158,000 km^2) and most important in Thailand. The CPRB supports the local community and economy and generates 66% of Thailand's gross domestic product (Mateo, 2012). The Sirikit reservoir, containing 9,510 million m3 of the total storage volume, has a significant role in effectively managing the water resources of the basin. However, the basin is located in a tropical climate with significant seasonal differences and uncertainty regarding the basin's hydrological condition. These uncertainties have a primary effect on reservoir operation, increasing the risk of water shortages (Tingsanchali and Boonyasirikul, 2006).

For reservoir operations, the reservoir outflow must be determined. However, the decision is challenging because of the uncertainty regarding river flows. These uncertainties are significant in a tropical climatic region where hydrological characteristics have large seasonal variations. In addition, climate change complicates future water resource management because of increasing extreme weather fluctuations (Miles *et al*., 2000; Stocker *et al*., 2013).

Incorporating weather forecast data may improve the efficiency of decision making (Hamlet *et al*., 2002; Lettenmaier and Wood, 1993; Zhu *et al*., 2002). However, forecast data have accuracy limitations (forecast uncertainty) with increasing forecast time. Therefore, mid- or long-term forecast data are not currently used frequently in reservoir management practices (Nohara and Hori, 2018).

Using an ensemble forecast rather than a single (deterministic) forecast is an ideal solution to reduce forecast uncertainty because a set of random, equally probable (independent) forecasts are associated with the ensemble forecast (Zhu, 2005). In recent decades, ensemble forecast techniques have been rapidly developed. Ensemble forecast techniques are now generally accepted as a reliable approach for estimating forecast confidence, especially for high-impact weather (Bougeault et al., 2010). Based on these advantages, several studies have been conducted using ensemble forecast data, such as storm track prediction (Lin *et al*., 2020; Nishimura and Yamaguchi, 2015; Weber, 2003),

reservoir inflow prediction (Fan et al., 2015), river flow prediction, and flood forecasting (Alfieri *et al*., 2012; Bao *et al*., 2011; He *et al*., 2010; Sayama *et al*., 2020).

Many studies have been conducted regarding ensemble streamflow predictions to improve reservoir operation efficiency (Alemu *et al*., 2011; Faber and Stedinger, 2001; Kim *et al*., 2007). In addition, some studies have introduced operational ensemble hydrometeorological predictions to reservoir operation for water use (Nohara *et al*., 2016; Nohara and Hori, 2018). Although these studies considered ensemble predictions for reservoir optimization, information regarding the methods for performing reservoir inflow forecasts using ensemble hydrometeorological predictions is scarce. This procedure becomes more important for a reservoir located in a tropical-climate basin with distinct wet and dry hydrological conditions, such as the CPRB.

This study investigates forecasting river flows using a distributed hydrological model with ensemble precipitation forecasts (EPF) for real-time reservoir optimization using dynamic programming (DP). For this purpose, a physical distributed hydrological model is adopted. An adaptive mode of operation (state variable update) with different update procedures to assess the effect of the model's initial state condition on the results of river flow forecasts is also utilized. Medium-range EPFs are used to determine the reservoir inflow two weeks in advance of reservoir inflow forecast. Then, the optimization of reservoir release is examined in different scenarios of optimization using the two-week inflow forecasts. In Section 5.2, the hydrological model is calibrated and validated prior to its adoption and use for forecasting. In Section 5.3, the methodology of implementing the real-time inflow forecast using precipitation forecasts is described, and the effect of the model's initial conditions with different model state update procedures on the inflow forecast results is evaluated. In Section 5.4, real-time reservoir optimization for one-week advanced release strategy using forecast inflows is examined with different scenarios regarding future long-term inflow assumptions. In Section 5.5, the advantages of introducing ensemble hydrometeorological forecasts are demonstrated for real-time optimization of Sirikit reservoir operation during 2019.

5.2 Reservoir inflow prediction model

5.2.1 Hydrological model

The improved 1K-DHM that incorporate the unconfined bedrock aquifer as described in Chapter 2 is applied for the reservoir inflow prediction in this chapter. The model should be calibrated and validated before applying it to the inflow forecast. To apply the model for long-term forecasting, periods should contain the seasonal hydrological characteristics of the basin (wet and dry seasons). The SCE-UA algorithm (Duan *et al*., 1994) was applied to optimize the model parameters by searching for the parameter with the smallest root mean square error (RMSE) when compared with observations. Designing the range of the parameters is important to identify the parameter set. The model calibration method was described by Meema and Tachikawa (2020).

The inflow of the Sirikit reservoir in 2014, which is considered a normal hydrological year, was selected as the calibration period. The optimized model parameters are listed in **Table 5.1**. The same parameter set was applied to the validation periods in 2008 and 1998, which were considered wet and dry, respectively.

The model performed well in both calibration and validation periods with an RMSE less than 63.9 million m^3 and Nash–Sutcliffe efficiency (NSE) coefficient greater than 0.82, as shown in the comparison between simulated and observed inflow of the reservoir in **Fig. 5.1**. The model efficiently represents the inflow characteristics of the basin for both the wet and dry seasons for all simulation periods. This model, with the optimized parameter set, was applied to produce real-time inflow forecasts for the 2019 Sirikit reservoir.

Table 5.1 Optimized parameters of the hydrologic model.

Parameter	Units	Value
n_s	$m^{-1/3}/s$	0.975
k_a	m/s	1.14×10^{-4}
d_a	m	3.179
d_m	m	2.984
β	-	19.906
k_u	m/s	8.46×10^{-5}
d_u	m	0.323
k_v	m/s	1.08×10^{-7}

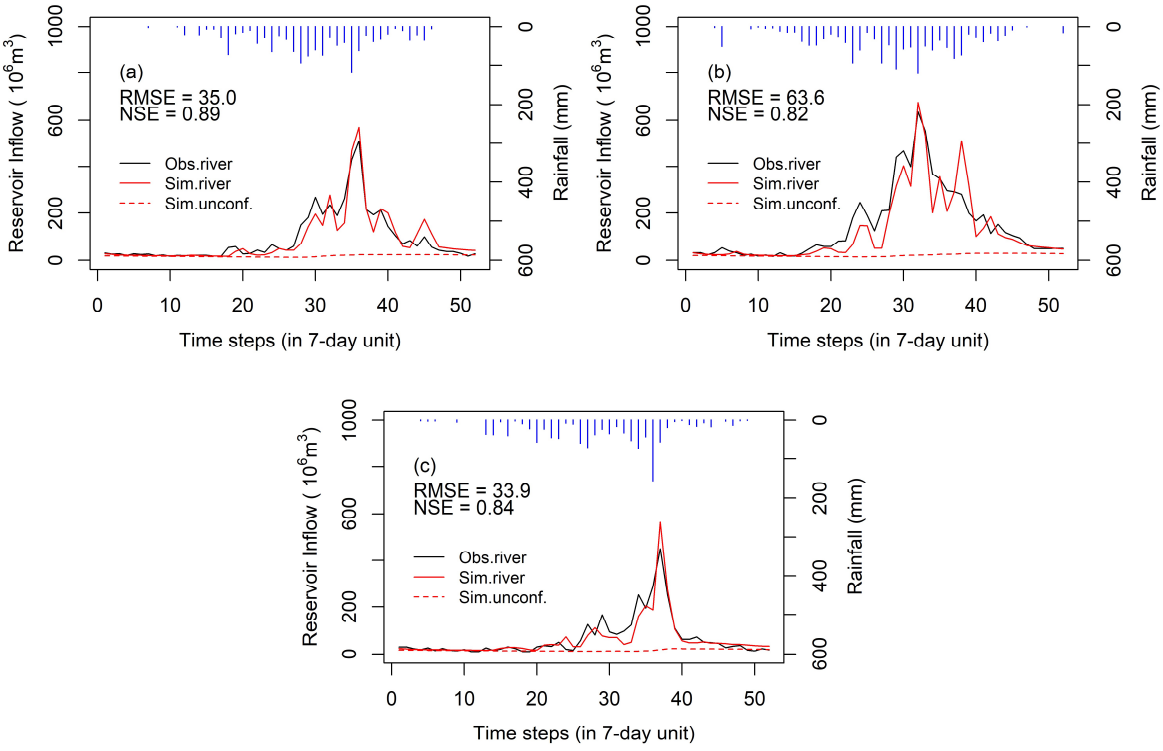

Fig. 5.1 Comparison between simulated and observed inflow at the Sirikit dam (a) during the calibration period (b) validation period 1 (c) validation period 2 (RMSE [million m^3] and NSE [-]).

5.2.2 Estimation of actual evapotranspiration

To predict the reservoir inflow in the Nan River Basin, the actual evapotranspiration (AET) is important especially during the dry season or less of precipitation period. For this study, the long-term estimation of daily average AET is adopted in inflow prediction period.

To estimate AET in Nan River Basin, assume that the error in the water balance calculated from AET is equal to zero, the annual AET can be estimated using **Eq. 3.6** which the inflow of Sirikit Dam is used as annual river discharge (Q). Thus, the estimation of annual AET for Nan River Basin is presented in **Fig. 5.2**.

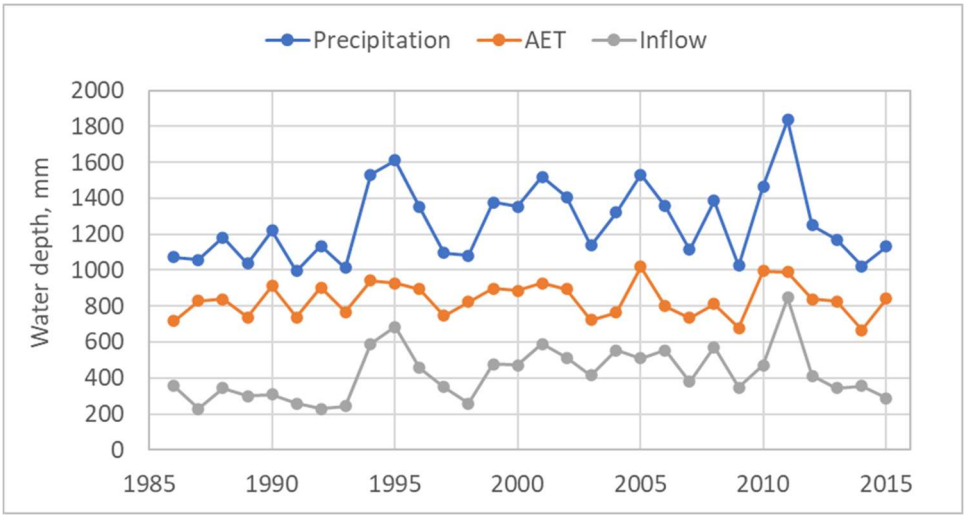

Fig. 5.2 Estimation of long-term AET for Nan River Basin

5.3 Ensemble inflow prediction using European Centre for Medium Range Weather Forecasts (ECMWF) precipitation forecast

5.3.1 Ensemble precipitation forecasts (EPF)

TIGGE (THORPEX Interactive Grand Global Ensemble) is a database of ensemble medium-range forecasts conducted by different forecasting centers worldwide for conducting scientific research (Bougeault *et al*., 2010). Ensemble Prediction System data are available from approximately ten of these forecasting centers.

Among all data on TIGGE, ECMWF has superior performance compared to other forecasting systems (Buizza *et al*., 2005). Therefore, it was selected as the EPF data for

generating reservoir inflow forecasts in this study.

The ECMWF forecasts consist of 51 members of precipitation with approximately 0.5° resolution for the whole globe. Initial uncertainties are considered using a singular vector technique. A stochastic scheme is used to model uncertainties resulting in possible variations in physical parameterizations (Buizza *et al*., 2007). The data are available twice a day at 00:00 UTC and 12:00 UTC with time steps of 6 h and 15 d.

5.3.2 Real-time state update of hydrological model

The update procedure of the model state variables is based on observed errors in river flow, and empirical methods or Kalman filtering has been used (Moore *et al*., 2005; Romanowicz *et al*., 2006). Using Kalman filtering with complex distributed and nonlinear models results in highly complex computations (O'Connell and Clarke, 1981). A cost-effective approach has been developed for computation using an empirical data assimilation procedure and applied to a large-scale hydrological model (Collischonn *et al*., 2005).

Therefore, we adopted this empirical data assimilation procedure to incorporate the large-scale distributed hydrological model (as explained in Section 5.2.1) to obtain the initial state of the basin (at *t*0) using observed and ensemble precipitation forecasts as the model input prior to performing reservoir inflow forecasts. The updating correction factor (*FCA*) is calculated at gauge station *k* using the following equation:

$$FCA_k = \frac{Q_{obs,k}}{Q_{cal,k}} \tag{5.1}$$

where $Q_{obs,\,k}$ and $Q_{cal,\,k}$ are the observed and calculated river discharges at gauge station *k*.

To evaluate the updating procedure during the warmup period, different empirical equations were investigated in this study. First (model states update type 1), the correction factor is directly applied to update the state variables for any cell *i* located upstream of gauge station *k* as expressed in **Eq. 5.2**. Second (model states update type 2), the correction factor is applied to correct the state variables for any cell *i* located upstream of gauge station *k* considering a drainage area factor of the upstream grids at each cell, as expressed in **Eq. 5.3**.

$$S_{up,i,k} = FCA_k \cdot S_{cal,i} \tag{5.2}$$

$$S_{up,i,k} = FCA_k \cdot S_{cal,i} \cdot \left(\frac{A_i}{A_k}\right) + S_{cal,i} \cdot \left(1 - \frac{A_i}{A_k}\right) \quad (5.3)$$

where $S_{up,\,i,\,k}$ are the updated model state variables at cell i located upstream of gauge station k, $S_{up,\,i,\,k}$ can be substitute with the variables of the hydrological model such as river discharge (Q), lateral discharge from the surface soil layer (q_s), and the bedrock aquifer layer (q_u); A_i and A_k are the drainage areas upstream of cell i and gauging station k.

5.3.3 Real-time reservoir inflow forecast algorithm

Fig. 5.3 illustrates the procedure of the reservoir inflow forecast using the EPF. The simulation can be divided into two periods: the warmup and forecast periods. For real-time forecasting, it is necessary to operate the model in adaptive mode (Moore *et al.*, 2005) for which the model output is based on previous model inputs as well as previously observed information that is used to update the model prior to a new forecast. Thus, this study proposes a warmup period to account for uncertainties in the model initial conditions before the forecast period is performed. For this purpose, data assimilation (as explained in Section 5.3.2) is adopted to improve the estimate of the initial states of the model and to reduce the simulation errors in the forecast period (Madsen and Skotner, 2005).

We not only considered model state variables for the data assimilation implementation, but also the errors due to model input. To assess the errors due to input data during the warmup period, two procedures of input precipitation data for the model were considered. First, a single pattern of observed data was applied to the model. Second, a combination of observed data and ensemble forecasts with 52 patterns (one pattern of observation + 51 patterns of ensemble forecasts) of precipitation was applied to the model. **Fig. 5.3a** describes the procedure of using observed precipitation and model state updates up to the starting time of the forecasts ($t0$). Then, the EPFs were applied to the model as forcing input data up to the lead time (t+15) for the 15-d reservoir inflow forecasts. **Fig. 5.3b** describes the procedure of using a combination of observed and ensemble forecast data and the update procedure of the model states up to the starting time of the forecasts ($t0$). Using 52 precipitation patterns during the warmup period, 52 flow patterns were obtained. To select the flow pattern that represents the model states at the starting time of the forecasts ($t0$), the highest NSE coefficient computed from the comparison between each

simulated flow pattern with the observation during the warmup period was selected.

Data assimilation methods used during the warmup period to reproduce the initial state of the model at the initial time of the forecast (*t*0) are summarized in **Table 5.2**. The model state variables were updated in forecast methods 1 and 2 using **Eq. 5.2** and in forecast methods 3 and 4 using **Eq. 5.3**. A single pattern of observed precipitation was used in forecast methods 1 and 3 (**Fig. 5.3a**). For forecast methods 2 and 4, 52 precipitation patterns were used (**Fig. 5.3b**). For the forecast period (all methods), precipitation forecasts were used, and the observed precipitation was applied in this study to evaluate the inflow forecast procedures as a possibly perfect forecast of precipitation.

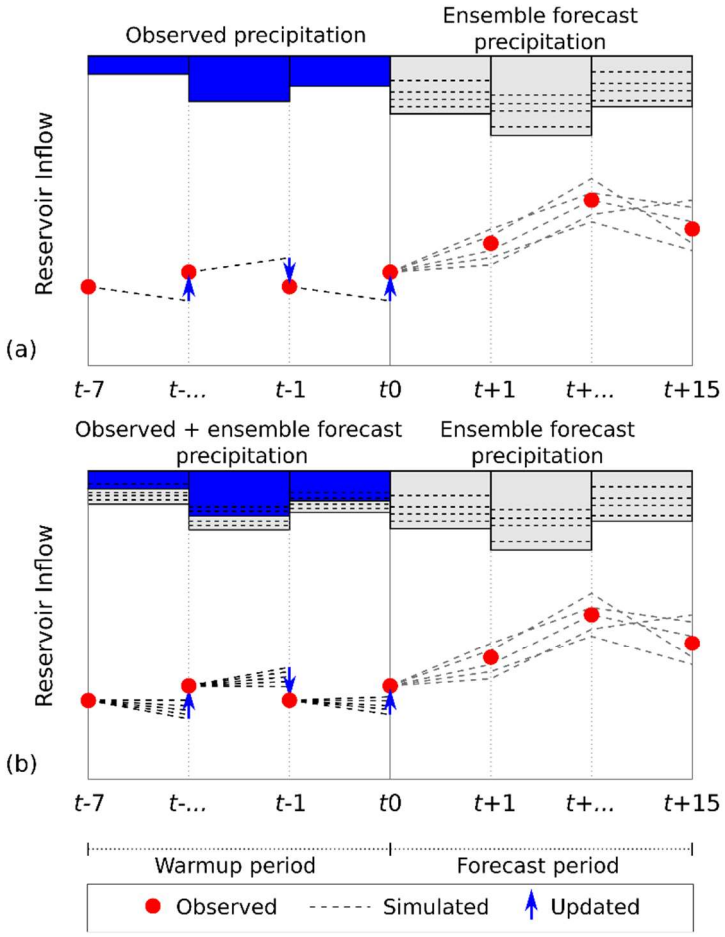

Fig. 5.3 Schematic of inflow forecast procedure using (a) observed rainfall and (b) a combination between observed and end ensemble forecasts up to the starting time of the forecasts (*t*0), and ensemble precipitation forecast up to the lead time.

Table 5.2 Description of data assimilation methods used in the warmup period and input forcing data for each simulation period

Method	Warmup period (t-7 − t0)			Forecast period (t0 − t+15)	
	State update type	Input data	No. input pattern	Input data	No. input pattern
1	1	Obs.	1	Obs. + Ens. Forecast	52
2	1	Obs. + Ens. Forecast	52		
3	2	Obs.	1		
4	2	Obs. + Ens. Forecast	52		

5.4 Reservoir optimization with ensemble inflow forecast in Sirikit Dam

5.4.1 Current reservoir operation of the Sirikit Dam

The Sirikit Dam contains 6,660 million m^3 of effective storage and 500 MW of power generation capacity located on the Nan River, the main tributary of the Chao Phraya River. The dam controls 13,130 km^2 of drainage area. The main functions of the dam include irrigation purposes, domestic and industrial use, flood control, ecological conservation, and power generation (Amnatsan *et al*., 2018). The location of the study basin is shown in **Fig. 5.4**.

Due to unpredicted inflow, reservoir operation faces significant challenges in controlling water for society. In 2019, the reservoir storage level was higher than the lower rule curve (LRC) at the beginning of the year, and the reservoir release was still above average because of the downstream demand and power supply requirement during the dry season. However, the low inflow volume from the beginning to the middle of the wet season was unexpected. This event presented difficulties for reservoir operation and resulted in a low storage level (lower than LRC) after mid-August.

Fig. 5.5 shows the operation records of the Sirikit reservoir during 2019. Compared to the 30 years historical data, the reservoir inflow volume is low (lower than 25th percentile), as shown in **Fig. 5.5a**, whereas the released volume is relatively high (close to the 75th percentile), as shown in **Fig. 5.5b**. This difference led to a low level of reservoir storage at the end of the year (significantly less than the LRC), as shown in **Fig. 5.5c**.

For effective basin water management, reservoir operation requires forecasting

information. Therefore, we selected this period as a case study to evaluate the performance of release strategy estimation forecasting one-week in advance using medium-range weather forecast information and the reservoir optimization process.

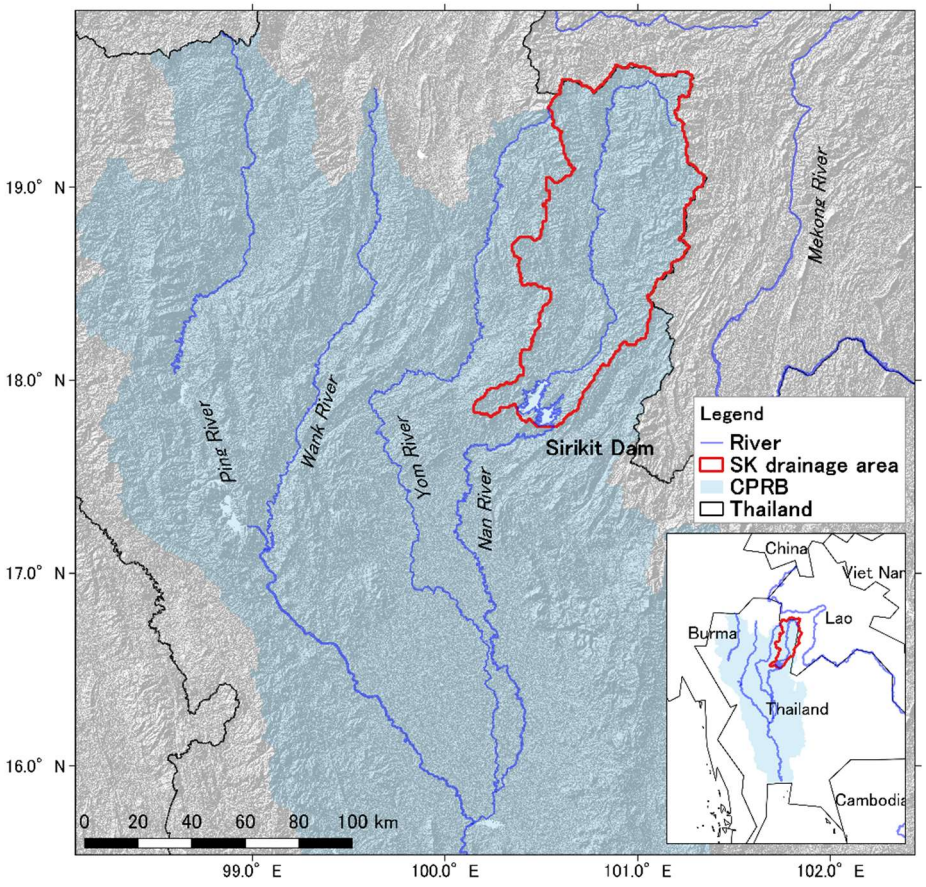

Fig. 5.4 Location of study basin and the Sirikit Reservoir (SK).

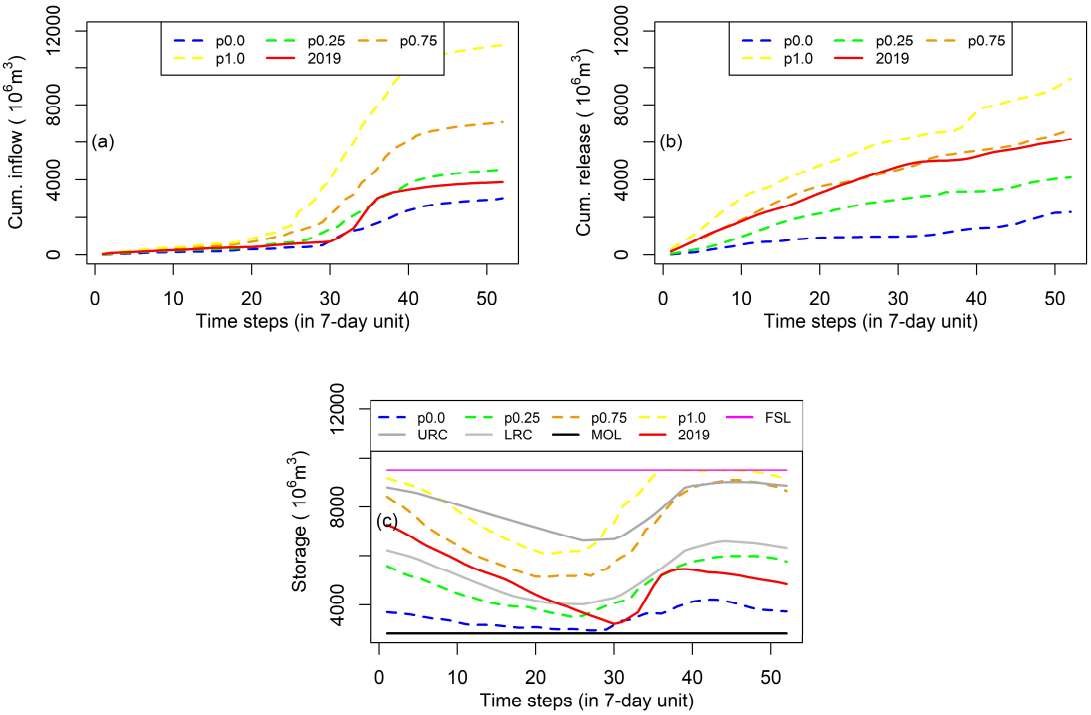

Fig. 5.5 Operation record of Sirikit Reservoir in 2019 (a) reservoir inflow compared to historical record (b) release compared to the historical record and (c) reservoir storage (p0.0 is minimum, p0.25 is 25th percentile, p0.75 is 75th percentile and p1.0 is maximum).

5.4.2 Optimization framework for dam release strategy using DP

The objective of this study is to develop a future release strategy for large-scale reservoirs using weather forecasts. For this purpose, the optimization process of the released strategy for long-term reservoir operation using EPF is illustrated in **Fig. 5.6**.

For real-time river flow forecasting, an initial condition setting of the hydrological model is necessary. The previous week's (*t*-1) flow condition was simulated with observed rainfall (forecast method 3 was selected, discussed in Section 5.5.2) as the model warmup in adaptive mode (data assimilation is associated). The model state variables at the beginning of the forecast period obtained from the simulation in the warmup period were assigned to the model as the initial state condition (see Section 5.3).

The two-week inflow forecast (Q_t and Q_{t+1}) obtained from the hydrological model (simulated with two-week advanced EPF) was input into the DP to optimize the one-week advanced release strategy (R_t) at any storage level (see Section 5.4.3). To optimize the release strategy, the future benefit at the end of the target period (F_{t+2}) is required to associate the penalties to lower storage levels of the reservoir (see Section 5.4.4). Objective functions such as irrigation and hydropower benefits are required for the optimization process (see Section 5.4.5). Reservoir information such as elevation-storage-area, maximum–minimum storage, evaporation rate from the water body at any stage, and generated power capacity are required. Furthermore, the minimum and maximum released capacities are assigned to the DP algorithm as the constraint for the reservoir release condition.

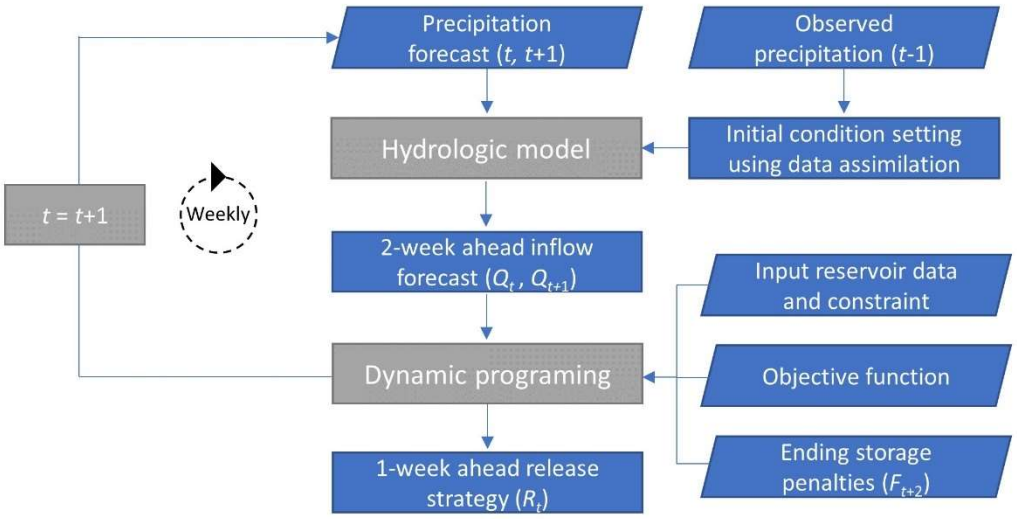

Fig. 5.6 Optimization of dam release strategy for long-term reservoir operation using EPF.

5.4.3 Application of DP for reservoir optimization

To interpret the results of the ensemble inflow forecast, the general method is to consider the mean value (ensemble mean) or median, which represents the tendency of all ensemble forecast members. To optimize the operation strategy of the reservoir using the ensemble mean or median of the ensemble inflow forecast, the deterministic DP (DDP) can be applied (Nohara and Hori, 2018).

By using DDP in reservoir problems, the reservoir storage at time t is divided into decision-making stages (S_t). The optimized water release (R_t) at each state is selected based on the maximum value of the sum of the current benefit ($B_t(R_t)$) and future benefit ($F_{t+1}(S_{t+1})$). The computation is started at the end of the optimization time (the final stage) and then moved backward to the beginning stage (Louoks and Falkson, 1970). The recursive equation for optimization can be defined by the following equation:

$$F_t(S_t) = \max\left[B_t(S_t, Q_t, R_t) + F_{t+1}(S_{t+1})\right] \tag{5.4}$$

where t is the time period, and $B_t(\cdot)$ is the benefit function of period t.

The storage (state variable) can be described using the reservoir continuity equation as follows:

$$S_{t+1} = S_t + Q_t - R_t - e_t(S_t, S_{t+1}) \tag{5.5}$$

where S_t is the storage at the beginning of period t, Q_t is the reservoir inflow for period t, $e_t(S_t, S_{t+1})$ is the loss due to reservoir evaporation during period t, which can be calculated as follows:

$$e_t(S_t, S_{t+1}) = A(S_t, S_{t+1}) \cdot ev_t \tag{5.6}$$

where $A(S_t, S_{t+1})$ is the reservoir surface area for period t, and ev_t is the evaporation rate from the water body during period t.

5.4.4 Implementation with the optimized strategy and scenarios

We assume that the simulation for 1-week in advance released strategy performs every Sunday. The volume of water released from the reservoir follows the simulated strategy throughout the week. A total of 52 weeks in 2019 was the target period of this study.

Fig. 5.7 presents the optimization scheme for a target week (t) release strategy using DP. To adopt DP, the penalties must be utilized at lower reservoir storage levels after the final time step of optimization. This is to ensure that the reservoir will not draw down to low storage levels by releasing excess water to generate quantified benefits during the optimized period. For this purpose, the sum of future benefits was applied to each storage level after the final time step of the optimization (F_{t+2}) as losses or penalties.

To calculate penalties at the stage of t+2 (F_{t+2}) for each storage level, the next year's benefits (possible future benefit in 2020) were also considered. However, to begin the calculation of the DP recursive equation, as expressed in **Eq. 5.4**, the initial assumption is that all future benefits (losses or penalties) will be zero at some point of time (Loucks

et al., 2005). For this purpose, a dummy year was proposed to quantify the benefits or penalties at the end of 2020 ($F_{T'+1}$), avoiding the assumption of terminating operation. The 50th percentile of the 30-year historical data was used for the reservoir inflow in the dummy year. Thus, all future benefits (losses or penalties) after the final stage of the dummy year (F_{T*+1}) were defined as 0. Following **Eq. 5.4**, we can start calculating the penalties (F) in each stage progressing backward to the stage after the optimization period (t+2). Finally, the penalties at the stage after the optimization period (F_{t+2}) for each storage level were obtained.

According to the limitation of forecast information (approximately two weeks), the future long-term reservoir inflow that is used to calculate the penalties after the optimization period (t+2) was proposed with different assumptions, which is summarized in **Table 5.3**. The general method for future inflow assumptions is to use the 50th percentile of historical data for all remaining periods (up to the end of 2020). This is proposed in Scenario 1. The 25th percentile of historical data was adopted in Scenario 2, assuming drought conditions.

To assess the effect of the future inflow assumption, it was assumed that the assumption is perfect, as proposed in Scenario 3. A combination of perfect forecasting and future assumptions was proposed in Scenario 4. To assess the effect of the use of forecast inflow in optimization, Scenario 5 was introduced with the general procedure using the 50th percentile of historical data as the future inflow assumption.

The one-week advanced release strategy (R_t) obtained from the optimized process can be implemented for any initial reservoir storage level (S_t) at the target time (t). This signifies that this strategy can be implemented under different flow patterns using linear interpolation among the release tables obtained from the optimization process.

To determine the strategy performance, the strategies were utilized on observed flow patterns (using a forward calculation). The strategy performance is evaluated based on the sum of the benefits from the present to the future using the same objective function. Storage of the target time (S_{t+1}) can be estimated using **Eq. 5.5**, which will be the initial storage of the following time step. The same procedure will be repeated with the next operation strategy.

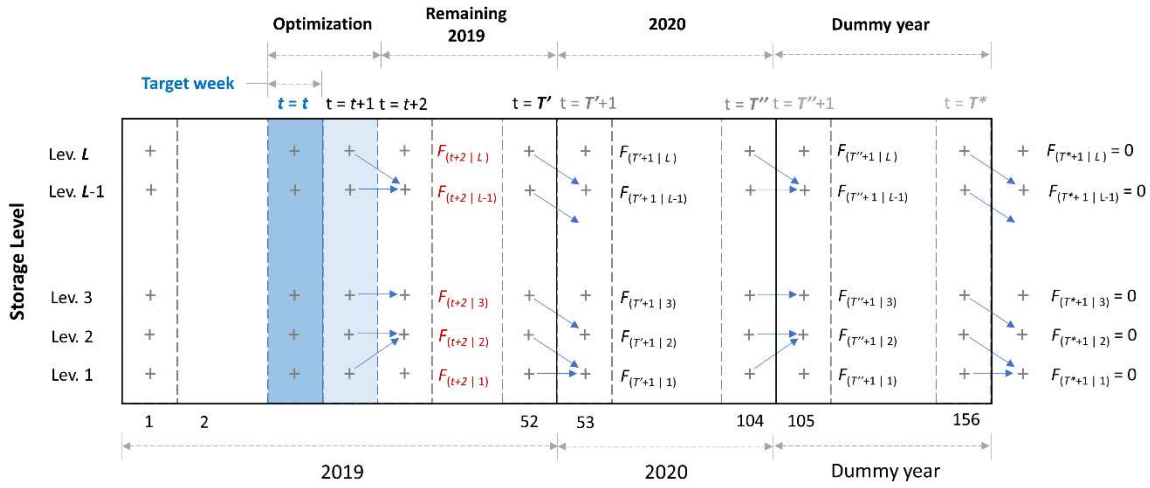

Fig. 5.7 Optimization scheme for any target week release strategy (R_t) and calculation of ending storage penalties ($F_{(t+2)}$) using DP.

Table 5.3 Description of optimization scenarios with different future long-term inflow assumptions for each period. (Hist. is historical data, p50 and p25 are 50th and 25th percentile respectively).

Scenarios	Periods			
	Optimization	**Remaining 2019**	**2020**	**Dummy**
Scenario 0	baseline scenario (actual operation)			
Scenario 1	Forecast mean	Hist. p50	Hist. p50	Hist. p50
Scenario 2	Forecast mean	Hist. p25	Hist. p25	
Scenario 3	Forecast mean	2019	2020	
Scenario 4	2019	2019	2020	
Scenario 5	Hist. p50			

5.4.5 Objective function

The objective function for the reservoir operation optimization may be defined as a maximization of the total benefit over the study period. In this study, irrigation and hydropower benefits were considered as functions of reservoir release. The objective function for this problem is expressed as follows:

$$max \sum_{t=1}^{T} B_t \tag{5.7}$$

where T is the number of optimization stages, and B_t is the total benefit at stage t, which can be expressed as follows:

$$B_t = B_t^{irr} + B_t^{hdp} \tag{5.8}$$

where B_t^{irr} and B_t^{hdp} are irrigation and hydropower benefits at stage t, respectively.

For the irrigation objective, the relationships between irrigation loss-benefit (B_t^{irr}) and the release of Sirikit reservoir (R_t) were obtained from Tingsanchali and Boonyasirikul (2006). To apply this relationship to this study, the present value of irrigation loss-benefit was estimated based on **Eq. 5.9**, as shown in **Fig. 5.8**.

$$B_t^{irr\,(2019)} = B_t^{irr\,(2006)} \cdot (1 + ir)^N \tag{5.9}$$

where $B_t^{irr\,(2006)}$ is irrigation loss-benefit in 2006, $B_t^{irr\,(2019)}$ is irrigation loss-benefit in 2019, N is the number of years, and ir is the interest rate, with an average rate of 2.4 % between 2006 and 2019 (Bank of Thailand, 2021).

For hydropower benefit (B_t^{hdp}), a fixed tariff rate of hydropower of 0.0375 per kWh is used according to the Electricity Generating Authority of Thailand (EGAT) (Tingsanchali and Boonyasirikul, 2006). As this fixed tariff rate is the official rate according to the power purchase agreement between EGAT and its customer, the hydropower benefit can be expressed as follows:

$$B_t^{hdp} = Tariff \cdot \eta \cdot g \cdot R_t \cdot H_t \tag{5.10}$$

where *Tariff* is the tariff rate, η is the turbine efficiency, g is the gravitational acceleration, R_t is the discharged discharge through the turbine (we assume that water is released downstream from the reservoir through the turbines), and H_t is the hydraulic head, which can be calculated as follows:

$$H_t = WL_t(S_t, S_{t+1}) - TWL - H_{loss} \tag{5.11}$$

where WL_t is the reservoir water level, TWL is the tailwater level downstream of the dam, and H_{loss} is the hydraulic head loss.

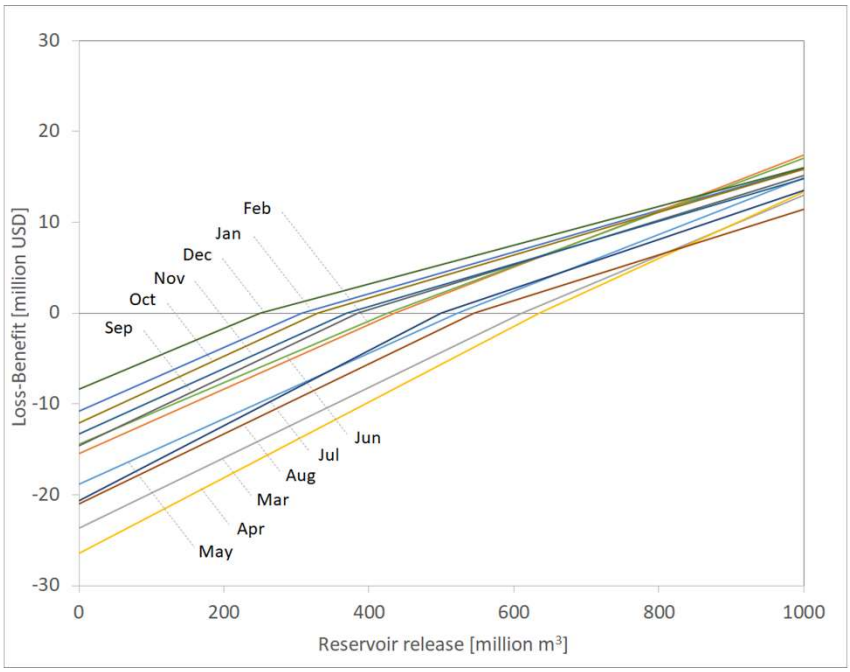

Fig. 5.8 Irrigation loss-benefit function base on the release of the Sirikit reservoir.

5.5 Results and discussion

5.5.1 Performance of EPF

Fig. 5.9a and **Fig. 5.9b** present the comparison of accumulated basin-averaged precipitation between forecasts and observations for accumulated 1 week (days 1–7) and accumulated 2 weeks (days 1–14), respectively. The forecast is capable of estimating precipitation during the dry season (around weeks 1–17 and weeks 45–52). However, during the wet season, there are some differences between precipitation forecasts and observation, especially during the start to mid of the wet season (around weeks 18–29), which resulted in an overestimation of the accumulated precipitation for both 1 week and 2 weeks.

In contrast, using the mean of forecast ensembles for accumulated basin precipitation, the forecast performed well, when compared to the observation, with an RMSE value of 22.6 mm (2.0% relative difference using annual precipitation) and 43.6 mm (3.9% relative

difference using annual precipitation) for 1 week and 2 weeks, respectively.

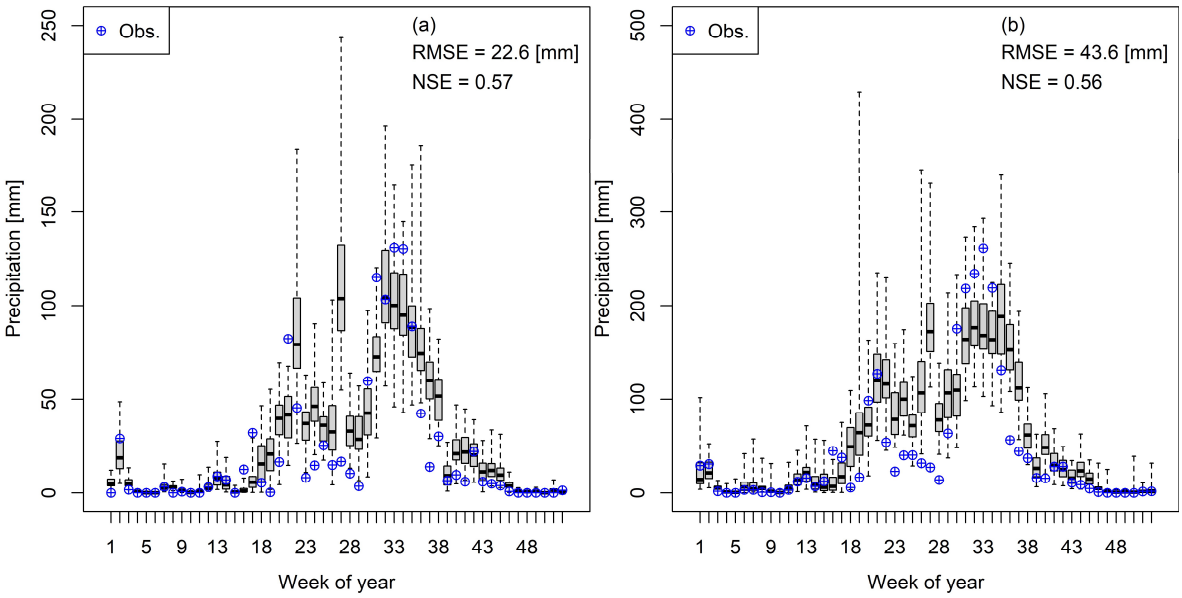

Fig. 5.9 Comparison of accumulated basin-averaged precipitation between observed and forecasts (a) one week of forecast (b) two weeks of forecast.

5.5.2 Performance of inflow forecasting

Fig. 5.10 and **Fig. 5.11** present the reservoir inflow comparison between forecasts (box plot) and observations in different forecast methods for one and two weeks accumulated inflows, respectively. Precipitation forecasts were used during the forecast period, and the observed precipitation was adopted to evaluate the forecast procedure as a possible perfect forecast. The performances of inflow forecasts such as RMSE and NSE in different forecast methods were calculated by comparing the mean of the forecast ensembles with the observations, as summarized in **Table 5.4**.

Table 5.4 performance of inflow forecasts in different forecast methods and input forcing data (RMSE [million m^3] and NSE [-]).

Method	One-week				Two-week			
	Forecasts		Observation		Forecasts		Observation	
	RMSE	NSE	RMSE	NSE	RMSE	NSE	RMSE	NSE
1	104.2	0.32	124.0	0.04	236.5	0.07	208.4	0.28
2	126.6	0.004	103.3	0.34	270.5	-	178.2	0.47
3	36.1	0.92	33.2	0.93	78.7	0.90	48.5	0.96
4	43.5	0.88	33.7	0.93	105.9	0.81	58.4	0.94

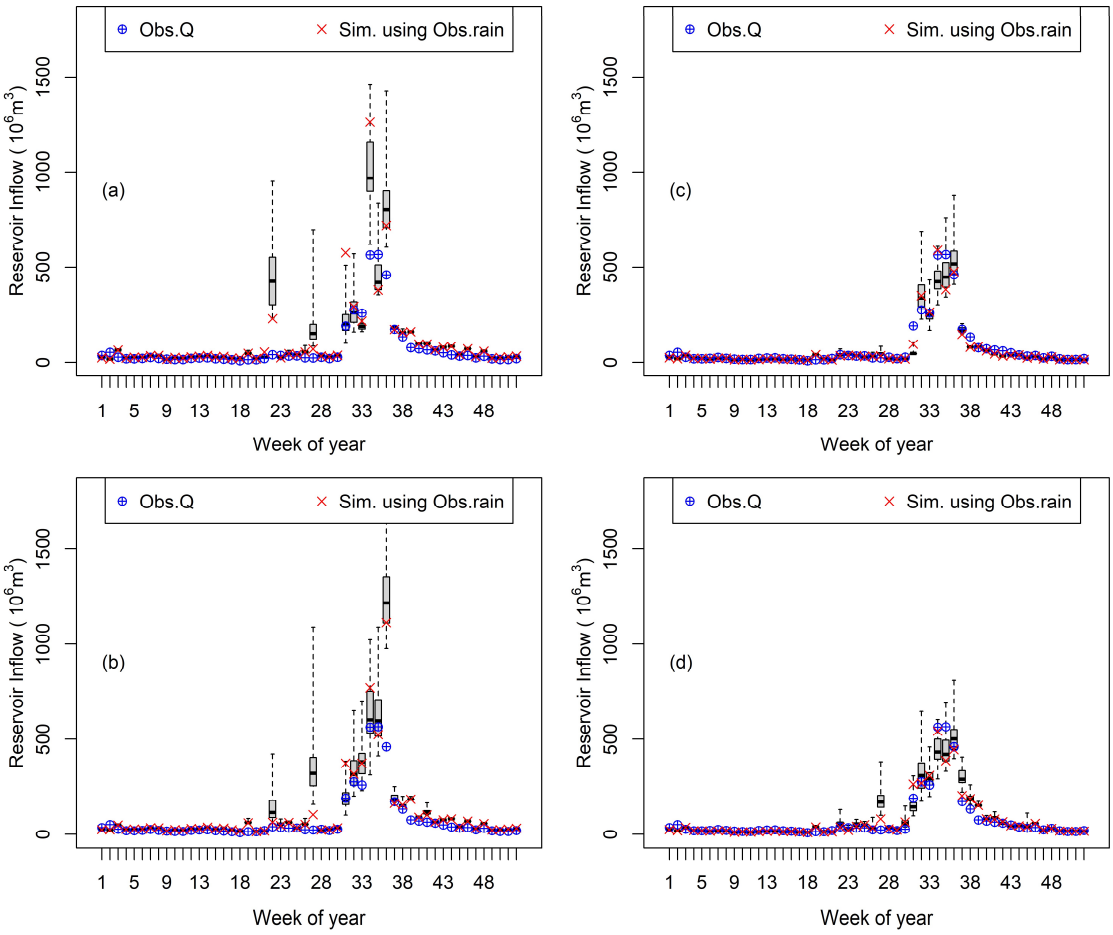

Fig. 5.10 Comparison of accumulated one week reservoir inflow between forecasts (box plot) and observation in different forecast methods (a) method 1 (b) method 2 (c) method 3 and (d) method 4.

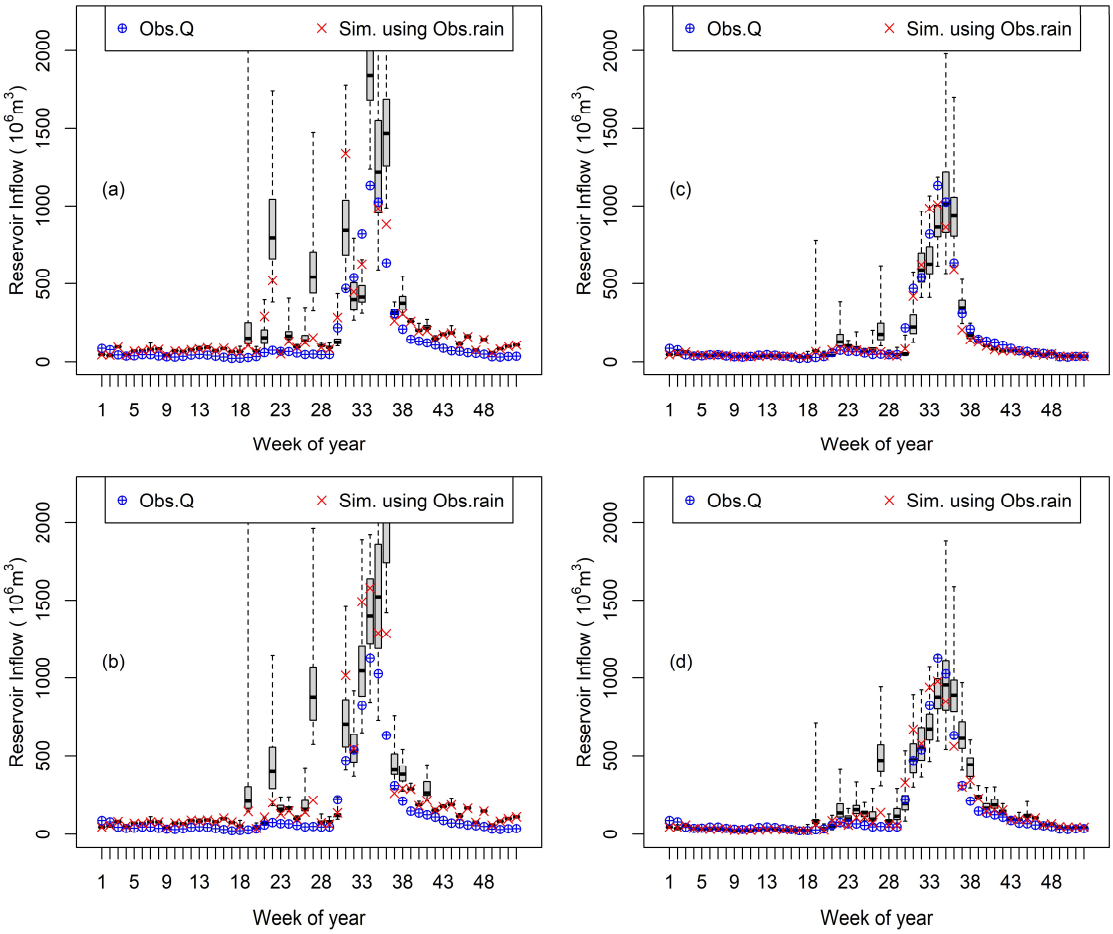

Fig. 5.11 Comparison of accumulated two weeks reservoir inflow between forecasts (box plot) and observation in different forecast methods (a) method 1 (b) method 2 (c) method 3 and (d) method 4.

According to the results obtained from different forecast methods, the model initial state condition (including its spatial distribution) has a primary effect on inflow forecasts. This results in a significant difference in the forecast inflow volume. Using the state update a type 1 scenario (applied same ratio to all upstream grids), the forecast inflow had a significant fluctuation among the forecast members compared to using the state update type 2. The use of forecast and observed precipitation resulted in a significant difference in the forecast volume, especially during high flow (see **Fig. 5.10a**, **5.10b**, **5.11a**, and **5.11b**). Moreover, the two-week accumulated inflow forecast resulted in a significant overestimation throughout the year compared to the observations (see **Fig. 5.11a** and **Fig. 5.11b**).

Using the state update type 2 (considered grid drainage area), the inflow forecast had more stable results among the members compared to the results obtained from the type 1 state update. There is no primary difference in the simulated results obtained using forecasts and observed precipitation (see **Fig. 5.10c**, **5.10d**, **5.11c**, and **5.11d**). Furthermore, the accumulated forecast inflow for one and two weeks corresponded well with observations.

This may be described by comparing the spatial distribution of the model's initial state (the model state at the initial forecast time, *t*0) that resulted in a difference in the forecast inflow. For example, **Fig. 5.12** presents a comparison of the initial model state spatial distribution for week 31 (July 28, 2019, 00:00 UTC) using different forecast methods. **Figs. 5.12a−5.12d** present the distributed grid discharge ranged from 0.0−265.0 m^3/s that emphasize the discharge state in the mainstream. **Figs. 5.12e−5.12h** present the distributed grid discharge ranged from 0.0−1.0 m^3/s that emphasize the discharge state for the most of catchment area (small streams). The spatial distribution of discharge state at the upstream grids shows a difference in value compared among different update methods (see the procedure in Section 4) in contrast to the river discharge at the basin outlet (observed station) having the same value for all methods. **Fig. 5.12a**, **5.12b, 5.12e** and **5.12f** present the spatial distribution of the initial model state resulting from update procedure type 1 that the correction factor (*FCA*) is directly applied to update the state variables for any upstream grid of the observed station as expressed in **Eq. 5.2**, which exhibited greater river discharge at the upstream grids than **Fig. 5.12c**, **5.12d, 5.12g** and **5.12h** resulting from update type 2 that the correction factor (*FCA*) is reduced when updating the state variables for any upstream grid based on a drainage area factor at each cell (the ratio of drainage area between any upstream grid and the observed station) as expressed in **Eq. 5.3**.

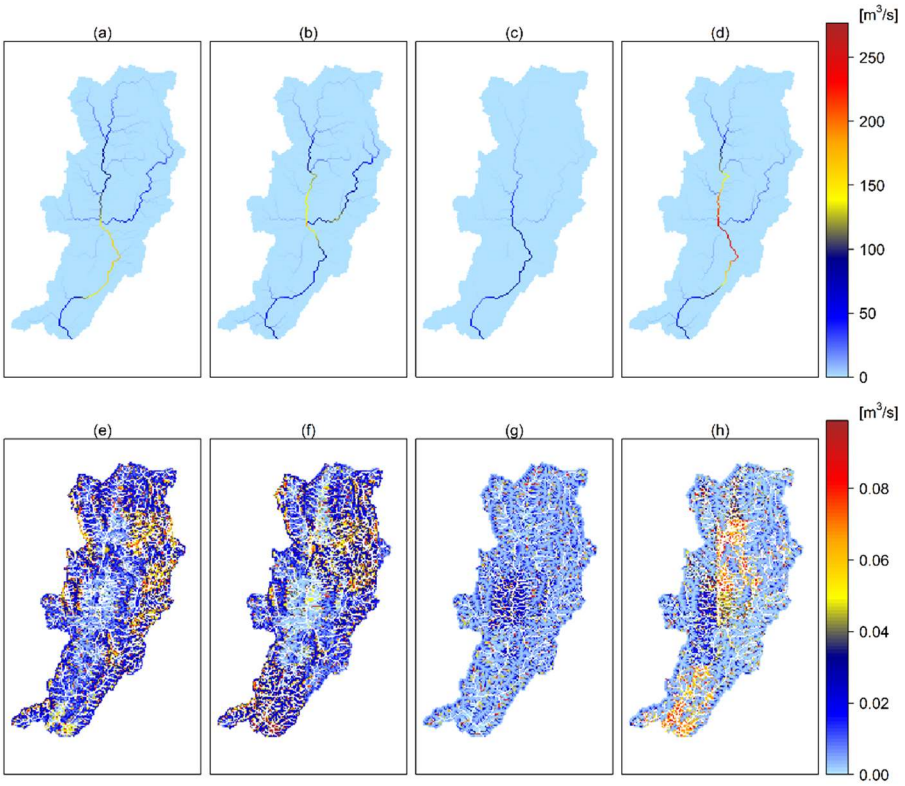

Fig. 5.12 Comparison of initial state conditions for the simulation of week 31 among different forecast methods (a) method 1 (b) method 2 (c) method 3 and (d) method 4 which value range from 0.0−265.0 m^3/s, (e) method 1 (f) method 2 (g) method 3 and (h) method 4 which value range from 0.0−1.0 m^3/s.

The difference in the initial state value resulted in different inflow forecasts, as shown in **Fig. 5.13**. The forecast hydrograph in **Fig. 5.13a** and **5.13b** resulting from state updated type 1 presented a higher forecast inflow than those (**Fig. 5.13c** and **5.13d)** from state updated type 2. Higher discharge from the upstream grids at the initial state of forecast simulation resulted from the higher update coefficient flow to the outlet, when the simulation time was extended.

There is no primary difference in the forecast results compared to the use of different forcing data during the warmup period. Using only observed precipitation during the warmup period, the inflow forecast resulted in higher performance and lower simulation cost. Therefore, it may be considered as a cost-effective procedure for setting the initial

states of the model prior to performing the forecast. As forecast method 3 resulted in satisfactory performance and reduced simulation cost, the result from this method was adopted to optimize the Sirikit Dam release strategy.

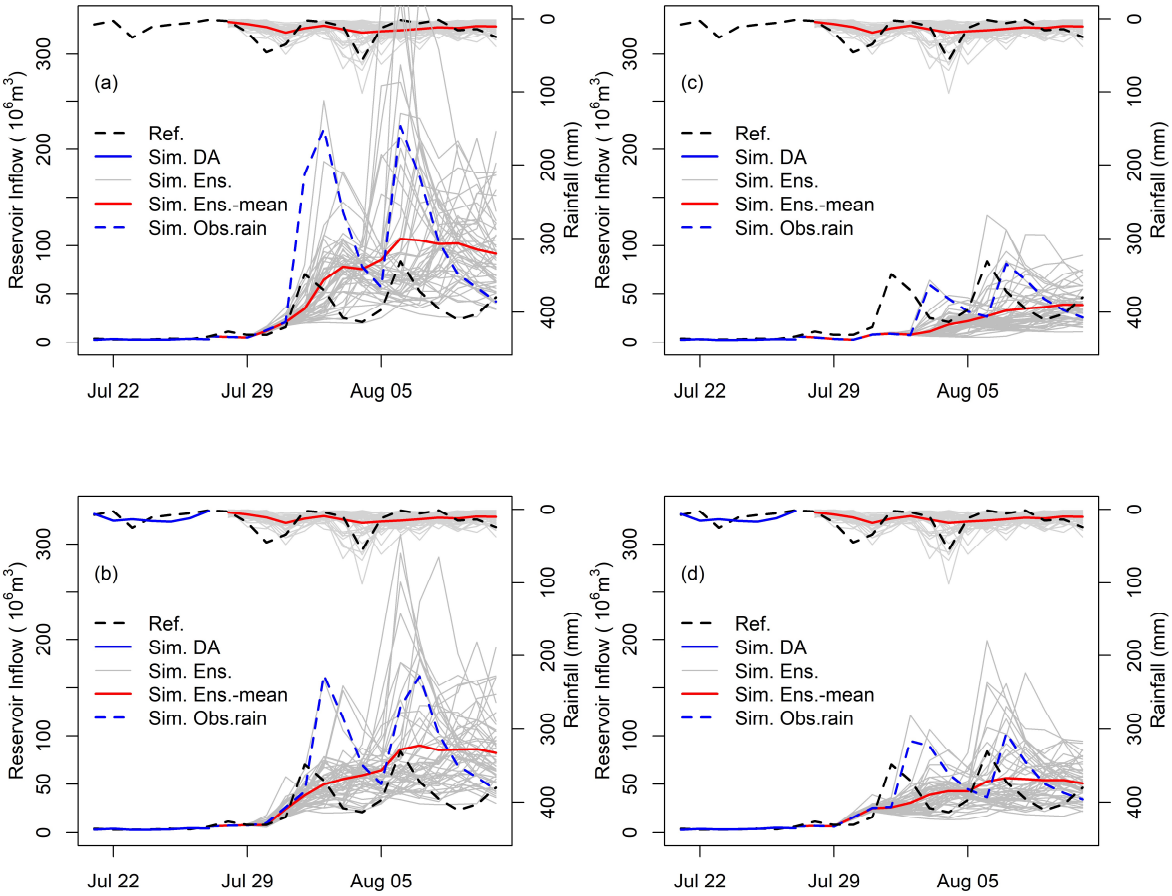

Fig. 5.13 Comparison of forecast hydrograph for simulation of week 31 among different forecast methods (a) method 1 (b) method 2 (c) method 3 and (d) method 4.

5.5.3 Reservoir optimization results

Fig. 5.14 presents the results of the reservoir operation by adopting the release strategies obtained from different scenarios of the real-time optimization process. **Fig. 5.14a** shows a comparison of the reservoir releases in different optimization scenarios. The actual release (Scenario 0) is large at the beginning of the year owing to increased demand for both downstream water and power during the dry season. The reservoir

storage might be considered to be at a high level (much higher than the LRC). The water release gradually decreased to low storage levels as a result of the imbalance between reservoir inflows and outflows. The water release hydrographs resulting from the optimization process (scenarios 1−5) have a similar tendency to increase water releases to mitigate the irrigation loss during March and April and to decrease releases during the wet season. This is a result of the irrigation sector requiring significant water from the reservoir for agricultural activities during the dry season. However, during the wet season, the water demand decreases due to seasonal rainfall.

Fig. 5.14b shows a comparison of the reservoir storage operated by the release strategies obtained from different optimization scenarios. Using an optimization process to determine the reservoir release decision, the reservoir storage at the end of 2019 was greater than that observed in operation (Scenario 0) for all scenarios. By associating forecast information in the real-time optimization of reservoir operation decision-making, such as scenarios 1−4, the overall reservoir water storage in 2019 is greater than that when predictions had not been considered (Scenario 5). Although Scenario 4 is considered as the perfect inflow forecast, there is no primary difference in the results obtained from Scenario 3. The forecast inflow for determining the release strategy in Scenario 3 has a similar tendency compared the actual inflow used in Scenario 4.

Fig. 5.14c presents a comparison of the accumulated total benefits of the reservoir operation in different optimization scenarios. Although increased releases provided a greater benefit at the end of the year as the benefit is a function of reservoir release, the remaining water budget for the future operation is different (difference in reservoir storage level at the end of the year). To compare the effectiveness of the optimization scenarios, the penalty might be considered for each storage level at the end of the year. This storage penalty can be calculated based on the future long-term inflow assumption using a backward calculation (**Eq. 5.4**). For this study, we used the actual inflow in 2020 and the 50^{th} percentile of the historical data in the dummy year. Thus, the penalties based on the end storage level for each scenario are summarized in **Table 5.5**.

The sum of the total benefit in 2019 and end year storage penalty were the greatest for scenarios 3 and 4 and had the highest value among all scenarios. Scenario 5 (without

considering forecast) had the highest benefit in 2019 among optimization scenarios (scenarios 1−5), but resulted in the smallest value when considering the storage penalty. This demonstrates that there are advantages when associating forecast information with real-time optimization for decision making in reservoir operation.

The future long-term inflow assumption (for penalty calculation) has a significant effect on the results of the reservoir operation. To improve optimization process efficiency, long-term forecasts with high performance should be utilized. In contrast, although the future long-term inflow is practically difficult to predict, the use of historical data, such as in scenarios 1 and 2, provided satisfactory results in this study.

Table 5.5 Summary of reservoir operation result using release strategy obtained from different optimization scenarios.

Scenarios	Total release [million m^3]	End year storage [million m^3]	End year storage penalties* [million USD]	Benefit [million USD]	
				within 2019	including penalties
Scenario 0	6175.9	4851.0	64.7	56.8	121.6
Scenario 1	5213.0	5786.4	104.3	33.1	137.5
Scenario 2	4473.2	6515.6	134.8	2.8	137.6
Scenario 3	4797.6	6197.6	121.6	16.2	137.8
Scenario 4	4796.9	6198.3	121.6	16.2	137.8
Scenario 5	5296.1	5703.9	100.9	36.5	137.4

* Possible max. future benefit at each storage level based on actual inflow in 2020 and Hist. p50 in dummy year

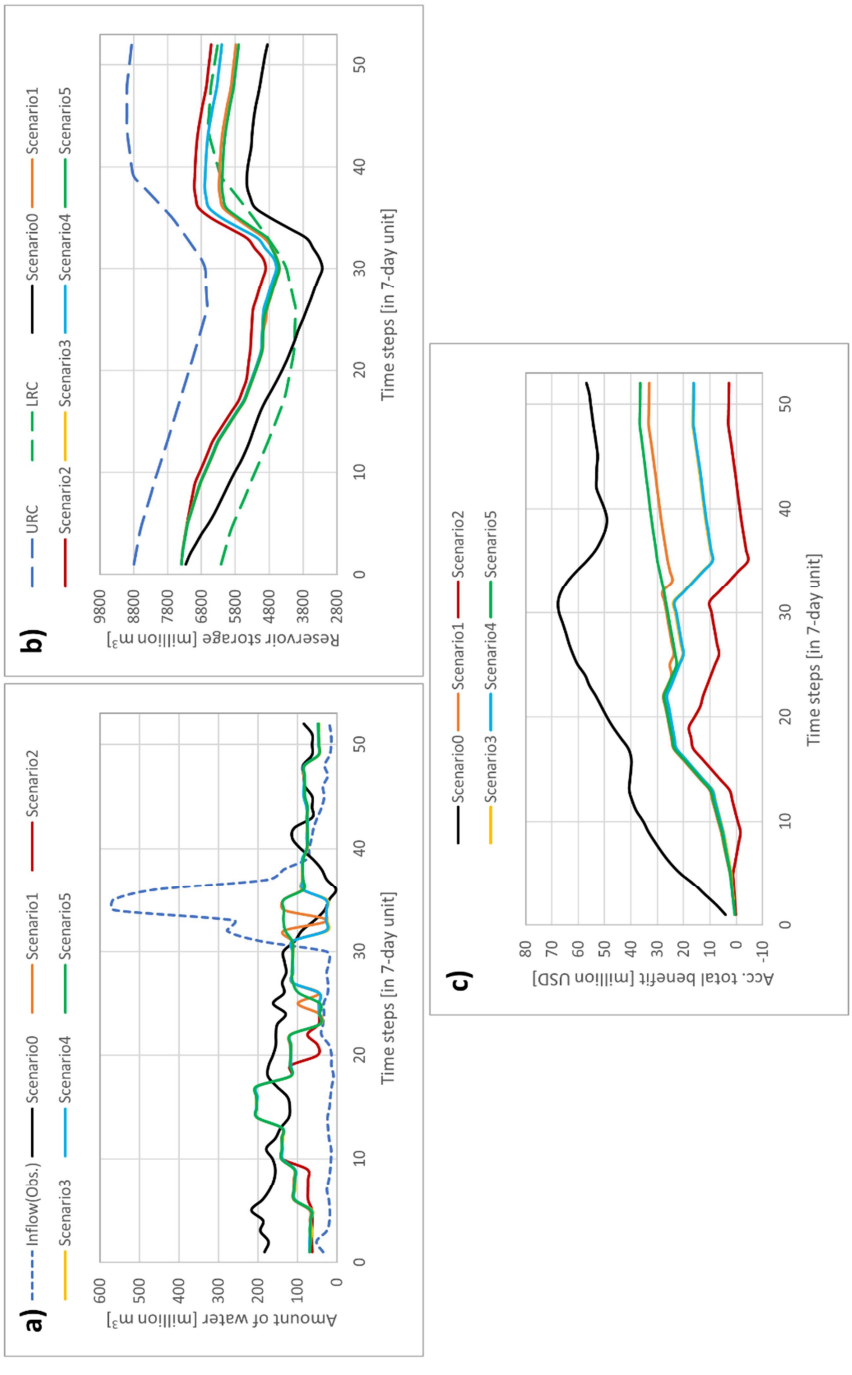

Fig. 5.14 Comparison of the Sirikit reservoir operation by adopting release strategies obtained from different scenarios of real-time optimization process.

5.6 Conclusions

This study presented a methodology to introduce ensemble weather forecast information collected from TIGGE archive data for real-time optimization of a one-week advanced release strategy of the Sirikit reservoir, Thailand. The basin is located in a tropical climate region with a distinct wet and dry season, which has high uncertainty regarding hydrological conditions. This uncertainty increases challenges for reservoir operation.

This study illustrates the importance of TIGGE, which provides forecast data from various centers worldwide, which provide the benefits of research development in regions where these advanced products are scarce.

To predict reservoir inflow, the hydrological model was operated in an adaptive mode during the warmup period to account for the uncertainties in the initial conditions of the model. The results showed that the state update that considers the drainage area factor (state update type 2) using observed precipitation as input forcing data has an advantage in terms of computation cost compared to other methods. By using this method to set the model initial condition, the two-week advanced inflow predictions using ECMWF perform well, which corresponds well with the observations throughout the year.

The ensemble mean of inflow predictions was introduced to the real-time optimization of Sirikit reservoir during 2019 using DP with different assumptions of optimization scenarios. The results showed that all optimization scenarios resulted in improved benefits (including end year storage penalties) compared to the observed operation. In conclusion, despite the reservoir's operational challenges resulting from the high uncertainty regarding hydrological conditions in a tropical-climate basin, the case study indicated that reservoir operation would benefit by considering ensemble weather forecasts. Such reservoir operation improvements would have positive impacts for long-term hydropower generation and irrigation purposes.

Although this study indicates potential advantages of considering ensemble weather predictions for the one-week advanced reservoir release strategy, further studies might consider updating the forecast and reservoir optimization in the shortest period possible to improve the efficiency of decision making in reservoir operation. Moreover, this study

presented significant differences in reservoir operation results driven by future long-term inflow assumptions (for a storage penalty estimation). Further studies might introduce long-range weather forecasts for more robust decision-making during reservoir operation.

Chapter 6 Concluding remarks

Regarding regional growth, water resources have become a highly essential resource for the countries in Southeast Asia where agriculture and hydropower are one of the main incomes for their economy. As a dam reservoir that controls rivers for both water use and flood control is an effective tool in water management, several dams have been developed in various stages ranged from operated to planned in this region.

Even though building dams can boost their economies, dam management becomes challenging due to the uncertainty (unpredictable) of hydrologic conditions in the tropical climate basin with distinct wet and dry seasons providing a primary effect on reservoir operation increased the risk of water disasters such as flood and drought. Furthermore, the effect of climate change on water resources results in more complicated efficient manage the dam.

In particular, this thesis focused on developing the approaches to assess the impact of climate change on reservoir operations and introduce the strategies to manage the reservoir coping with the uncertainty of water resources. Thus, the achievements in this thesis are as follows;

1) Improvement of the distributed hydrological model to improve the long-term river flow prediction in a tropical climate basin,
2) Development of an integrated model that coupled reservoir-hydropower plant model with a distributed hydrological model,
3) Applying the integrated model to assess the effect of climate change on reservoir operation and introducing the strategies to cope with the effect.
4) Introducing weather forecast to the real-time reservoir optimization using DP.

In Chapter 2, the original 1K-DHM was applied to the Nam Ngum River Basin, Laos PDR where the basin characteristic is distinct between wet and dry season for long-term river flow estimation. Even though the result is satisfactory, the optimized parameters such as soil depth is unreasonable (much larger than the available physical data).

Regarding this reason, the model structure of the 1K-DHM has been improved for a better estimation of long-term river discharge by incorporating bedrock aquifer into the original model structure. Based on different structures of bedrock aquifer, the model structure that combined the soil layer (original model) and the unconfined aquifer component with the estimation of the vertical infiltration based on vertical hydraulic conductivity best reproduced the long-term river discharge phenomena. The improved model structure not only improved river flow estimation but produced a reasonable set of parameters that agreed with physical data sets also.

In Chapter 3, the integrated model combined hydrological model (Chapter 2) and reservoir-hydropower model has been developed to assess the effect of dam operation in the Nam Ngum River Basin, Laos PDR. The integrated model performed well in calibration and validation processes that the result agrees with the actual operation record of the Nan Ngum 1 dam. The integrated model was applied to assess the impact of hydropower development in the Nam Ngum River Basin. The result indicated a primary change in annual and seasonal river flow due to regulated flow by the cascade dams in full development compared to natural river flow conditions. Furthermore, regulated flow by the upstream cascade dams also resulted in benefits in energy production of the Nam Ngum 1 power station.

In Chapter 4, the integrated model (Chapter 3) was applied to assess the combined effect of climate change and hydropower development in the Nam Ngum River Basin. The future climate has been projected using a large ensemble of future climate projections (d4PDF). The simulation results indicated a slight reduction trend of river flow (including dam inflow) and hydropower production due to a combination of precipitation reduction and high temperature in the mean climate projection of +2K and +4K scenarios. Therefore, to mitigate the impact of climate change on long-term reservoir operation, adaptive implementations are required to consider.

In Chapter 5, the methodology that introduced ensemble weather forecasting for real-time reservoir optimization for hydropower and irrigation facilities of Sirikit Dam in Thailand was conducted using dynamic programming. The real-time reservoir inflow prediction using medium-range ensemble precipitation forecasts with a hydrological

model in adaptive mode performed well compared to the observation. The result of reservoir implementation presented that considering ensemble forecasts in real-time reservoir optimization provided more efficient operating decisions than employing historical data.

This thesis successfully proposed a methodology for assessing the impact of water resource uncertainty in tropical climate basin with a distinct wet and dry season on reservoir operation and introduced adaptive implementations to cope with this uncertainty included a real-time optimization approach. The resulting information will be useful for water resources management, which may be adapted to other basins in the study region.

This thesis indicates the potential advantages of hydropower production and irrigation in reservoir management using adaptive implementations. For further research, the other multi-purposes of the reservoir (flood control, drought, etc.) may be taken into account to perform robust decision-making during reservoir operation. For this purpose, the real-time river flow forecast requires the accuracy of prediction in a shorter time step. Uncertainties in river flow forecast such as initial condition, precipitation, model parameters, and model structure might be taken into account, especially initial condition uncertainty as provided a primary effect on river flow prediction (mentioned in Chapter 5). By achieving this, supporting information for decision-making would be more reliable, leading to efficient water resources management and contributing benefits to society.

Bibliography

Abu-Zeid, M., Shiklomanov, I.A., 2004. Water Resources as a Challenge of the Twenty-First Century, World Meteorological Organization.

ADB, 2019. Lao People's Democratic Republic Energy Sector Assessment, Strategy, and Road Map.

Alemu, E.T., Palmer, R.N., Polebitski, A., Meaker, B., 2011. Decision Support System for Optimizing Reservoir Operations Using Ensemble Streamflow Predictions. J. Water Resour. Plan. Manag. 137, 72–82. https://doi.org/10.1061/(asce)wr.1943-5452.0000088

Alfieri, L., Thielen, J., Pappenberger, F., 2012. Ensemble hydro-meteorological simulation for flash flood early detection in southern Switzerland. J. Hydrol. 424–425, 143–153. https://doi.org/10.1016/j.jhydrol.2011.12.038

Amnatsan, S., Yoshikawa, S., Kanae, S., 2018. Improved forecasting of extreme monthly reservoir inflow using an analogue-based forecasting method: A case study of the Sirikit Dam in Thailand. Water (Switzerland) 10. https://doi.org/10.3390/w10111614

Arnold, J.G., Srinivasan, R., Muttiah, R.S., Williams, J.R., 1998. Large area hydrologic modeling and assessment part I: model development. J. Am. Water Resour. Assoc. 34, 73–89. https://doi.org/10.1111/j.1752-1688.1998.tb05961.x

Ayers, J., Ficklin, D.L., Stewart, I.T., Strunk, M., 2016. Comparison of CMIP3 and CMIP5 projected hydrologic conditions over the Upper Colorado River Basin. Int. J. Climatol. 36, 3807–3818. https://doi.org/10.1002/joc.4594

Bank of Thailand, 2021. Interest Rates in Financial Market [WWW Document]. URL https://www.bot.or.th/English/Statistics/FinancialMarkets/InterestRate/Pages/StatInterestRate.aspx (accessed 4.20.21).

Banks, E.W., Simmons, C.T., Love, A.J., Cranswick, R., Werner, A.D., Bestland, E.A., Wood, M., Wilson, T., 2009. Fractured bedrock and saprolite hydrogeologic controls

on groundwater/surface-water interaction: A conceptual model (Australia). Hydrogeol. J. 17, 1969–1989. https://doi.org/10.1007/s10040-009-0490-7

Bao, H.J., Zhao, L.N., He, Y., Li, Z.J., Wetterhall, F., Cloke, H.L., Pappenberger, F., Manful, D., 2011. Coupling ensemble weather predictions based on TIGGE database with Grid-Xinanjiang model for flood forecast. Adv. Geosci. 29, 61–67. https://doi.org/10.5194/adgeo-29-61-2011

Bates, B., Kundzewicz, Z., Wu, S., Palutikof, J., 2008. Climate change and water. Technical Paper of the Intergovernmental Panel on Climate Change, Geneva.

Beven, K., 1979. On the generalized kinematic routing method. Water Resour. Res. 15, 1238–1242. https://doi.org/10.1029/WR015i005p01238

Beyene, T., Lettenmaier, D.P., Kabat, P., 2010. Hydrologic impacts of climate change on the Nile River Basin: Implications of the 2007 IPCC scenarios. Clim. Change 100, 433–461. https://doi.org/10.1007/s10584-009-9693-0

Blackshear, B., Crocker, T., Drucker, E., Filoon, J., Knelman, J., Skiles, M., 2011. Hydropower Vulnerability and Climate Change A Framework for Modeling the Future of Global Hydroelectric Resources, Middlebury College Environmental Studies Senior Seminar.

Bougeault, P., Toth, Z., Bishop, C., Brown, B., Burridge, D., De Chen, H., Ebert, B., Fuentes, M., Hamill, T.M., Mylne, K., Nicolau, J., Paccagnella, T., Park, Y.Y., Parsons, D., Raoult, B., Schuster, D., Dias, P.S., Swinbank, R., Takeuchi, Y., Tennant, W., Wilson, L., Worley, S., 2010. The thorpex interactive grand global ensemble. Bull. Am. Meteorol. Soc. 91, 1059–1072. https://doi.org/10.1175/2010BAMS2853.1

Bourke, R.H., Garrett, R.P., 1987. Sea ice thickness distribution in the Arctic Ocean. Cold Reg. Sci. Technol. 13, 259–280. https://doi.org/10.1016/0165-232X(87)90007-3

Buizza, R., Bidlot, J.-R., Wedi, N., Fuentes, M., Hamrud, M., Holt, G., Vitart, F., 2007. The new ECMWF VAREPS (Variable Resolution Ensemble Prediction System). Q. J. R. Meteorol. Soc. 133, 681–695. https://doi.org/10.1002/qj.75

Buizza, R., Houtekamer, P.L., Toth, Z., Pellerin, G., Wei, M., Zhu, Y., 2005. A comparison of the ECMWF, MSC, and NCEP global ensemble prediction systems. Mon. Weather Rev. 133, 1076–1097. https://doi.org/10.1175/MWR2905.1

Carvajal, P.E., Anandarajah, G., Mulugetta, Y., Dessens, O., 2017. Assessing uncertainty of climate change impacts on long-term hydropower generation using the CMIP5 ensemble—the case of Ecuador. Clim. Change 144, 611–624. https://doi.org/10.1007/s10584-017-2055-4

Collischonn, W., Haas, R., Andreolli, I., Tucci, C.E.M., 2005. Forecasting River Uruguay flow using rainfall forecasts from a regional weather-prediction model. J. Hydrol. 305, 87–98. https://doi.org/10.1016/j.jhydrol.2004.08.028

Duan, Q., Sorooshian, S., Gupta, V.K., 1994. Optimal use of the SCE-UA global optimization method for calibrating watershed models. J. Hydrol. 158, 265–284. https://doi.org/10.1016/0022-1694(94)90057-4

Endo, H., Kitoh, A., Mizuta, R., Ishii, M., 2017. Future changes in precipitation extremes in East Asia and their uncertainty based on large ensemble simulations with a high-resolution AGCM. Sci. Online Lett. Atmos. 13, 7–12. https://doi.org/10.2151/sola.2017-002

ESCAP-UNISDR, 2012. Reducing Vulnerability and Exposure to Disasters 2012: The Asia-Pacific Disaster Report.

Faber, B.A., Stedinger, J.R., 2001. Reservoir optimization using sampling SDP with ensemble streamflow prediction (ESP) forecasts. J. Hydrol. 249, 113–133. https://doi.org/10.1016/S0022-1694(01)00419-X

Fan, J.-L., Hu, J.-W., Zhang, X., Kong, L.-S., Li, F., Mi, Z., 2020. Impacts of climate change on hydropower generation in China. Math. Comput. Simul. 167, 4–18. https://doi.org/10.1016/j.matcom.2018.01.002

Ferket, B.V.A., Samain, B., Pauwels, V.R.N., 2010. Internal validation of conceptual rainfall-runoff models using baseflow separation. J. Hydrol. 381, 158–173. https://doi.org/10.1016/j.jhydrol.2009.11.038

Freeze, R.A., Cherry, J.A., 1979. Groundwater. Prentice-Hall. Inc., Englewood Cliffs, New Jersey, USA.

Fujita, M., Mizuta, R., Ishii, M., Endo, H., Sato, T., Okada, Y., Kawazoe, S., Sugimoto, S., Ishihara, K., Watanabe, S., 2019. Precipitation Changes in a Climate With 2-K Surface Warming From Large Ensemble Simulations Using 60-km Global and 20-km Regional Atmospheric Models. Geophys. Res. Lett. 46, 435–442. https://doi.org/10.1029/2018GL079885

Grijsen, J., Patel, H., 2014. Understanding the Impact of Climate Change on Hydropower: the case of Cameroon Understanding the Impact of Climate Change on Hydropower: the case of Cameroon Climate Risk Assessment for hydropower generation in Cameroon. Africa Energy Pract. 151.

Hamlet, A.F., Huppert, D., Lettenmaier, D.P., 2002. Economic Value of Long-Lead Streamflow Forecasts for Columbia River Hydropower. J. Water Resour. Plan. Manag. 128, 91–101. https://doi.org/10.1061/(asce)0733-9496(2002)128:2(91)

Hamlet, A.F., Lee, S.-Y., Mickelson, K.E.B., Elsner, M.M., 2010. Effects of projected climate change on energy supply and demand in the Pacific Northwest and Washington State. Clim. Change 102, 103–128. https://doi.org/10.1007/s10584-010-9857-y

Hamududu, B., Killingtveit, A., 2012. Assessing climate change impacts on global hydropower. Energies 5, 305–322. https://doi.org/10.3390/en5020305

Hanittinan, P., Tachikawa, Y., Ram-Indra, T., 2020. Projection of hydroclimate extreme indices over the Indochina region under climate change using a large single-model ensemble. Int. J. Climatol. 40, 2924–2952. https://doi.org/10.1002/joc.6374

Hawkins, E., Sutton, R., 2009. The Potential to Narrow Uncertainty in Regional Climate Predictions. Bull. Am. Meteorol. Soc. 90, 1095–1108. https://doi.org/10.1175/2009BAMS2607.1

Hay, L.E., Wilby, R.L., Leavesley, G.H., 2000. A comparison of delta change and downscaled GCM scenarios for three mountainous basins in the United States. J. Am. Water Resour. Assoc. 36, 387–397. https://doi.org/10.1111/j.1752-

1688.2000.tb04276.x

He, Y., Wetterhall, F., Bao, H., Cloke, H., Li, Z., Pappenberger, F., Hu, Y., Manful, D., Huang, Y., 2010. Ensemble forecasting using TIGGE for the July-September 2008 floods in the Upper Huai catchment: A case study. Atmos. Sci. Lett. 11, 132–138. https://doi.org/10.1002/asl.270

Hibino, K., Takayabu, I., Wakazuki, Y., Ogata, T., 2018. Physical responses of convective heavy rainfall to future warming condition: Case study of the hiroshima event. Front. Earth Sci. 6, 1–9. https://doi.org/10.3389/feart.2018.00035

Hirahara, S., Ishii, M., Fukuda, Y., 2014. Centennial-Scale Sea Surface Temperature Analysis and Its Uncertainty. J. Clim. 27, 57–75. https://doi.org/10.1175/JCLI-D-12-00837.1

Hunukumbura, P.B., Tachikawa, Y., 2012. River discharge projection under climate change in the Chao Phraya River basin, Thailand, using the MRI-GCM3.1S dataset. J. Meteorol. Soc. Japan 90, 137–150. https://doi.org/10.2151/jmsj.2012-A07

Hunukumbura, P.B., Tachikawa, Y., Shiiba, M., 2012. Distributed hydrological model transferability across basins with different hydro-climatic characteristics. Hydrol. Process. 26, 793–808. https://doi.org/10.1002/hyp.8294

IEA, 2020. Climate Impacts on African Hydropower [WWW Document]. URL https://www.iea.org/reports/climate-impacts-on-african-hydropower (accessed 1.10.21).

JICA, 2010. Preparatory survey on Nam Ngum 1 Hydropower Station Expansion in Lao People's Democratic Republic : final report.

Katsura, S., Kosugi, K., Mizutani, T., Okunaka, S., Mizuyama, T., 2008. Effects of bedrock groundwater on spatial and temporal variations in soil mantle groundwater in a steep granitic headwater catchment. Water Resour. Res. 44. https://doi.org/10.1029/2007WR006610

Kim, S., Tachikawa, Y., Nakakita, E., Yorozu, K., Shiiba, M., 2011. Climate change impact on river flow of the Tone River Basin, Japan. J. Japan Soc. Civ. Eng. Ser. B1

(Hydraulic Eng. 67, I_85-I_90. https://doi.org/10.2208/jscejhe.67.I_85

Kim, Y.-O., Eum, H.-I., Lee, E.-G., Ko, I.H., 2007. Optimizing Operational Policies of a Korean Multireservoir System Using Sampling Stochastic Dynamic Programming with Ensemble Streamflow Prediction. J. Water Resour. Plan. Manag. 133, 4–14. https://doi.org/10.1061/(asce)0733-9496(2007)133:1(4)

Kılıç, Z., 2020. The importance of water and conscious use of water. Int. J. Hydrol. 4, 239–241. https://doi.org/10.15406/ijh.2020.04.00250

Kolka, R.K., Wolf, A.T., 1998. Estimating Actual Evapotranspirationfor Forested Sites: Modifications tothe Thornthwaite Model. United StatesDepartment ofAgriculture, For. Serv. South. Res. Stn. Res. Note SRS-6 7 pp.

Kopytkovskiy, M., Geza, M., McCray, J.E., 2015. Climate-change impacts on water resources and hydropower potential in the Upper Colorado River Basin. J. Hydrol. Reg. Stud. 3, 473–493. https://doi.org/10.1016/j.ejrh.2015.02.014

Kummu, M., Varis, O., 2007. Sediment-related impacts due to upstream reservoir trapping, the Lower Mekong River. Geomorphology 85, 275–293. https://doi.org/10.1016/j.geomorph.2006.03.024

Lauri, H., De Moel, H., Ward, P.J., Räsänen, T.A., Keskinen, M., Kummu, M., 2012. Future changes in Mekong River hydrology: Impact of climate change and reservoir operation on discharge. Hydrol. Earth Syst. Sci. 16, 4603–4619. https://doi.org/10.5194/hess-16-4603-2012

Lehner, B., Czisch, G., Vassolo, S., 2005. The impact of global change on the hydropower potential of Europe: A model-based analysis. Energy Policy 33, 839–855. https://doi.org/10.1016/j.enpol.2003.10.018

Lehner, B., Verdin, K., Jarvis, A., 2006. HydroSHEDS Technical Documentation Version 1.0, World Wildlife Fund US. Washington, DC.

Lettenmaier, D.P., Wood, E.F., 1993. Hydrologic forecasting, in: Maidment, D.R. (Ed.), Handbook of Hydrology. McGraw-Hill, New York.

Lin, J., Emanuel, K., Vigh, J.L., 2020. Forecasts of hurricanes using large-ensemble

outputs. Weather Forecast. 35, 1713–1731. https://doi.org/10.1175/WAF-D-19-0255.1

Loucks, D.P., Beek, E. van, Stedinger, J.R., Dijkman, J.P.M., Villars, M.T., 2005. Water Resources Planning and Management : An Overview, Water Resources Systems Planning and Management An Introduction to Methods, Models and Applications.

Louoks, D.P., Falkson, L.M., 1970. a Comparison of Some Dynamic, Linear and Policy Iteration Methods for Reservoir Operation. JAWRA J. Am. Water Resour. Assoc. 6, 384–400. https://doi.org/10.1111/j.1752-1688.1970.tb00489.x

Luo, Y., Arnold, J., Allen, P., Chen, X., 2012. Baseflow simulation using SWAT model in an inland river basin in Tianshan Mountains, Northwest China. Hydrol. Earth Syst. Sci. 16, 1259–1267. https://doi.org/10.5194/hess-16-1259-2012

Madsen, H., Skotner, C., 2005. Adaptive state updating in real-time river flow forecasting - A combined filtering and error forecasting procedure. J. Hydrol. 308, 302–312. https://doi.org/10.1016/j.jhydrol.2004.10.030

Manee, D., 2016. Impact of climate change on reservoir water storage and operation of large scale dams in Thailand. Kyoto University.

Maréchal, J.C., Dewandel, B., Subrahmanyam, K., 2004. Use of hydraulic tests at different scales to characterize fracture network properties in the weathered-fractured layer of a hard rock aquifer. Water Resour. Res. 40. https://doi.org/10.1029/2004WR003137

Mateo, C., 2012. Hydrological modeling with reservoir operation in the Chao Phraya River Basin for flood mitigation. University of Tokyo.

Meema, T., Tachikawa, Y., 2020. Structural improvement of a kinematic wave-based distributed hydrologic model to estimate long-term river discharge in a tropical climate basin. Hydrol. Res. Lett. 14, 104–110. https://doi.org/10.3178/hrl.14.104

Meema, T., Tachikawa, Y., Ichikawa, Y., Yorozu, K., 2021. Uncertainty assessment of water resources and long-term hydropower generation using a large ensemble of future climate projections for the Nam Ngum River in the Mekong Basin. J. Hydrol.

Reg. Stud. 36, 100856. https://doi.org/10.1016/j.ejrh.2021.100856

Meema, T., Tachikawa, Y., Ichikawa, Y., Yorozu, K., 2020. Integrated reservoir-hydropower-hydrologic model for water resources and energy assessment. J. Japan Soc. Civ. Eng. Ser. B1 (Hydraulic Eng. 67, I_811-I_816.

Miles, E.L., Snover, A.K., Hamlet, A.F., Callahan, B., Fluharty, D., 2000. Pacific Northwest regional assessment: The impacts of climate variability and climate change on the water resources of the Columbia River Basin. J. Am. Water Resour. Assoc. 36, 399–420. https://doi.org/10.1111/j.1752-1688.2000.tb04277.x

Milly, P.C.D., Dunne, K.A., Vecchia, A. V., 2005. Global pattern of trends in streamflow and water availability in a changing climate. Nature 438, 347–350. https://doi.org/10.1038/nature04312

Mizuta, R., Murata, A., Ishii, M., Shiogama, H., Hibino, K., Mori, N., Arakawa, O., Imada, Y., Yoshida, K., Aoyagi, T., Kawase, H., Mori, M., Okada, Y., Shimura, T., Nagatomo, T., Ikeda, M., Endo, H., Nosaka, M., Arai, M., Takahashi, C., Tanaka, K., Takemi, T., Tachikawa, Y., Temur, K., Kamae, Y., Watanabe, M., Sasaki, H., Kitoh, A., Takayabu, I., Nakakita, E., Kimoto, M., 2017. Over 5,000 years of ensemble future climate simulations by 60-km global and 20-km regional atmospheric models. Bull. Am. Meteorol. Soc. 98, 1383–1398. https://doi.org/10.1175/BAMS-D-16-0099.1

Mohammed, I.N., Bomblies, A., Wemple, B.C., 2015. The use of CMIP5 data to simulate climate change impacts on flow regime within the Lake Champlain Basin. J. Hydrol. Reg. Stud. 3, 160–186. https://doi.org/10.1016/j.ejrh.2015.01.002

Mohor, G.S., Rodriguez, D.A., Tomasella, J., Siqueira Júnior, J.L., 2015. Exploratory analyses for the assessment of climate change impacts on the energy production in an Amazon run-of-river hydropower plant. J. Hydrol. Reg. Stud. 4, 41–59. https://doi.org/10.1016/j.ejrh.2015.04.003

Moore, R.J., Bell, V.A., Jones, D.A., 2005. Forecasting for flood warning. Comptes Rendus - Geosci. 337, 203–217. https://doi.org/10.1016/j.crte.2004.10.017

MRC, 2018. Basin-Wide Assessment of Climate Change Impacts on Hydropower

Production Final Report 41 pp.

MRC, 2005. Hydrology of the Mekong Basin, Mekong River Commission, Vientiane.

Ngo, L.A., Masih, I., Jiang, Y., Douven, W., 2018. Impact of reservoir operation and climate change on the hydrological regime of the Sesan and Srepok Rivers in the Lower Mekong Basin. Clim. Change 149, 107–119. https://doi.org/10.1007/s10584-016-1875-y

Nishimura, M., Yamaguchi, M., 2015. Selective Ensemble Mean Technique for Tropical Cyclone Track Forecasts Using Multi-Model Ensembles. Trop. Cyclone Res. Rev. 4, 71–78. https://doi.org/10.6057/2015TCRR02.03

Nohara, D., Hori, T., 2018. Reservoir operation for water supply considering operational ensemble hydrological predictions. J. Disaster Res. 13, 650–659. https://doi.org/10.20965/jdr.2018.p0650

Nohara, D., Nishioka, Y., Hori, T., Sato, Y., 2016. Real-Time Reservoir Operation for Flood Management Considering Ensemble Streamflow Prediction and Its Uncertainty, in: Advances in Hydroinformatics. pp. 333–347. https://doi.org/10.1007/978-981-287-615-7_23

O'Connell, P.E., Clarke, R.T., 1981. Adaptive hydrological forecasting—a review. Hydrol. Sci. Bull. 26, 179–205. https://doi.org/10.1080/02626668109490875

Pahl-Wostl, C., 2007. Transitions towards adaptive management of water facing climate and global change, in: Water Resources Management. Springer, pp. 49–62. https://doi.org/10.1007/s11269-006-9040-4

Palmer, M.A., Reidy Liermann, C.A., Nilsson, C., Flörke, M., Alcamo, J., Lake, P.S., Bond, N., 2008. Climate change and the world's river basins: Anticipating management options. Front. Ecol. Environ. https://doi.org/10.1890/060148

Paz, V.P. da S., Teodoro, R.E.F., Mendonça, F.C., 2000. Water resources, irrigated agriculture and the environment. Rev. Bras. Eng. Agrícola e Ambient. e Ambient. 4, 465–473.

Perera, E.D.P., Sayama, T., Magome, J., Hasegawa, A., Iwami, Y., 2017. RCP8.5-Based

future flood hazard analysis for the lower mekong river basin. Hydrology 4. https://doi.org/10.3390/hydrology4040055

Piman, T., Cochrane, T.A., Arias, M.E., 2016. Effect of Proposed Large Dams on Water Flows and Hydropower Production in the Sekong, Sesan and Srepok Rivers of the Mekong Basin. River Res. Appl. 32, 2095–2108. https://doi.org/10.1002/rra.3045

Piman, T., Cochrane, T.A., Arias, M.E., Dat, N.D., Vonnarart, O., 2015. Managing Hydropower Under Climate Change in the Mekong Tributaries, in: Shrestha, S., Anal, A.K., Salam, P.A., van der Valk, M. (Eds.), Managing Water Resources under Climate Uncertainty. Springer International Publishing, Cham, pp. 223–248. https://doi.org/10.1007/978-3-319-10467-6_11

Rittima, A., Saleekij, K., Samarnwongrak, K., Sritamma, P., Cheeranoravanich, I., Udomthara, M., 2013. The Study on Evaporation Losses from Medium and Small Reservoirs in Thailand. Res. Dev. J. 24, 27–36.

Romanowicz, R.J., Young, P.C., Beven, K.J., 2006. Data assimilation and adaptive forecasting of water levels in the river Severn catchment, United Kingdom. Water Resour. Res. 42, 1–12. https://doi.org/10.1029/2005WR004373

Samuel, J., Coulibaly, P., Metcalfe, R.A., 2012. Identification of rainfall-runoff model for improved baseflow estimation in ungauged basins. Hydrol. Process. 26, 356–366. https://doi.org/10.1002/hyp.8133

Sayama, T., Tachikawa, Y., Takara, K., Ichikawa, Y., 2006. Distributed rainfall-runoff analysis in a flow regulated basin having multiple multi-purpose dams. IAHS-AISH Publ. 371–381.

Sayama, T., Yamada, M., Sugawara, Y., Yamazaki, D., 2020. Ensemble flash flood predictions using a high-resolution nationwide distributed rainfall-runoff model: case study of the heavy rain event of July 2018 and Typhoon Hagibis in 2019. Prog. Earth Planet. Sci. 7. https://doi.org/10.1186/s40645-020-00391-7

Shangguan, W., Hengl, T., Mendes de Jesus, J., Yuan, H., Dai, Y., 2017. Mapping the global depth to bedrock for land surface modeling. J. Adv. Model. Earth Syst. 9, 65–88. https://doi.org/10.1002/2016MS000686

Shrestha, S., Bajracharya, A.R., Babel, M.S., 2016. Assessment of risks due to climate change for the Upper Tamakoshi Hydropower Project in Nepal. Clim. Risk Manag. 14, 27–41. https://doi.org/10.1016/j.crm.2016.08.002

Sirisena, T.A.J.G., Maskey, S., Ranasinghe, R., Bamunawala, J., 2020. Climate change and reservoir impacts on 21st century streamflow and fluvial sediment loads in the Irrawaddy River, Myanmar. Front. Earth Sci. Hydrosph. 9:644527, 1–16. https://doi.org/10.3389/feart.2021.644527

Stocker, T.F., Qin, D., Plattner, G.K., Tignor, M.M.B., Allen, S.K., Boschung, J., Nauels, A., Xia, Y., Bex, V., Midgley, P.M., 2013. Climate change 2013 the physical science basis: Working Group I contribution to the fifth assessment report of the intergovernmental panel on climate change, Climate Change 2013 the Physical Science Basis: Working Group I Contribution to the Fifth Assessment Report of the Intergovernmental Panel on Climate Change. https://doi.org/10.1017/CBO9781107415324

Tachikawa, Y., Nagatani, G., Takara, K., 2004. Development of stage-discharge relationship equation incorporating saturated-unsaturated flow mechanism. Proc. Hydraul. Eng. 48, 7–12. https://doi.org/10.2208/prohe.48.7

Takasao, T., Shiiba, M., 1988. Incorporation of the effect of concentration of flow into the kinematic wave equations and its applications to runoff system lumping. J. Hydrol. 102, 301–322. https://doi.org/10.1016/0022-1694(88)90104-7

Tanaka, T., 2016. Extreme flood frequency analysis and flood risk curve development considering spatiotemporal rainfall variabilit. Kyoto University.

Tanaka, T., Kiyohara, K., Tachikawa, Y., 2020. Comparison of fluvial and pluvial flood risk curves in urban cities derived from a large ensemble climate simulation dataset: A case study in Nagoya, Japan. J. Hydrol. 584, 124706. https://doi.org/10.1016/j.jhydrol.2020.124706

Tanaka, T., Tachikawa, Y., 2015. Testing the applicability of a kinematic wave-based distributed hydrological model in two climatically contrasting catchments. Hydrol. Sci. J. 60, 1361–1373. https://doi.org/10.1080/02626667.2014.967693

Tebaldi, C., Knutti, R., 2007. The use of the multi-model ensemble in probabilistic climate projections. Philos. Trans. R. Soc. A Math. Phys. Eng. Sci. 365, 2053–2075. https://doi.org/10.1098/rsta.2007.2076

Thompson, J.R., Crawley, A., Kingston, D.G., 2017. Future river flows and flood extent in the Upper Niger and Inner Niger Delta: GCM-related uncertainty using the CMIP5 ensemble. Hydrol. Sci. J. 62, 2239–2265. https://doi.org/10.1080/02626667.2017.1383608

Thornthwaite, C.W., 1948. An Approach toward a Rational Classification of Climate. Geogr. Rev. 38, 55. https://doi.org/10.2307/210739

Tingsanchali, T., Boonyasirikul, T., 2006. Stochastic Dynamic Programming with Risk Consideration for Transbasin Diversion System. J. Water Resour. Plan. Manag. 132, 111–121. https://doi.org/10.1061/(asce)0733-9496(2006)132:2(111)

Trzaska, S., Schnarr, E., 2014. A review of downscaling methods for climate change projections. United States Agency Int. Dev. by Tetra Tech ARD 1–42.

van Vliet, M.T.H., Wiberg, D., Leduc, S., Riahi, K., 2016. Power-generation system vulnerability and adaptation to changes in climate and water resources. Nat. Clim. Chang. 6, 375–380. https://doi.org/10.1038/nclimate2903

Vinayak, H., Thompson, F., Tonby, O., 2014. Understanding ASEAN: Seven things you need to know, McKinsey&Company.

Viossanges, M., Pavelic, P., Rebelo, L.M., Lacombe, G., Sotoukee, T., 2018. Regional mapping of groundwater resources in data-scarce regions: The case of Laos. Hydrology 5. https://doi.org/10.3390/hydrology5010002

Weber, H.C., 2003. Hurricane track prediction using a statistical ensemble of numerical models. Mon. Weather Rev. 131, 749–770. https://doi.org/10.1175/1520-0493(2003)131<0749:HTPUAS>2.0.CO;2

Wichakul, S., Tachikawa, Y., Shiiba, M., Yorozu, K., 2015. River discharge assessment under a changing climate in the Chao Phraya River Thailand by using MRI-AGCM3.2S. Hydrol. Res. Lett. 9, 84–89. https://doi.org/10.3178/hrl.9.84

Winter, T.C., 1981. Uncertainties in estimating the water balance of lakes. J. Am. Water Resour. Assoc. 17, 82–115. https://doi.org/10.1111/j.1752-1688.1981.tb02593.x

Wittenberg, H., 1999. Baseflow recession and recharge as nonlinear storage processes. Hydrol. Process. 13, 715–726. https://doi.org/10.1002/(SICI)1099-1085(19990415)13:5<715::AID-HYP775>3.0.CO;2-N

Zhu, Y., 2005. Ensemble Forecast : A New Approach. Adv. Atmos. Sci. 22, 781–788.

Zhu, Y., Toth, Z., Wobus, R., Richardson, D., Mylne, K., 2002. The Economic Value Of Ensemble-Based Weather Forecasts. Bull. Am. Meteorol. Soc. 83, 73–83. https://doi.org/10.1175/1520-0477(2002)083<0073:TEVOEB>2.3.CO;2

Appendix

Table A1 Inflow of the Nam Ngum 1 reservoir in mcm.

Year	Jan	Feb	Mar	Apr	May	Jun	Jul	Aug	Sep	Oct	Nov	Dec	Annual
2001	255.3	154.6	385.4	163.9	810.3	1761.2	2714.9	2747.3	1958.3	1120.9	508.9	388.3	12969.4
2002	297.2	237.2	204.4	143.8	818.0	2222.0	3061.0	3364.6	1506.8	957.7	602.8	468.2	13883.8
2003	328.5	233.0	219.0	174.7	377.3	891.0	1644.5	2210.3	1817.1	676.0	345.8	277.6	9194.7
2004	253.8	225.0	184.7	319.3	601.1	1113.0	2621.9	2773.9	2964.0	732.1	392.8	315.9	12497.6
2005	286.1	259.1	229.7	296.8	267.2	1388.6	2759.3	4025.2	2638.8	1274.6	559.6	357.9	14343.0
2006	294.4	238.4	269.8	275.3	704.0	802.5	2785.5	2447.3	1396.8	811.8	394.4	290.3	10710.4
2007	246.7	220.7	201.7	188.7	405.1	719.1	1098.0	1889.0	2071.2	1291.0	432.3	312.1	9075.6
2008	253.0	199.2	228.5	233.1	769.0	2576.4	3520.3	3021.3	1471.6	1055.4	573.5	338.4	14239.8
2009	291.2	256.4	257.2	199.9	598.7	1159.0	2707.7	1851.4	1147.0	700.8	324.1	238.3	9731.6
2010	290.3	177.7	157.1	127.9	153.4	828.5	1472.3	1888.6	1543.3	552.7	332.2	260.4	7784.5
2011	164.0	165.5	346.2	829.1	1228.4	2206.4	2646.6	2698.2	2346.6	1289.5	702.5	361.7	14984.7
2012	445.5	475.9	727.0	810.2	845.9	1089.2	1378.5	1764.7	1220.6	744.8	525.6	363.0	10391.1

Table A2 Released flow of the Nam Ngum 1 reservoir in mcm.

Year	Jan	Feb	Mar	Apr	May	Jun	Jul	Aug	Sep	Oct	Nov	Dec	Annual
2001	743.8	695.2	887.5	906.9	867.8	970.4	1097.5	1127.8	1098.6	1149.7	886.7	970.5	11402.5
2002	771.5	764.4	890.7	924.8	956.1	1045.1	1129.0	1151.3	1122.1	1158.7	910.4	1014.7	11838.8
2003	881.1	753.0	782.3	919.9	945.3	724.2	863.3	961.0	681.4	725.5	708.4	782.6	9728.1
2004	755.3	726.0	929.0	962.7	888.6	978.9	1002.8	1181.5	1162.7	1003.0	745.5	808.5	11144.5
2005	884.4	941.9	1165.4	1061.9	707.5	533.2	1106.7	1174.5	1154.5	1198.2	951.2	849.1	11728.6
2006	906.3	901.9	1000.8	970.2	977.3	982.9	1013.3	1141.5	755.3	751.4	675.7	694.2	10770.8
2007	713.3	733.9	888.8	923.3	896.0	744.0	942.7	732.9	601.6	595.4	751.5	694.4	9217.6
2008	671.9	660.4	836.7	889.3	1031.1	1058.9	1156.9	1160.4	1118.3	1145.0	780.3	785.0	11294.1
2009	797.6	812.6	873.3	830.0	820.2	888.7	1138.0	1167.9	961.7	778.3	523.2	527.8	10119.1
2010	576.9	574.9	736.7	714.1	829.3	739.4	543.6	582.8	745.5	774.7	667.5	982.9	8468.3
2011	896.7	820.0	837.0	807.6	768.9	741.0	1097.1	1188.9	1155.9	1182.2	1006.4	1026.5	11528.1
2012	1042.1	1005.6	875.6	820.7	840.8	815.6	846.0	859.4	842.5	834.4	826.4	892.4	10501.5

Table A3 Delta change of precipitation from present climate scenario in different future climate scenarios for the Nam Ngum River Basin.

Scenario	Jan	Feb	Mar	Apr	May	Jun	Jul	Aug	Sep	Oct	Nov	Dec
HFB_2K_CC	1.362	1.119	1.040	0.951	0.981	1.061	1.153	1.059	0.981	0.940	0.989	1.165
HFB_2K_GF	1.003	0.983	0.897	0.951	0.998	1.013	1.062	1.001	1.049	1.047	1.002	1.030
HFB_2K_HA	1.074	1.210	1.076	1.005	1.041	1.018	1.033	0.975	1.063	1.122	0.971	1.010
HFB_2K_MI	0.878	0.734	0.871	0.957	1.006	1.050	0.934	0.820	0.995	0.924	0.982	0.929
HFB_2K_MP	1.073	0.986	0.994	0.959	1.010	1.013	0.948	0.907	0.928	0.966	1.210	1.327
HFB_2K_MR	1.196	1.335	0.900	0.987	1.025	1.017	1.020	1.025	1.051	0.944	0.906	0.945
HFB_2K_AVR	1.098	1.061	0.963	0.968	1.010	1.029	1.025	0.965	1.011	0.990	1.010	1.068
HFB_4K_CC	1.162	0.937	0.953	0.957	1.009	1.030	0.990	0.889	1.056	1.209	1.037	1.058
HFB_4K_GF	0.765	0.706	0.871	0.956	1.028	1.056	1.000	1.030	1.153	1.228	1.020	0.744
HFB_4K_HA	1.032	1.303	1.143	1.022	1.062	1.032	0.985	0.959	1.302	1.503	1.220	0.847
HFB_4K_MI	1.125	0.922	0.959	1.036	1.016	0.987	0.761	0.731	1.055	1.037	1.127	1.256
HFB_4K_MP	1.119	1.005	0.959	0.965	1.021	1.063	0.925	0.855	0.937	0.790	0.889	0.961
HFB_4K_MR	1.335	1.437	1.026	1.021	1.073	0.985	0.924	0.942	1.176	1.151	0.837	0.903
HFB_4K_AVR	1.090	1.052	0.985	0.993	1.035	1.026	0.931	0.901	1.113	1.153	1.022	0.961

Table A4 Delta change of actual evapotranspiration from present climate scenario in different future climate scenarios for the Nam Ngum River Basin.

Scenario	Jan	Feb	Mar	Apr	May	Jun	Jul	Aug	Sep	Oct	Nov	Dec
HFB_2K_CC	1.025	1.012	0.996	1.023	1.032	1.023	0.981	1.005	1.051	1.054	1.027	1.015
HFB_2K_GF	1.026	0.998	0.961	0.996	1.035	1.034	1.045	1.047	1.040	1.036	1.038	1.032
HFB_2K_HA	1.031	1.034	1.030	1.062	1.095	1.034	1.007	1.008	1.029	1.029	1.032	1.034
HFB_2K_MI	1.016	0.953	0.908	0.987	1.004	1.006	1.035	1.012	1.045	1.052	1.026	1.019
HFB_2K_MP	1.027	1.003	0.984	1.011	1.032	1.020	1.024	1.071	1.074	1.053	1.009	1.023
HFB_2K_MR	1.028	1.033	0.971	1.035	1.079	1.037	1.024	1.035	1.029	1.052	1.029	1.017
HFB_2K_AVR	1.025	1.006	0.975	1.019	1.046	1.026	1.019	1.030	1.045	1.046	1.027	1.023
HFB_4K_CC	1.064	1.028	0.979	1.057	1.055	1.008	1.030	1.061	1.062	1.060	1.074	1.064
HFB_4K_GF	1.060	0.972	0.912	1.036	1.088	1.043	1.076	1.086	1.085	1.095	1.093	1.067
HFB_4K_HA	1.085	1.089	1.079	1.119	1.141	1.029	1.012	1.019	1.025	1.046	1.078	1.090
HFB_4K_MI	1.085	1.013	0.960	1.063	1.052	1.005	1.110	1.047	1.056	1.099	1.068	1.060
HFB_4K_MP	1.050	0.967	0.923	1.068	1.127	1.055	1.043	1.124	1.126	1.113	1.029	1.014
HFB_4K_MR	1.085	1.077	1.007	1.096	1.147	1.059	1.106	1.068	1.056	1.086	1.083	1.057
HFB_4K_AVR	1.072	1.024	0.977	1.073	1.102	1.033	1.063	1.068	1.069	1.083	1.071	1.059

Table A5 Delta change of reservoir evaporation from present climate scenario in different future climate scenarios for the Nam Ngum River Basin.

Scenario	Jan	Feb	Mar	Apr	May	Jun	Jul	Aug	Sep	Oct	Nov	Dec
HFB_2K_CC	1.123	1.092	1.121	1.127	1.115	1.117	1.103	1.104	1.120	1.112	1.087	1.164
HFB_2K_GF	1.084	1.101	1.139	1.138	1.127	1.134	1.137	1.131	1.130	1.112	1.086	1.132
HFB_2K_HA	1.129	1.119	1.122	1.153	1.141	1.117	1.105	1.104	1.115	1.117	1.107	1.148
HFB_2K_MI	1.000	1.059	1.152	1.126	1.125	1.118	1.113	1.110	1.132	1.163	1.139	1.086
HFB_2K_MP	1.073	1.095	1.136	1.145	1.133	1.120	1.117	1.127	1.131	1.155	1.223	1.193
HFB_2K_MR	1.157	1.139	1.179	1.193	1.145	1.128	1.121	1.120	1.121	1.088	1.074	1.138
HFB_2K_AVR	1.094	1.101	1.141	1.147	1.131	1.122	1.116	1.116	1.125	1.125	1.119	1.144
HFB_4K_CC	1.204	1.275	1.375	1.387	1.322	1.292	1.282	1.290	1.318	1.280	1.206	1.253
HFB_4K_GF	1.197	1.317	1.439	1.418	1.359	1.360	1.367	1.358	1.371	1.337	1.261	1.231
HFB_4K_HA	1.249	1.319	1.342	1.389	1.344	1.297	1.274	1.276	1.305	1.320	1.264	1.244
HFB_4K_MI	1.205	1.310	1.428	1.396	1.353	1.324	1.319	1.297	1.324	1.419	1.408	1.324
HFB_4K_MP	1.272	1.324	1.426	1.443	1.390	1.349	1.321	1.345	1.362	1.350	1.411	1.349
HFB_4K_MR	1.379	1.387	1.450	1.473	1.385	1.346	1.340	1.331	1.341	1.288	1.243	1.336
HFB_4K_AVR	1.251	1.322	1.410	1.417	1.359	1.328	1.317	1.316	1.337	1.332	1.299	1.289

Table A6 Delta change of basin-averaged temperature from present climate scenario in different future climate scenarios for the Nam Ngum River Basin.

Scenario	Jan	Feb	Mar	Apr	May	Jun	Jul	Aug	Sep	Oct	Nov	Dec
HFB_2K_CC	1.116	1.081	1.074	1.069	1.062	1.063	1.059	1.059	1.066	1.072	1.083	1.132
HFB_2K_GF	1.105	1.088	1.082	1.074	1.067	1.070	1.073	1.070	1.071	1.074	1.085	1.124
HFB_2K_HA	1.123	1.095	1.076	1.079	1.073	1.063	1.061	1.060	1.065	1.076	1.093	1.130
HFB_2K_MI	1.065	1.069	1.086	1.068	1.066	1.063	1.063	1.062	1.071	1.092	1.104	1.101
HFB_2K_MP	1.106	1.090	1.083	1.078	1.071	1.065	1.066	1.070	1.073	1.093	1.142	1.154
HFB_2K_MR	1.138	1.106	1.099	1.095	1.075	1.068	1.068	1.067	1.068	1.066	1.083	1.131
HFB_2K_AVR	1.109	1.088	1.083	1.077	1.069	1.066	1.065	1.065	1.069	1.079	1.098	1.129
HFB_4K_CC	1.218	1.192	1.179	1.165	1.141	1.132	1.132	1.135	1.145	1.154	1.175	1.235
HFB_4K_GF	1.230	1.213	1.200	1.175	1.153	1.153	1.159	1.156	1.162	1.175	1.203	1.242
HFB_4K_HA	1.237	1.208	1.170	1.166	1.148	1.133	1.131	1.131	1.141	1.167	1.196	1.235
HFB_4K_MI	1.233	1.211	1.197	1.169	1.151	1.143	1.145	1.138	1.148	1.199	1.249	1.273
HFB_4K_MP	1.262	1.219	1.198	1.182	1.162	1.150	1.146	1.153	1.160	1.181	1.253	1.287
HFB_4K_MR	1.295	1.237	1.204	1.190	1.161	1.149	1.152	1.149	1.154	1.162	1.200	1.281
HFB_4K_AVR	1.246	1.213	1.191	1.175	1.153	1.143	1.144	1.143	1.152	1.173	1.213	1.259

Table A7 Inflow of the Sirikit Reservoir in mcm.

Year	Jan	Feb	Mar	Apr	May	Jun	Jul	Aug	Sep	Oct	Nov	Dec	Annual
1986	124.3	115.1	131.4	164.1	466.2	410.2	912.7	865.7	812.1	384.3	208.0	121.4	4715.5
1987	75.9	66.4	72.1	61.6	88.0	160.6	142.1	951.6	661.1	414.9	221.7	89.8	3005.6
1988	78.8	66.0	50.0	89.2	310.8	346.5	817.8	1464.3	635.6	413.6	165.3	103.5	4541.4
1989	74.0	76.1	63.1	47.2	279.4	237.2	642.8	828.5	941.2	492.3	173.7	93.0	3948.5
1990	84.0	80.4	59.4	48.6	239.9	360.7	730.5	884.0	885.6	395.5	219.8	97.2	4085.6
1991	86.4	44.6	29.3	68.5	226.6	260.8	347.9	826.9	846.4	413.1	167.4	85.7	3403.4
1992	81.9	66.5	64.2	45.0	58.5	91.1	418.0	693.1	741.5	440.2	176.5	150.9	3027.3
1993	93.7	49.9	75.2	69.8	125.5	205.6	787.3	643.0	649.7	322.2	130.6	80.9	3233.4
1994	65.6	58.2	91.8	67.2	218.3	411.3	875.1	3272.4	1665.4	631.5	254.6	183.9	7795.4
1995	119.3	84.8	55.9	51.7	133.5	211.3	1019.3	3300.1	2614.2	744.4	510.4	210.7	9055.5
1996	156.6	149.1	95.8	151.2	194.6	387.6	886.3	1592.5	1196.9	744.5	316.0	161.0	6032.2
1997	124.2	99.3	50.6	96.8	107.4	69.8	460.9	1125.3	1367.8	738.8	248.7	134.1	4623.7
1998	111.7	73.4	71.8	96.1	103.4	144.3	503.9	657.6	1155.4	265.2	159.5	84.0	3426.3
1999	71.3	67.1	74.4	115.9	237.8	432.0	458.8	1578.6	2193.7	685.6	285.2	128.1	6328.4
2000	141.7	146.3	101.2	111.1	421.0	517.4	1181.0	1054.8	1433.0	643.2	287.5	175.8	6214.0
2001	138.3	107.8	201.8	83.3	283.6	333.3	1202.8	2740.7	1642.4	609.8	286.1	176.7	7806.7
2002	146.4	123.3	91.0	61.4	547.1	653.4	777.7	1531.1	1668.5	621.5	327.5	219.9	6768.8
2003	186.5	143.0	158.8	102.2	120.3	268.0	934.0	1243.6	1607.0	370.2	215.7	132.7	5482.0
2004	137.7	105.1	81.4	127.1	221.6	665.7	1239.2	1596.0	2225.2	511.3	258.7	178.0	7347.0
2005	168.5	108.3	111.8	114.2	108.0	450.6	685.8	1771.7	1867.7	847.8	322.1	203.3	6759.7
2006	169.3	124.5	92.5	165.5	467.9	287.2	727.8	2356.7	1535.5	936.3	265.8	213.3	7342.1
2007	163.7	139.9	121.8	105.1	264.6	361.1	391.4	1091.9	1035.0	896.1	275.9	184.0	5030.4
2008	136.8	144.8	103.6	135.7	301.5	772.4	1503.1	2095.1	1136.9	654.1	367.8	223.1	7575.0
2009	180.7	142.6	129.4	140.8	205.2	329.3	1103.8	769.6	775.0	466.0	215.9	142.5	4600.7
2010	135.5	97.4	84.1	68.9	115.0	154.9	634.6	2288.4	1761.2	513.1	207.2	188.9	6249.1
2011	116.1	93.5	117.3	134.3	525.7	1237.7	1945.6	3096.0	2320.7	1031.1	365.0	243.8	11226.6
2012	215.7	142.9	119.9	147.2	448.4	273.2	628.4	1290.7	1211.9	454.0	300.4	211.0	5443.8
2013	122.5	108.1	92.0	78.5	133.5	160.3	598.3	1404.2	1060.0	429.1	198.0	150.7	4535.1
2014	118.8	98.4	86.0	88.0	181.7	209.4	728.0	1094.7	1287.5	430.8	262.4	126.6	4712.4
2015	133.6	94.1	92.3	106.5	127.2	149.5	353.4	944.3	812.2	618.7	215.3	170.7	3817.6
2016	117.8	82.6	66.9	46.5	199.0	275.6	799.3	1919.2	1407.7	630.2	242.2	143.0	5929.8
2017	178.1	94.8	52.4	129.4	209.6	209.1	1163.1	1101.7	1167.4	885.4	266.8	212.2	5670.0
2018	178.1	113.8	127.9	179.8	265.2	605.1	1639.4	1919.8	1271.8	493.8	239.3	166.3	7200.4

Table A8 Released flow of the Sirikit Reservoir in mcm.

Year	Jan	Feb	Mar	Apr	May	Jun	Jul	Aug	Sep	Oct	Nov	Dec	Annual
1986	193.2	544.1	849.6	728.7	679.0	681.5	556.3	397.1	302.5	422.4	667.4	233.3	6255.0
1987	319.3	686.9	657.8	633.5	571.4	266.2	452.7	303.7	118.4	71.9	188.8	45.6	4316.0
1988	192.6	542.5	412.3	237.1	140.0	63.5	147.5	120.2	180.1	140.7	171.6	77.2	2425.3
1989	208.5	339.8	356.9	556.4	557.8	143.6	168.5	429.7	475.5	202.9	342.5	105.9	3888.0
1990	267.0	428.8	727.4	635.9	479.8	374.8	410.9	411.9	431.6	321.0	329.7	169.1	4987.9
1991	209.1	506.7	655.5	587.4	318.1	149.9	331.8	313.3	59.9	181.7	261.0	160.1	3734.6
1992	215.6	340.4	465.9	465.0	320.2	118.9	118.5	24.9	57.4	39.2	208.3	210.1	2584.3
1993	148.9	292.1	411.0	417.5	353.2	295.0	426.2	735.7	257.7	125.5	457.2	195.3	4115.1
1994	174.7	238.2	274.6	136.7	103.0	30.1	14.5	101.0	302.4	160.0	446.5	341.5	2323.1
1995	369.2	629.0	824.4	745.6	598.2	472.6	268.9	822.8	1177.0	753.6	526.7	375.6	7563.7
1996	482.8	799.3	1081.0	939.2	793.8	737.9	645.6	734.4	358.6	212.8	373.6	244.1	7403.1
1997	382.5	615.0	775.4	721.3	634.1	409.7	446.4	331.8	177.7	199.4	462.8	338.5	5494.8
1998	421.1	658.5	658.6	614.0	330.6	226.1	157.0	334.6	50.3	183.2	320.2	233.6	4187.7
1999	375.7	448.9	545.8	277.3	66.5	38.5	134.3	158.2	103.4	11.4	40.5	81.5	2281.9
2000	599.1	917.3	1006.4	777.8	452.1	371.5	273.0	333.6	127.6	280.6	332.0	526.7	5997.6
2001	765.3	894.8	806.7	969.9	406.2	148.2	407.1	724.8	1280.5	230.3	186.8	479.2	7299.8
2002	683.4	830.0	979.5	943.0	739.7	379.8	628.7	473.8	42.9	217.1	285.6	244.1	6447.4
2003	683.5	786.7	847.3	638.8	884.4	494.8	517.3	428.8	96.8	234.3	629.0	549.8	6791.4
2004	572.8	699.5	802.4	762.8	440.2	167.5	406.3	186.7	372.7	339.3	667.4	830.5	6248.0
2005	875.6	838.9	948.8	744.8	806.7	420.0	406.1	215.2	101.1	229.2	298.8	683.3	6568.5
2006	804.9	817.7	930.8	864.5	374.4	288.3	222.5	264.0	255.0	413.5	300.2	788.6	6324.5
2007	939.0	813.7	850.3	739.8	264.3	500.2	526.4	527.1	276.3	208.6	449.2	642.6	6737.3
2008	756.1	673.4	722.0	778.8	488.7	427.4	483.0	349.1	275.7	248.8	330.5	719.0	6252.5
2009	854.5	790.1	940.3	878.3	683.7	394.4	286.5	392.1	297.3	247.6	354.2	596.6	6715.6
2010	594.7	589.5	541.6	366.2	250.6	328.5	265.8	131.8	60.0	110.9	180.6	511.7	3931.9
2011	926.4	927.9	769.6	395.4	213.0	183.1	508.8	1558.4	1723.0	903.8	422.7	864.3	9396.3
2012	1235.0	1377.8	935.8	762.0	696.4	691.6	478.9	361.0	121.3	191.2	541.3	760.8	8153.1
2013	883.3	656.5	479.2	346.0	427.3	342.6	277.2	181.8	113.7	87.5	121.4	368.4	4284.8
2014	520.3	562.5	501.2	391.3	601.4	537.9	523.7	200.9	76.5	93.9	91.3	199.1	4300.0
2015	274.6	298.0	354.6	510.7	956.3	723.7	449.5	315.1	191.7	123.2	250.5	264.4	4712.3
2016	295.8	291.7	312.5	301.5	317.2	313.7	257.5	170.9	65.7	79.2	141.0	556.4	3103.2
2017	757.0	772.0	754.8	474.7	421.2	243.9	201.5	110.9	88.7	20.4	104.6	765.9	4715.5
2018	824.0	758.3	743.5	631.5	659.5	545.8	476.0	862.7	324.3	299.9	539.0	783.1	7447.6

Table A9 Reservoir storage at the end of month for Sirikit Dam in mcm.

Year	Jan	Feb	Mar	Apr	May	Jun	Jul	Aug	Sep	Oct	Nov	Dec
1986	8144.7	7683.0	6930.1	6328.5	6079.3	5782.1	6117.0	6565.1	7053.0	6992.5	6511.0	6377.6
1987	6110.7	5462.9	4846.9	4244.7	3733.0	3607.7	3280.9	3914.3	4440.8	4766.1	4780.7	4806.4
1988	4669.8	4169.0	3782.3	3606.2	3749.9	4012.4	4664.4	5989.8	6424.8	6676.2	6647.8	6652.2
1989	6493.7	6201.2	5876.2	5333.3	5022.4	5092.4	5546.3	5925.7	6371.2	6639.1	6448.4	6414.0
1990	6207.5	5831.1	5130.5	4507.4	4237.9	4202.5	4503.9	4958.5	5393.9	5449.1	5319.6	5228.4
1991	5084.8	4598.0	3946.3	3400.9	3283.6	3375.7	3375.7	3874.6	4644.6	4858.0	4746.0	4653.6
1992	4500.4	4202.5	3776.1	3330.0	3043.0	2997.3	3275.5	3928.7	4596.2	4979.1	4926.7	4845.1
1993	4769.7	4502.2	4140.6	3765.3	3510.8	3402.3	3746.8	3639.1	4015.7	4195.8	3852.6	3722.3
1994	3595.8	3395.3	3190.3	3096.1	3186.3	3548.7	4392.0	7543.4	8882.1	9327.4	9108.5	8924.7
1995	8646.1	8068.1	7263.3	6530.4	6027.2	5739.4	6467.8	8899.6	9476.4	9440.3	9396.6	9204.9
1996	8849.7	8164.0	7143.1	6317.8	5682.7	5307.9	5528.4	6366.9	7183.8	7692.3	7610.7	7504.1
1997	7220.1	6674.0	5917.4	5259.4	4700.6	4338.5	4335.1	5111.5	6281.7	6799.3	6562.9	6337.0
1998	6004.3	5392.0	4777.1	4229.5	3973.6	3871.5	4200.8	4507.5	5594.3	5656.5	5476.8	5307.9
1999	4984.7	4578.4	4081.1	3892.1	4035.2	4407.7	4713.3	6114.9	8183.2	8832.2	9050.4	9070.6
2000	8584.6	7779.0	6839.1	6135.9	6068.9	6188.5	7073.3	7772.0	9052.9	9388.9	9317.1	8939.7
2001	8284.5	7464.8	6825.8	5903.0	5745.5	5905.0	6678.4	8670.9	9007.6	9360.7	9432.6	9103.4
2002	8537.9	7797.8	6874.5	5956.7	5729.3	5977.4	6104.5	7140.9	8742.7	9121.2	9136.4	9085.7
2003	8560.0	7882.7	7158.9	6584.7	5784.2	5532.4	5927.7	6722.3	8209.7	8320.8	7882.7	7441.8
2004	6981.4	6356.2	5604.3	4936.0	4686.1	5161.1	5973.2	7361.4	9189.6	9335.1	8899.6	8221.7
2005	7487.9	6726.6	5857.8	5193.8	4463.5	4472.3	4733.3	6271.0	8015.6	8609.2	8606.7	8101.6
2006	7439.5	6715.7	5845.5	5113.4	5174.6	5149.7	5634.4	7706.4	8962.3	9458.4	9396.6	8794.8
2007	7991.8	7286.0	6523.9	5853.7	5818.9	5654.5	5498.6	6043.9	6781.6	7446.4	7249.6	6768.4
2008	6125.4	5568.3	4921.1	4248.1	4032.0	4355.7	5356.7	7082.3	7920.6	8301.4	8313.6	7793.1
2009	7093.5	6416.2	5574.2	4804.6	4295.7	4209.2	5007.3	5366.5	5825.0	6023.0	5863.9	5390.0
2010	4910.0	4393.8	3911.1	3587.0	3424.9	3232.6	3585.5	5725.2	7405.0	7783.7	7786.1	7439.5
2011	6604.2	5741.5	5060.2	4767.9	5048.8	6079.4	7492.5	8919.7	9394.1	9494.5	9409.5	8762.5
2012	7713.4	6446.3	5598.3	4951.0	4671.6	4231.2	4362.6	5274.9	6345.5	6586.8	6324.2	5753.6
2013	4971.6	4399.0	3986.5	3691.8	3371.5	3170.7	3476.2	4682.5	5610.3	5931.9	5987.7	5749.6
2014	5323.5	4834.0	4392.0	4059.7	3612.2	3264.7	3453.3	4331.6	5524.4	5841.4	5991.9	5898.9
2015	5735.4	5504.5	5213.0	4775.2	3915.9	3321.8	3210.0	3824.3	4428.5	4906.2	4852.5	4740.5
2016	4542.8	4309.4	4038.5	3756.1	3610.7	3553.1	4077.8	5808.6	7129.6	7657.3	7734.4	7297.4
2017	6693.7	5987.7	5255.5	4878.4	4635.6	4578.4	5520.4	6491.5	7548.0	8388.8	8525.6	7946.7
2018	7274.7	6599.9	5952.5	5466.9	5039.4	5075.3	6218.1	7254.2	8178.4	8347.5	8022.8	7382.1